

OVERCOMING IONOSPHERIC SCINTILLATION FOR
WORLDWIDE GPS AVIATION

A DISSERTATION
SUBMITTED TO THE DEPARTMENT OF AERONAUTICS AND
ASTRONAUTICS
AND THE COMMITTEE ON GRADUATE STUDIES
OF STANFORD UNIVERSITY
IN PARTIAL FULFILLMENT OF THE REQUIREMENTS
FOR THE DEGREE OF
DOCTOR OF PHILOSOPHY

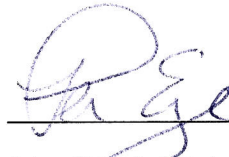
Jiwon Seo

June 2010

© Copyright by Jiwon Seo 2010

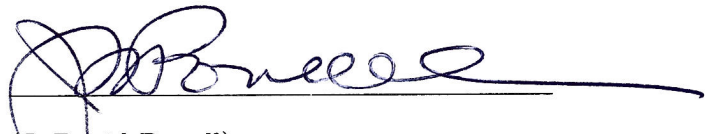
All Rights Reserved

I certify that I have read this dissertation and that, in my opinion, it is fully adequate in scope and quality as a dissertation for the degree of Doctor of Philosophy.




(Per Enge) Principal Adviser

I certify that I have read this dissertation and that, in my opinion, it is fully adequate in scope and quality as a dissertation for the degree of Doctor of Philosophy.



(J. David Powell)

I certify that I have read this dissertation and that, in my opinion, it is fully adequate in scope and quality as a dissertation for the degree of Doctor of Philosophy.



(Todd Walter)

Approved for the University Committee on Graduate Studies.

Abstract

Together, the Global Positioning System (GPS) and the Wide Area Augmentation System (WAAS) can guide aircraft down to 200 ft above the runway. This approach procedure is referred to as Localizer Performance with Vertical guidance (LPV)-200. Approach guidance using GPS and WAAS has many advantages over traditional precision approach guidance using the Instrument Landing System (ILS) and the number of published LPV approaches in the U. S. is now greater than the number of published Category I ILS approaches. Given the success of LPV service in the U. S., worldwide expansion of the LPV service is being actively pursued.

One of the main challenges for the LPV service in the equatorial area, including Brazil and India, is ionospheric scintillation. Due to electron density irregularities inside the ionosphere, transionospheric radio waves interfere constructively and destructively; consequently, a GPS receiver can experience deep and frequent signal fading. This phenomenon is known as ionospheric scintillation. Although the physics of the ionospheric scintillation has been studied for several decades, its impact on GPS aviation has not been well understood. As a result, the current GPS aviation receiver performance standards (RTCA/DO-229D) do not have any specific performance requirements to mitigate the impact of scintillation.

Although current aviation receivers do not protect against scintillation, currently it

is not a problem because they are only used in the mid-latitude area where scintillation is not usually observed. The advent of a new GPS civilian signal at the L5 frequency and dual frequency airborne receivers will eliminate ionospheric delay errors in the equatorial and arctic regions, but it will not solve the scintillation problems that will arise in those areas. This dissertation analyzes and proposes a solution to scintillation for the dual frequency era so that the LPV service will become practical worldwide.

Specifically, this research investigates the characteristics of GPS signal fades due to scintillation from the perspective of GPS aviation. Using high rate GPS data collected during the past solar maximum, scintillation impact on the operational availability of LPV-200 is analyzed. In order to mitigate scintillation impact, satellite-to-satellite correlation and frequency-to-frequency correlation of GPS signal fades under strong scintillation are investigated. Based on the observed data and availability analyses, a new requirement for the future dual frequency aviation receiver performance standards to mitigate the impact of scintillation is proposed. This new requirement mandating fast reacquisition after a very brief outage is under discussion at the standards committee working group (RTCA Special Committee-159, Working Group-2). Without this requirement, a certified aviation receiver may provide less than 50% availability of LPV-200 during severe scintillation. It is demonstrated that with this new requirement in place, it will be possible to achieve high level of availability (more than 99% availability) even during severe scintillation.

Acknowledgements

There are many people who have guided and supported this research. I am heartily thankful to my advisor, Professor Per Enge, for his generous support and encouragement during my Ph.D. study. He has been a great role model for me in my academic career. I hope that one day I would become as good an advisor as he has been to me. I would also like to thank the chair of the Ph.D. oral examination committee, Professor Teresa Meng, and other committee members, Professors Ilan Kroo, J. David Powell, and Dr. Todd Walter. I am particularly grateful to Dr. Walter for his invaluable guidance and discussion throughout this research. I will never forget the delightful years of working with him. Outside Stanford, Drs. Theodore Beach and Eurico de Paula helped this research by providing scintillation data sets. I am indebted to Professor Changdon Kee for his broad support. Also, I appreciate Fiona Walter's careful proofreading of this dissertation and my other publications.

I gratefully acknowledge the five year support of the Samsung Lee Kun Hee Fellowship Foundation and the support of the Federal Aviation Administration for the remaining years. With the tuition support of the fellowship, I was able to pursue an M.S. in electrical engineering in addition to an M.S. and a Ph.D. in aeronautics and astronautics. The knowledge that I gained in electrical engineering was definitely helpful for GPS research which is interdisciplinary in nature.

The GPS group members and alumni include many good friends, colleagues, and mentors. Professors Dennis Akos, Seebany Datta-Barua, Shau-Shiun Jan, Jiyun Lee, Brad Parkinson, Jason Rife, Jim Spilker; Drs. Juan Blanch, Lee Boyce, Dave De Lorenzo, Juyong Do, Alex Ene, Grace Gao, Euiho Kim, Ung-Suok Kim, Hiro Konno, Sherman Lo, Eric Phelts, Sam Pullen, and Di Qiu; Doug Archdeacon, Alan Chen, Tsung-Yu Chiou, Jun Choi, Sherann Ellsworth, Liang Heng, Ming Luo, Dana Parga, Young Shin Park, Shankar Ramakrishnan, Haochen Tang, Gabriel Wong, and Godwin Zhang: thank every single one of you. I feel privileged to be a member of this GPS family.

This long journey toward Ph.D. has started from Korea Science Academy (formerly Busan Science High School) where I cultivated my spirit of science and engineering. I am grateful to all teachers, especially Dr. Doo-Young Jung, for their excellent lectures and cares. I also thank all high school classmates for their lifelong friendship. Further, I cannot forget to acknowledge the faculty of aerospace engineering at Korea Advanced Institute of Science and Technology. Due to their superior undergraduate training, I had no academic difficulty while pursuing Ph.D. at Stanford. My sincere thanks go to Professors Chun-Gon Kim, Oh Joon Kwon, Seung O Park, and Min-Jea Tahk, who have either encouraged me to study in the U. S. or written recommendation letters when I applied for Stanford.

Finally, and most importantly, I extend my deepest love and gratitude to my parents, Taeik Seo and Hangbun Chung, and my brother, Hyowon Seo. I cannot imagine completing my Ph.D. study without their support, love, and prayer, and for that I dedicate this dissertation to them.

Contents

Abstract	v
Acknowledgements	vii
1 Introduction	1
1.1 Overview	1
1.2 GPS Applications for Aviation	2
1.2.1 Space-Based Augmentation for Landing Approach Guidance of Aircraft	3
1.2.2 GNSS Evolutionary Architecture Study Toward Worldwide LPV Service	5
1.3 Scintillation as a Challenge for GPS Aviation	7
1.3.1 Strong Ionospheric Scintillation in the Equatorial Latitudes	7
1.3.2 Aviation Receiver Performance Standards Regarding Scintillation	10
1.4 Previous Work	11
1.5 Contributions	13
2 Characteristics of GPS Signal Fading Due to Scintillation	16
2.1 Overview	16

2.2	Scintillation Data Set	17
2.2.1	Ascension Island Data	17
2.2.2	Brazil Data	20
2.3	Definition of Deep Signal Fading	21
2.4	Fading Duration Model	23
2.5	Time Between Deep Fades	29
2.6	Effects of Different Definitions of Deep Fading	31
2.7	Summary	35
3	Impact of Scintillation on GPS Aviation Availability	36
3.1	Overview	36
3.2	Ionospheric Scintillation and GPS Aviation	37
3.2.1	Simultaneous Loss of Satellites and Reacquisition Time	37
3.2.2	Frequent Signal Fading and Shortened Carrier Smoothing Time	40
3.3	Operational Availability During Strong Scintillation	43
3.3.1	Availability Analysis Procedure	44
3.3.2	Availability of Vertical Navigation (LPV-200)	47
3.3.3	Availability of Horizontal Navigation (RNP-0.1)	54
3.4	Summary	56
4	Satellite-to-Satellite Correlation of GPS Signal Fades Under Strong Scintillation	58
4.1	Overview	58
4.2	Deep GPS Signal Fades and Correlation Coefficients	59
4.3	Satellite-to-Satellite Correlation	63

4.3.1	Satellite-to-Satellite Correlation During a Past Solar Maximum Period	63
4.3.2	Correlation of Closely-Spaced Satellites During a Strong Scin- tillation Period of Solar Minimum	67
4.4	A Method to Generate Correlated Fading Processes	70
4.5	Availability of LPV-200 Under Severe Scintillation	76
4.6	Summary	80
5	Dual Frequency GPS Aviation Under Scintillation	82
5.1	Overview	82
5.2	Availability Analysis of Dual Frequency Aviation	83
5.2.1	Availability Analysis Procedure	84
5.2.2	Availability Results Depending on Ionospheric Delay Estimation	86
5.3	Sensitivity Analysis of the Availability Results	94
5.3.1	Sensitivity to the Fading Rate of the L5 channel	94
5.3.2	Sensitivity to the Maximum Bounded Ionospheric Gradient . .	96
5.3.3	Impact of Satellite-to-Satellite Correlation of Deep Fades . . .	97
5.4	Summary	101
6	Suggestion for Future Dual Frequency Aviation Receiver Perform-	
	ance Standards	103
6.1	Overview	103
6.2	Benefit of Fast Reacquisition Capability	104
6.3	Reacquisition Performance of a Certified Receiver	105
6.4	New Performance Requirement	108
6.5	Summary	110

7 Conclusion	111
7.1 Overview	111
7.2 Proposed Strategy to Provide High Availability	112
7.3 Effectiveness of the Proposed Strategy	113
7.4 Real World Action Regarding the Strategy	115
7.5 Direction of Future Work	116
A Acronyms	118
B Covariance Between Correlated Poisson Random Variables	121
C Doubly-Correlated Fading Process Model	123
Bibliography	129

List of Tables

4.1	Correlation coefficients of loss of lock between two satellite channels .	66
-----	---	----

List of Figures

1.1	Conceptual illustration of current GPS and WAAS-based aviation in the US	4
1.2	Example of deep signal fading due to strong ionospheric scintillation .	8
1.3	Potential hazard to aircraft navigation due to ionospheric scintillation	9
1.4	Global depth of scintillation fading during low and moderate solar activity	10
2.1	Satellites affected by scintillation	18
2.2	C/N_0 outputs of all eight satellite channels during strong scintillation of the past solar maximum	19
2.3	Example of deep signal fades according to the definition of this work .	21
2.4	Definition of fading duration	23
2.5	Examples of unreliable C/N_0 outputs from NordNav receiver	24
2.6	Fading durations obtained at all C/N_0 data points of deep fades . . .	25
2.7	Histograms of fading durations at 25 dB-Hz and 30 dB-Hz	26
2.8	Empirical fading duration model	27
2.9	Definition of time between deep fades	29
2.10	Histogram of time between deep fades during strong scintillation . . .	30
2.11	Comparison of different definitions of deep fading	32

2.12	Effect of shallower fading on observed statistics	33
3.1	Example of C/N_0 outputs of all satellites in view during strong scintillation of the past solar maximum	38
3.2	Number of simultaneously tracked satellites depending on various reacquisition times	39
3.3	Decreasing code noise by Hatch filtering under a nominal condition without scintillation	41
3.4	Frequent reset of Hatch filter and high code noise level under strong scintillation	42
3.5	Availability analysis procedure	45
3.6	Simulated vertical protection level without considering scintillation effects	47
3.7	C/N_0 and vertical protection level considering satellite outages only	48
3.8	Impact of shortened carrier smoothing times due to frequent fades	49
3.9	Availability benefit of a shorter reacquisition time	50
3.10	Availability benefit of a shorter reacquisition time	52
3.11	Availability contour for vertical navigation (LPV-200)	53
3.12	Availability contour for horizontal navigation (RNP-0.1)	54
3.13	Horizontal protection level during strong scintillation	55
4.1	Comparison of 50 Hz C/N_0 outputs of nominal and scintillation cases	60
4.2	Weakness of the conventional sample correlation coefficient	61
4.3	Correlation of deep fades between two satellite channels during a strong scintillation period of the previous solar maximum	64
4.4	Locations of loss of satellites during 5 hours	68

4.5	Empirical probability density function of time between deep fades . . .	70
4.6	Modeling a fading process as a Poisson process	72
4.7	Generation of two correlated Poisson processes from three independent Poisson processes	73
4.8	Procedure to simulate the availability of LPV-200 under severe scintil- lation scenarios	77
4.9	Availability of LPV-200 under severe scintillation scenarios with vari- ous satellite-to-satellite correlation coefficients of deep fades	78
5.1	Availability simulation procedure considering frequency-to-frequency correlation	85
5.2	Inflation of vertical protection level while ionospheric delay cannot be directly measured	87
5.3	Availability contour of LPV-200 under the most conservative approach to bound the ionospheric delay error	90
5.4	Availability contour of LPV-200 under the most optimistic approach to bound the ionospheric delay error	91
5.5	Maximum temporal pseudorange error under the worst-case combina- tion of the geometry	93
5.6	Availability contour of LPV-200 under the maximum observed iono- spheric gradient and the worst-case geometries	94
5.7	Availability of LPV-200 with various L5 fading rates	95
5.8	Availability of LPV-200 with various inflation rates of the new VPL equation	96
5.9	Availability contour of LPV-200 with the consideration of both satellite- to-satellite correlation and frequency-to-frequency correlation	99

5.10 Comparison between the observed strong scintillation and the simulated severe scintillation	100
6.1 Observed reacquisition times of a certified WAAS receiver during the 36 day campaign in Brazil	106
C.1 Generation of four doubly-correlated Poisson processes from eight independent Poisson processes	124

Chapter 1

Introduction

1.1 Overview

Beyond familiar applications of the Global Positioning System (GPS), such as car and marine navigation, GPS [Parkinson and Gilbert, 1983; Misra and Enge, 2006; Kaplan and Hegarty, 2006] has been beneficial to aircraft navigation as well. This chapter introduces GPS applications to current civil aviation. The future Global Navigation Satellite Systems (GNSS) including GPS and Galileo (the European GNSS under development) envision a worldwide guidance of aircraft down to 200 ft above the runway. One of the main challenges to worldwide GPS-based aviation is deep signal fading due to ionospheric scintillation which is the topic of this research. After a brief review of previous work regarding the impact of ionospheric scintillation on GPS aviation, a summary of the contributions of this dissertation is provided.

1.2 GPS Applications for Aviation

Different from car and marine navigation, a GPS application for civil aviation is very challenging because aviation requires an extremely high level of safety. If one GPS satellite malfunctions, for example, it can cause hundreds or thousands of meters of error in its position output. If a pilot trusts this erroneous position output without timely warning in poor visibility and bad weather, a disaster such as an aircraft crash can occur. Therefore, there must be a way to guarantee that the current position output from a GPS receiver is reliable enough for aviation applications. Receiver Autonomous Integrity Monitoring (RAIM) is one of the ways to guarantee the “integrity” of position solutions [ION, 1998]. The basic idea of RAIM is to cross-check the position solutions calculated from subsets of the GPS satellites in view. If the position solutions from the subsets do not closely match each other, it is an indication that a range measurement from a certain satellite is unreliable. Hence, a receiver must raise a flag indicating that the current position output is unreliable in this situation. RAIM is able to guarantee aviation integrity in the en route phase of flight which requires a relatively low level of integrity [Lee, 1992].

The most stringent integrity requirement arises in the approach and landing phase of flight, but the current RAIM cannot satisfy this requirement. In order to satisfy the stringent integrity requirement for landing approach, integrity augmentation systems, such as the Wide Area Augmentation System (WAAS) [Enge *et al.*, 1996] and the Local Area Augmentation System (LAAS) [Enge, 1999] of the United States (US) Federal Aviation Administration (FAA) have been developed. This research focuses on the space-based augmentation system, WAAS, which is currently operational in the US. The most challenging phase of flight (i.e., the approach and landing phase) is mainly considered in this work, although other phases of flight are also supported

by GPS and WAAS.

1.2.1 Space-Based Augmentation for Landing Approach Guidance of Aircraft

For the last 50 years, the Instrument Landing System (ILS) [Kayton and Fried, 1997] has been widely used to guide aircraft landing in poor visibility conditions. ILS provides horizontal and vertical guidance by forming a radio wave “beam” and a pilot follows the beam towards a runway. Category I ILS can guide aircraft down to 200 ft above the runway, and Category III ILS enables automatic landing in zero visibility. Although ILS is a proven technology, it has several limitations. The installation and maintenance cost of ILS is high. ILS requires periodic calibration by flight inspection [Kim *et al.*, 2008] which can overwhelm the initial installation cost. Since ground facilities, such as a glide slope and a localizer, must be installed for each runway to make a beam for guidance, a big airport with multiple runways needs multiple ILS installations which causes even more cost. Further, advanced landing approaches such as a curved approach cannot be supported by ILS because ILS forms a straight beam.

Satellite-based navigation resolves many of these problems. WAAS reference stations monitor the health status and the signal quality of GPS satellites. They also monitor the signal delay due to the ionosphere using L1/L2 semi-codeless dual frequency receivers. (This signal delay cannot be directly measured by GPS avionics onboard because they are only single frequency receivers.) This information is broadcast by geostationary satellites (usually called WAAS satellites) above the conterminous United States (CONUS). A GPS/WAAS receiver uses this information from the WAAS satellites to ensure the integrity of its position solutions. In this way, GPS and

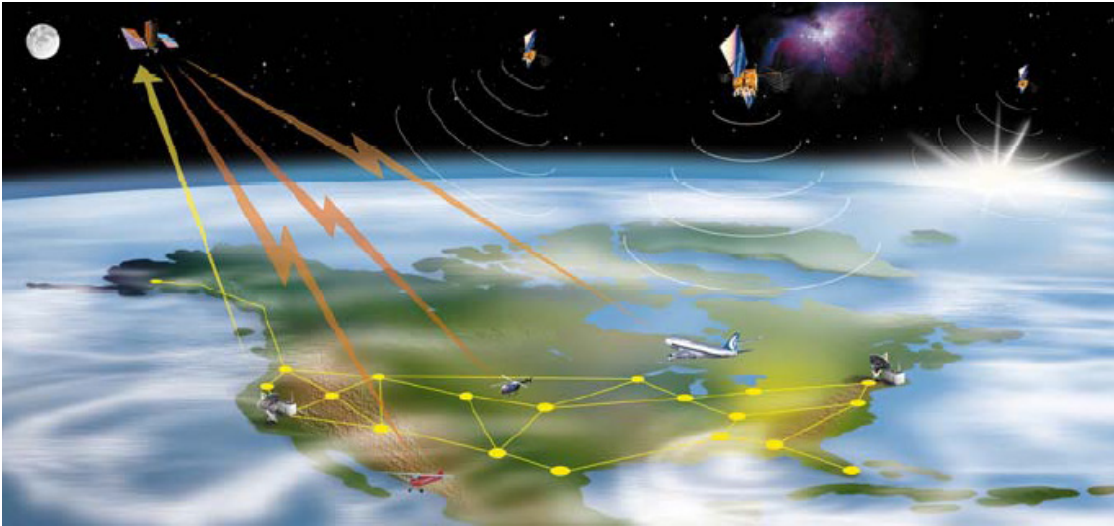


Figure 1.1: Conceptual illustration of current GPS and WAAS-based aviation in the US. WAAS geostationary satellites broadcast integrity information generated by WAAS reference stations to aircraft. GPS and WAAS can guide aircraft down to 200 ft above the runway. (Figure courtesy of FAA.)

WAAS can satisfy the extremely high integrity requirement of aircraft approach guidance and provide enough availability of the guidance service at the same time. (The system is conceptually illustrated in Figure 1.1.) About 40 WAAS reference stations and 2–3 WAAS geostationary satellites can cover North America without a glide slope and a localizer at each runway. This is a significant benefit over the current ILS which are not installed and maintained at small airports due to its high cost. The number of general aviation users is rapidly growing. (General aviation refers to all flights other than military and scheduled airline flights.) GPS and WAAS provide approach guidance to those general aviation planes equipped with cost-efficient GPS/WAAS avionics in poor visibility conditions at small airports. Hence, the accessibility of small airports in bad weather is significantly increased.

Currently, GPS with the integrity augmentation from WAAS can guide aircraft horizontally and vertically down to 200 ft above the runway, which is comparable to

the Category I ILS approach. This approach procedure is referred to as Localizer Performance with Vertical guidance (LPV)-200 [Cabler and DeCleene, 2002]. Due to the benefits of GPS and WAAS, the number of published LPV approaches is currently greater than the number of published ILS approaches in the US.

1.2.2 GNSS Evolutionary Architecture Study Toward Worldwide LPV Service

Given the success of LPV service in the US, worldwide expansion of LPV service is being actively pursued. Currently, a GPS aviation receiver onboard uses the GPS civilian signal at the L1 frequency only. Hence, the ionospheric delay of the GPS signal, which is the biggest error source for GPS aviation, cannot be directly measured by a receiver onboard. A GPS/WAAS aviation receiver in a plane relies on the broadcast information for ionospheric delay from the WAAS satellites. The WAAS reference stations use the semi-codeless technique [Woo, 2000] to estimate ionospheric delays and broadcast the estimated delays using geostationary satellites. The semi-codeless technique utilizes the civilian signal with known codes at the L1 frequency (1.575 GHz) and the military signal with encrypted codes, unknown to civilian applications, at the L2 frequency (1.227 GHz). This technique is applicable to a stationary receiver such as a WAAS reference station receiver, but it is not adequate for a non-stationary receiver such as an aviation receiver onboard. Also, the reference receivers are at controlled FAA facilities where Radio Frequency Interference (RFI) can be more readily treated.

Although the broadcast ionospheric delay information is currently used for LPV service in the US, the direct airborne measurement of ionospheric delay is much more desirable. The broadcast information contains ionospheric delay amounts at each grid

point only. Hence, a receiver interpolates the broadcast delays of nearby grid points for estimating a delay at a particular point of interest. A conservative estimate of error bounds on this interpolation is required to guarantee the aviation integrity, but it reduces the aviation availability. Future GPS will provide a new civilian code at the L5 frequency (1.176 GHz) [Hegarty and Chatre, 2008]. (As of April 2010, one GPS satellite is broadcasting the L5 test signal [Gao *et al.*, 2009b; Gunawardena *et al.*, 2009].) Since the L1 and L5 frequencies are within Aeronautical Radionavigation Service (ARNS) bands, a future GPS aviation receiver can use civilian codes at both frequencies for direct ionospheric delay measurements.

Given the scheduled upgrade of GPS with a new civilian signal at the L5 frequency and the new GNSS under development (e.g., Galileo of Europe, Compass of China [Gao *et al.*, 2009a]), LPV service will be expanded worldwide. Three potential architectures to provide worldwide aviation integrity have been proposed through the GNSS Evolutionary Architecture Study (GEAS). The proposed architectures are explained in [Walter *et al.*, 2008]. These are: the GNSS Integrity Channel (GIC), Relative Receiver Autonomous Integrity Monitoring (RRAIM), and Absolute/Advanced Receiver Autonomous Integrity Monitoring (ARAIM). Among these architectures, the GIC architecture is assumed in the availability studies of this work. In the GIC architecture, integrity information is provided by WAAS-like channels.

1.3 Ionospheric Scintillation as a Challenge for World-wide GPS Aviation

1.3.1 Strong Ionospheric Scintillation in the Equatorial Latitudes

The ionosphere has a practical importance to GPS applications because it influences transionospheric radio wave propagation. Although the ionospheric delay is the biggest error source for GPS navigation, it can be directly measured by future dual frequency GPS avionics, and higher-order ionosphere errors are not problematic for LPV-200 [Datta-Barua *et al.*, 2008]. However, deep and frequent GPS signal fades due to electron density irregularities in the ionosphere raise a concern about the operational availability of LPV-200. Transionospheric radio waves interfere constructively and destructively when they pass through electron density irregularities. This phenomenon can be understood as multipath inside the ionosphere. As a result, a receiver experiences amplitude fading and phase jitter of the received signal. This phenomenon is referred to as ionospheric scintillation [Crane, 1977; Gwal *et al.*, 2004]. The signal fades are rapid with decorrelation times of several seconds or less depending on scintillation intensities [Basu *et al.*, 1985].

Figure 1.2 compares the carrier to noise density ratio (C/N_0) of a received GPS signal during a nominal period without scintillation and the C/N_0 during a strong scintillation period. The C/N_0 varies slowly without scintillation as in Figure 1.2 (top). However, if strong scintillation occurs, C/N_0 fluctuates rapidly and sometimes drops more than 25 dB as in Figure 1.2 (bottom). These deep signal fades were observed in an equatorial area during the past solar maximum (2001). Solar activity

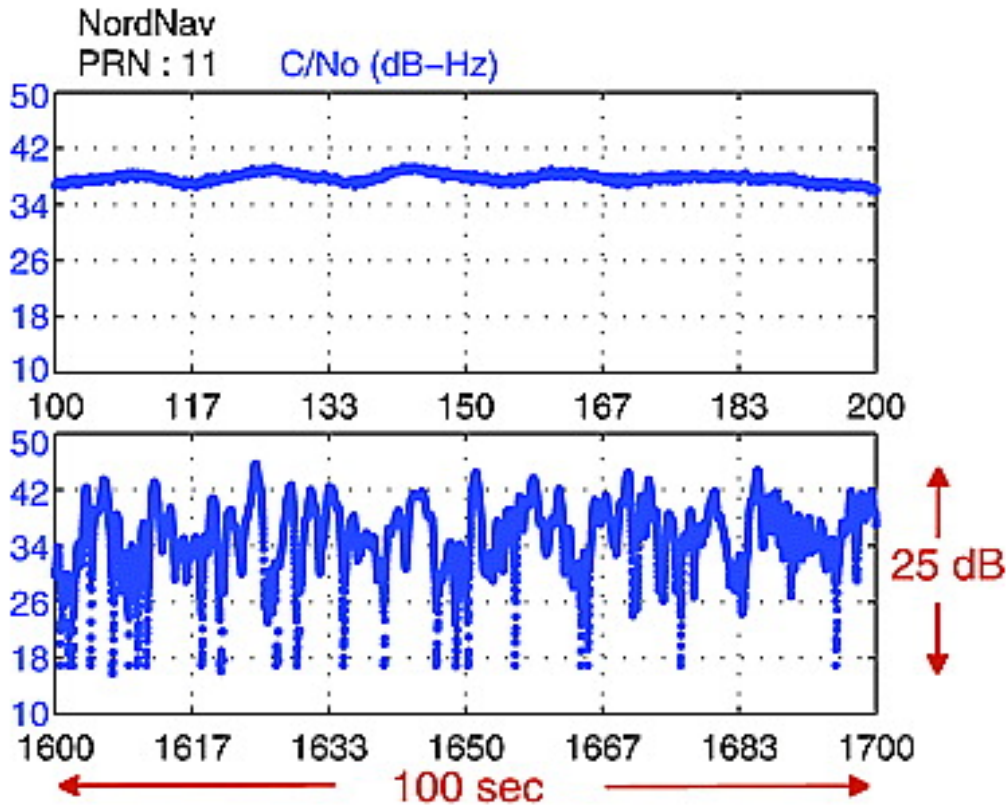


Figure 1.2: Example of deep signal fading due to strong ionospheric scintillation. Top plot shows C/N_0 during a nominal period and the bottom plot shows C/N_0 during a strong scintillation period. Data collected on 18 March 2001 at Ascension Island.

follows about an 11-year average solar cycle, and strong scintillation with deep signal fades is frequently observed for several hours after local sunset during solar maxima (high solar activity).

These deep signal fades may break a receiver's carrier tracking lock. Since GPS avionics rely on both code and carrier measurements, the loss of carrier tracking lock of a certain satellite channel can be effectively considered as the loss of the corresponding satellite until the carrier tracking lock is reestablished. GPS aviation requires a minimum of four simultaneously tracked satellites with good geometry

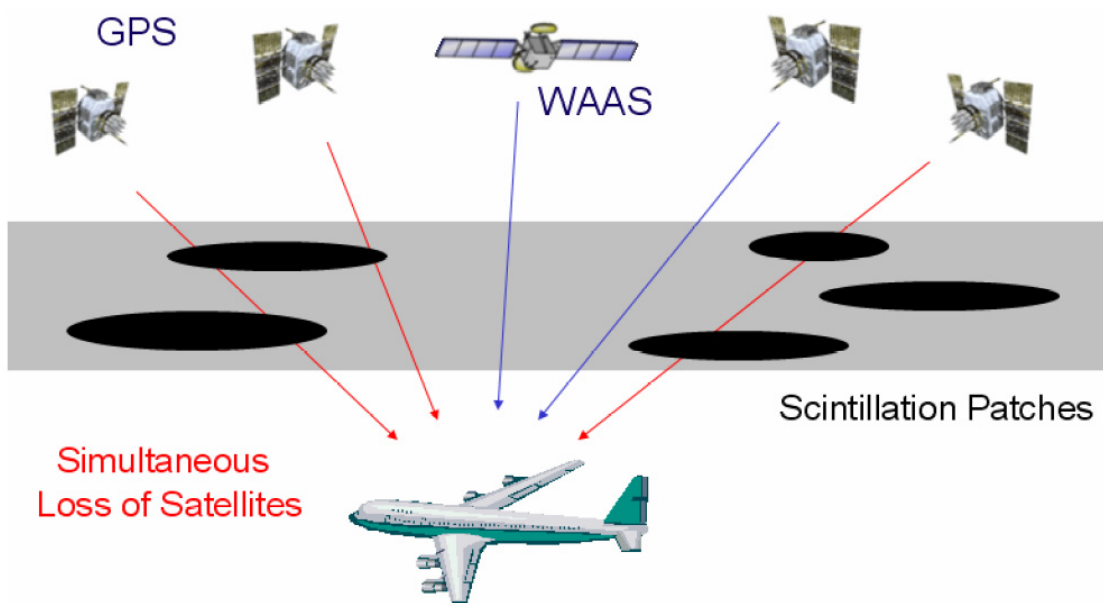


Figure 1.3: Potential hazard to aircraft navigation due to ionospheric scintillation. Simultaneous loss of satellites under scintillation reduces the availability of GPS aviation.

[Misra and Enge, 2006; Kaplan and Hegarty, 2006]. If electron density irregularities cover a large portion of the sky as in Figure 1.3, there is a chance that a receiver may lose more than one satellite simultaneously. Simultaneous loss of a significant number of satellites discontinues GPS navigation. Therefore, strong ionospheric scintillation could be hazardous in terms of continuity and availability for GPS aviation. Note that ionospheric scintillation is not usually observed in the mid-latitude region including the US, but it is frequently observed in the equatorial region including Brazil and India during solar maxima after local sunset [Basu, 1981; Aarons, 1982] and is potentially limiting to GPS aviation in this region. The global morphology of scintillation activity is shown in Figure 1.4.

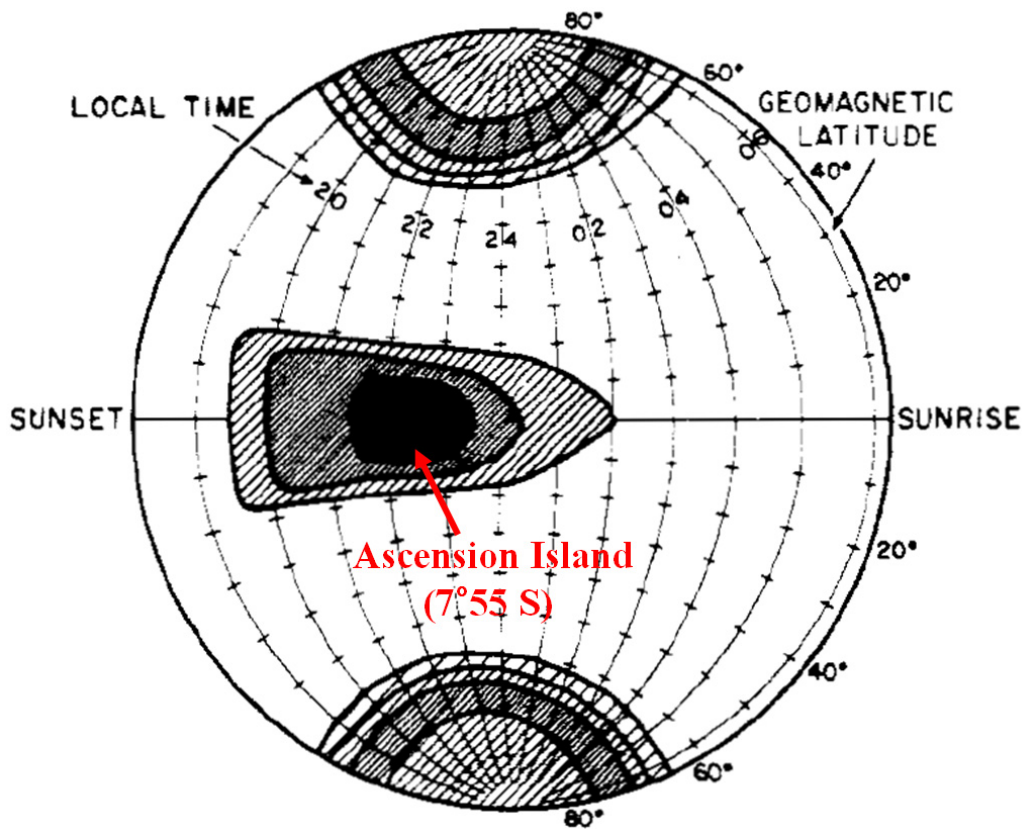


Figure 1.4: Global depth of scintillation fading during low and moderate solar activity. (Figure courtesy of Aarons [1982].)

1.3.2 Aviation Receiver Performance Standards Regarding Scintillation

A GPS/WAAS aviation receiver must satisfy all the requirements in the WAAS Minimum Operational Performance Standards (MOPS) [RTCA, 2006] in order to be certified. In fact, the current WAAS MOPS addresses scintillation in the following statement, “There is insufficient information to characterize scintillation and define appropriate requirements and tests for inclusion in this MOPS. . . . New requirements may be defined when ionospheric effects can be adequately characterized [RTCA,

2006].”

Since the current MOPS does not have specific requirements and tests for an aviation receiver under scintillation, certified aviation receivers currently in use in the US, where scintillation is not a concern, may not achieve the same levels of performance in equatorial areas during solar maxima. Therefore, it is necessary to characterize scintillation and recommend appropriate performance requirements under scintillation for the next version of MOPS in order to expand LPV service to equatorial areas. This is the motivation for this research.

1.4 Previous Work

Although the physics of the ionospheric scintillation has been studied for several decades (e.g., [Singleton *et al.*, 1961]) and scintillation effects on generic GPS applications are summarized in [Kintner *et al.*, 2007; Beniguel and Adam, 2007], the impact of scintillation on GPS aviation is not yet well understood. Hence, the current WAAS MOPS does not specify performance requirements regarding scintillation, as mentioned in the previous section.

As an effort to characterize GPS signal fading under scintillation, El-Arini *et al.* [2003] analyzed the depth and the duration of fading based on a strong scintillation data set collected in Naha, Japan during the past solar maximum (2002). It is essential to use high rate GPS data (20 Hz or preferably 50 Hz) to characterize signal environment in the time-domain, but a very limited number of high rate GPS data sets under strong scintillation is available from the past solar maximum. As already mentioned, solar maxima follow an 11-year average solar cycle. Hence, high rate scintillation data of solar maxima cannot be collected until the next solar maximum

occurs (around 2013). The lack of high rate scintillation data is one of the main difficulties in understanding scintillation impact on GPS aviation.

The availability of LPV-200 service under strong scintillation in equatorial areas is one of the main interests of this work. The availability study of GPS and Satellite-Based Augmentation System (SBAS)-based aviation under scintillation has been performed by Conker *et al.* [2003]. This previous research used the Wide-band scintillation model (WBMOD) [Secan *et al.*, 1997] for simulating scintillation parameters. WBMOD provides the level of intensity and phase scintillation based on a power law phase-screen propagation model and globally collected data. This approach is useful to illustrate the global trend of GPS/SBAS availability under scintillation. As Conker *et al.* [2003] mentioned, a realistic estimate of the probability of simultaneous loss of multiple satellites is needed for evaluating scintillation impact on GPS aviation. However, WBMOD does not provide this probability and consequently this previous study showed very conservative results.

In addition to the probability of simultaneous loss of multiple satellites, the probability of simultaneous loss of multiple frequencies is also important for predicting the operational availability of future dual frequency GPS aviation. If future dual frequency GPS avionics track both L1 and L5 frequencies of the same satellite, they may be able to rely on one frequency when it briefly loses the other frequency under scintillation. A recent study reported correlation coefficients of about 0.7 among signal intensities of L1 and L2 channels based on early GPS data collected at Thule, Greenland during 1989-1991 [El-Arini *et al.*, 2009]. Although the correlation coefficient between two time series of signal intensity used in the study shows the similarity of the trends of the two time series, it does not describe how often two frequencies are lost simultaneously. Hence, it is not a good metric for assessing scintillation impact

on GPS aviation.

Other research efforts have focused on a scintillation-robust receiver design. Knight [2000] quantified the effect of scintillation on the performance of the code and carrier tracking loops of a GPS receiver using a stochastic model of scintillation and various tracking loop models. There are several possible strategies for reducing the probability of loss of lock during signal fading. For example, Doppler aiding [Chiou *et al.*, 2008] and Vector Phase Lock Loops (VPLL) [Henkel *et al.*, 2008] are being investigated to determine their effectiveness. A caveat of a receiver with a novel design is that it is much harder to be certified as an aviation receiver than a receiver with a conventional design although the novel design could be preferred in non-aviation applications.

1.5 Contributions

As mentioned in Section 1.3.2, the strong motivation for this research is the fact that current aviation receiver performance standards do not have specific performance requirements under scintillation. Hence, the current standards do not guarantee the performance of aviation receivers under strong scintillation of equatorial areas during solar maxima. With this motivation, this work contributes to suggesting a new performance requirement for future standards, which can mitigate the impact of scintillation on GPS aviation. Specifically, this research:

1. Characterized signal environment under ionospheric scintillation from the perspective of GPS aviation [Seo *et al.*, 2009a].
2. Analyzed scintillation impact on GPS aviation availability [Seo *et al.*, 2009b].

3. Suggested and validated a new requirement for future dual frequency aviation receiver performance standards [Seo *et al.*, 2009c; 2009d].

First, Chapter 2 studies the characteristics of signal fades under strong scintillation based on real scintillation data from the past solar maximum. In particular, the impact of very frequent deep fades on GPS aviation is discussed. Other characteristics such as fading depth and fading duration are comparable to the previous study with other data sets [El-Arini *et al.*, 2003].

Under the very frequent deep fades observed during the past solar maximum, the operational availabilities of vertical and horizontal navigation are assessed in Chapter 3. For a more realistic analysis, a carrier smoothing filter model considering shortened carrier smoothing time under very frequent fades is developed. The proposed method to analyze operational availability of GPS aviation is applicable to any real scintillation period if GPS scintillation data are available.

As a previous study mentioned [Conker *et al.*, 2003], the probability of simultaneous loss of multiple satellites under scintillation is important to understand for GPS aviation, but it has not been previously studied. Chapter 4 proposes a new correlation metric to measure the probability of simultaneous loss of multiple channels. Based on this correlation metric, satellite-to-satellite correlation of loss of lock is studied based on real scintillation data sets. Further, a method to generate correlated fading channels for the availability study is proposed. Using this method, the impact of severe scintillation with arbitrary fading rates and correlation levels can be parametrically studied. This is useful because high rate GPS scintillation data from the past solar maximum are very limited.

Future GPS will provide a civilian code on the L5 frequency (1.176 GHz) in addition to the current L1 frequency (1.575 GHz). Hence, future dual frequency GPS

avionics can provide better availability depending on the correlation level between frequencies. Although L5 strong scintillation data are not yet available, the availability of LPV-200 under severe scintillation scenarios is parametrically studied in Chapter 5 using the method proposed in Chapter 4.

Based on the study in Chapters 2–5, a simple receiver strategy to provide high aviation availability under scintillation is suggested in Chapter 6. The strategy is to coast a receiver’s tracking loops for 1 s after a brief outage caused by scintillation. With this strategy in place, it will be possible to achieve a high level of availability (more than 99% availability) even under severe scintillation scenarios which are much worse than the real observations from the past solar maximum. Without this strategy, a certified aviation receiver may provide less than 50% availability under severe scintillation. Therefore, this research suggests an additional performance requirement mandating this strategy for future dual frequency aviation receiver performance standards. This new requirement was presented at the standards committee working group (RTCA Special Committee-159, Working Group-2) meeting on 24 June 2009 [Seo *et al.*, 2009d].

Chapter 2

Characteristics of GPS Signal Fading Due to Ionospheric Scintillation

2.1 Overview

Before investigating ionospheric scintillation effects on GPS aviation, it is necessary to understand the GPS signal environment under scintillation. This chapter analyzes two important characteristics of signal fading (fading duration and time between deep fades) based on a strong scintillation data set from the past solar maximum. The solar maximum data analyzed in this chapter demonstrates very frequent deep signal fades of almost all satellites in view (Section 2.2.1). This could significantly reduce the number of simultaneously tracked satellites and consequently decrease aviation availability. Forty-five minutes of strong scintillation, which was the worst scintillation period of a nine day campaign at Ascension Island in 2001, are analyzed

in this chapter. Based on the Ascension Island data set, a fading duration model is presented in Section 2.4. The time between deep fades observed in this data set shows very frequent deep fades which can significantly impact the benefit of carrier smoothing filters in aviation receivers (Section 2.5).

2.2 Scintillation Data Set

Two scintillation data sets are used for this research. One data set contains very strong scintillation from the previous solar maximum. This data set is valuable because raw Intermediate Frequency (IF) GPS scintillation data collected during solar maxima are very limited. The other data set contains strong scintillation during a solar minimum period. Although this data was collected during a solar minimum, it is valuable for aviation research because a certified aviation receiver was used for the data collection campaign.

2.2.1 Ascension Island Data

The Ascension Island data were collected during the previous solar maximum period at Ascension Island in the South Atlantic Ocean. Ascension Island is located near the crest of equatorial anomaly where strong scintillation is highly expected (see Figure 1.4, p. 10). The campaign was performed from 13 March 2001 to 26 March 2001 and reliable data was obtained for nine days. Theodore Beach of the US Air Force Research Laboratory (AFRL) provided S_4 plots and raw IF data for this research [Ganguly *et al.*, 2004]. The most severe scintillation period was selected based on the S_4 index. (The S_4 index is a widely-used amplitude scintillation index, which is a normalized standard deviation of detrended signal intensity [Fremouw *et al.*, 1980;

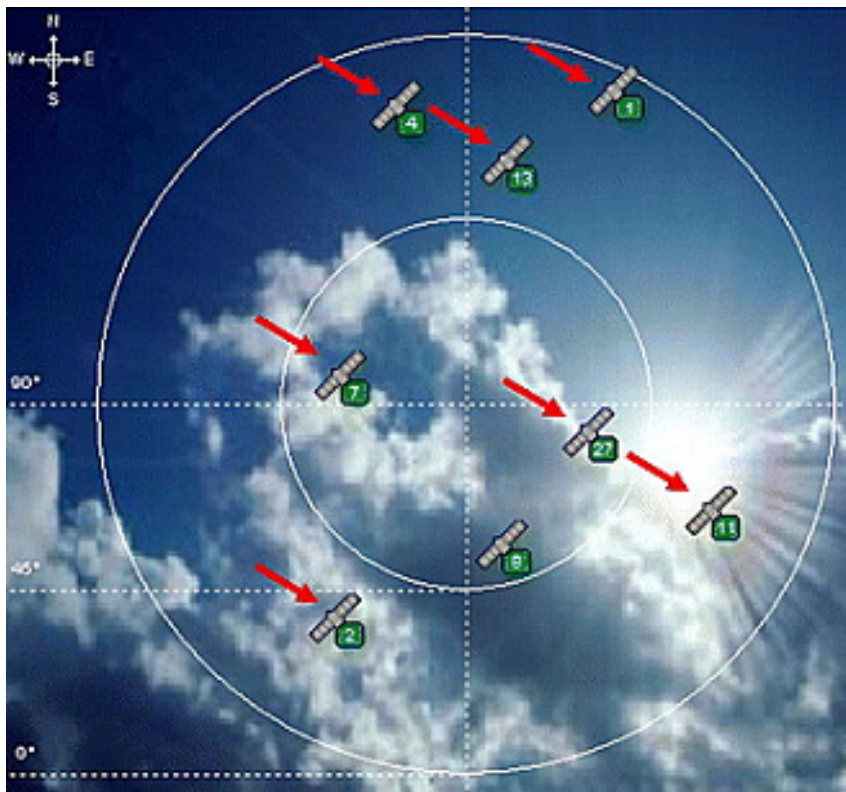


Figure 2.1: Satellites affected by scintillation. Seven out of eight satellite channels were affected during the 45 min of strong scintillation, which was the worst case from the 9 day campaign at Ascension Island during the past solar maximum (2001).

Fremouw and Ishimaru, 1992].) The selected period was from 8:45 P.M. to 9:30 P.M. on 18 March 2001 (UTC, also local time). The analyses in this work are based on this 45 minute worst-case data set. (Remember that strong scintillation usually persists for several hours after local sunset in the equatorial area.)

Raw IF data was collected using a NAVSYS DSR-100 receiver [May *et al.*, 1999] with a Rubidium frequency standard. The raw data was processed using a NordNav commercial software receiver [Normark and Stahlberg, 2005]. The 50 Hz C/N_0 outputs from the NordNav receiver are used for this research. A benefit of raw IF data

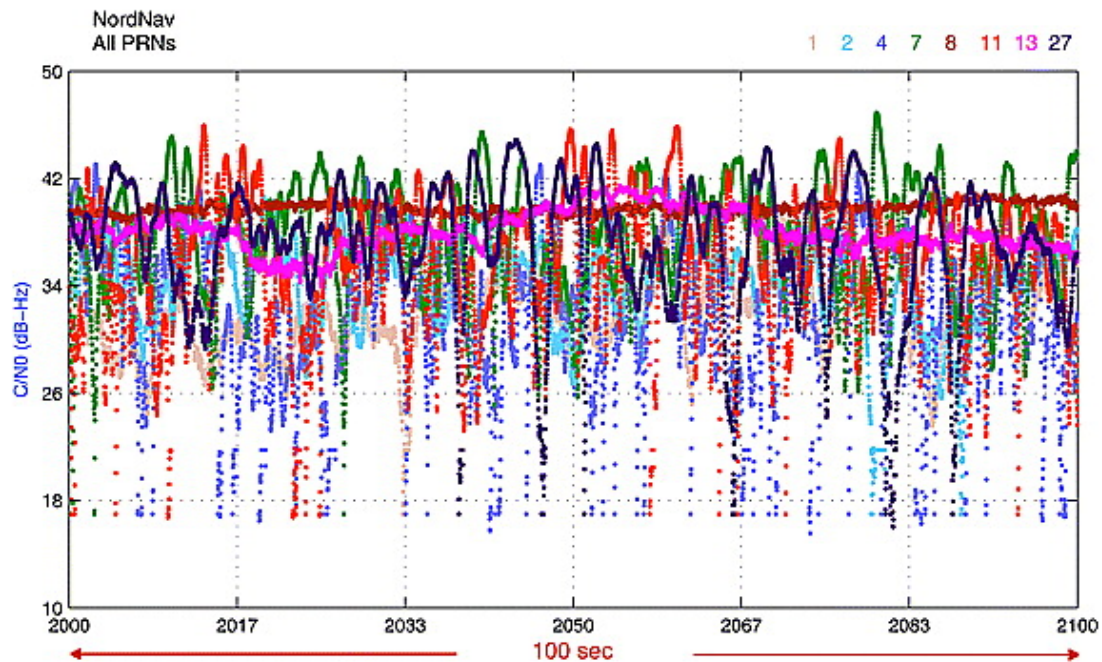


Figure 2.2: C/N_0 outputs of all eight satellite channels during strong scintillation of the past solar maximum (100 s example from the 45 min worst-case data). Different colors represent different satellite channels. The receiver experienced very frequent deep signal fades within 100 s which is the carrier smoothing time constant of aviation receivers.

and postprocessing using a software receiver is that tracking loop algorithms and settings can be adjusted to maximize tracking capability for a specific data set. Raw IF data are ideal to investigate characteristics of weak signals for short timescales. The NordNav processing was set up to maximize its ability to track each signal into and out of each fade. Commercial and aviation receivers with more limited resources running in real time may not be able to track as deep into each signal fade or reacquire the signal after a fade as quickly. Despite the benefit, the size of raw IF data is very large and data storage is a problem for a long-term data collection campaign.

As shown in Figure 2.1, seven (with red arrows) out of eight satellites were affected by strong scintillation in this data set, which is a very stressing case. Figure 2.2

shows an example of C/N_0 outputs of all eight satellite channels from a 100 s period of the severe scintillation data. Frequent deep signal fades of almost all channels are observed in Figure 2.2. As will be discussed in Section 2.3 (p. 21), this data set has lower than typical C/N_0 values.

2.2.2 Brazil Data

It is informative to observe performance of a currently-used certified aviation receiver during scintillation. Unfortunately, there was no certified GPS/WAAS aviation receiver available during the past solar maximum, so solar maximum scintillation data have not been collected by a certified receiver. As an alternative, a data collection campaign using a certified GPS/WAAS receiver was performed during a solar minimum period with the help of Eurico de Paula at the Instituto Nacional de Pesquisas Espaciais (INPE), Brazil [de Paula *et al.*, 2007]. Although it was a solar minimum period, strong scintillations with S_4 index of about 1.0 were sometimes observed during the 36 day campaign.

The Brazil data were collected at Sao Jose dos Campos, Brazil from December 2005 to January 2006 (36 days). Four different GPS receivers were deployed for the campaign. These included a certified WAAS receiver, a Cornell Scintillation Monitor receiver [Beach and Kintner, 2001], an Ashtech dual frequency receiver, and a NovAtel receiver. The primary interest of this research is the performance of the certified WAAS receiver. Since the certified WAAS receiver used for this study was the only certified WAAS receiver for aircraft navigation with vertical guidance, its performance evaluation during scintillation is essential to assess scintillation impact on GPS aviation. The WAAS receiver output position solutions and lock statuses of satellite tracking channels with a 1 Hz rate. During the campaign, signal fades

between two closely-spaced satellites were observed. This data is used to study the correlation of signal fades between closely-spaced satellites (Section 4.3.2, p. 67). Observed performance of the certified WAAS receiver will be discussed in detail in Section 6.3. The observed threshold of the certified WAAS receiver during the Brazil campaign is used to define “deep signal fading” in Section 2.3. The remaining analyses in this chapter (Sections 2.4 – 2.6) are all based on the solar maximum data from Ascension Island.

2.3 Definition of Deep Signal Fading

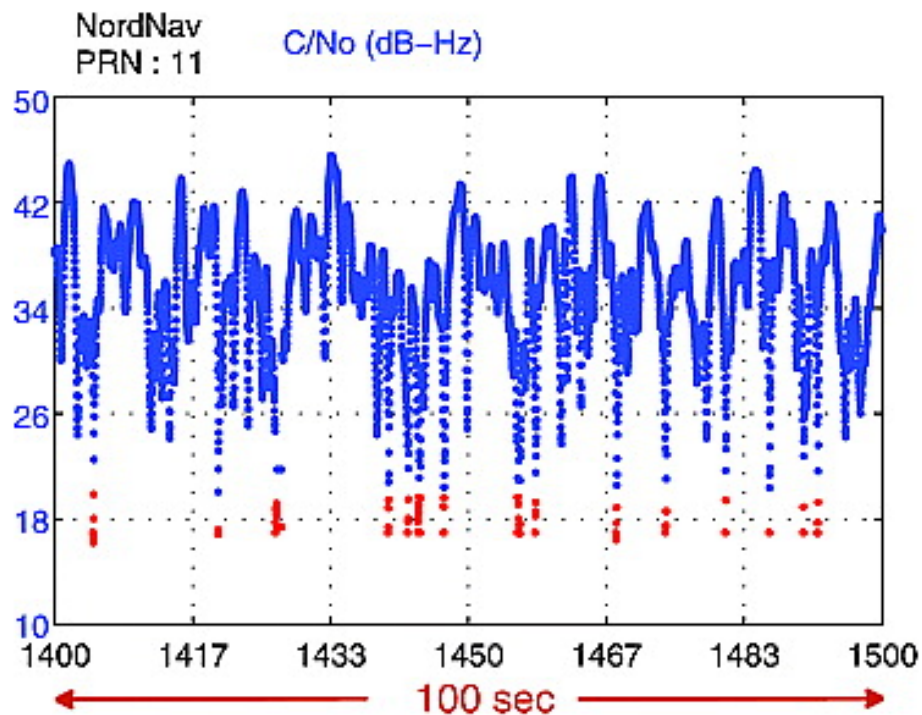


Figure 2.3: Example of deep signal fades according to the definition of this work. Samples below the 20 dB-Hz threshold are marked in red. Data are from the Ascension Island campaign.

Before investigating the characteristics of deep GPS signal fading under scintillation, it is necessary to give a proper definition of “deep fading.” If a signal fade is deep enough to break the receiver’s carrier tracking loop, the fade can be detrimental to GPS navigation. Hence, at least from GPS navigation’s point of view, it is logical to define deep fading in the context of a receiver’s carrier tracking loop performance.

A “deep fading” in this research is defined as a signal fading with a minimum C/N_0 of 20 dB-Hz or less in this particular data set (Ascension Island data). Based on the observations during the Brazil campaign (Section 2.2.2, p. 20), the certified WAAS receiver tracked signal down to 28-30 dB-Hz. Due to the early IF capture technology of DSR-100 incorporating one-bit sampling, narrow bandwidth, and aliasing caused by a low sampling frequency, the C/N_0 level of the Ascension Island data is 8-10 dB lower than the C/N_0 level from a current IF recorder such as the NordNav IF recorder. Hence, the 20 dB-Hz threshold in the Ascension Island data is comparable to 28-30 dB-Hz threshold of the certified aviation receiver in the Brazil campaign. Among various C/N_0 fluctuations, only deep fades are selected and samples below the threshold are marked in red in Figure 2.3.

Since different receivers have different tracking loop performances, other definitions of deep fading may make more sense for other types of receivers. Effects of different definitions of deep fading on the results of this chapter will be also discussed in Section 2.6 (p. 31) after analyzing two important characteristics of deep fading in Sections 2.4 and 2.5.

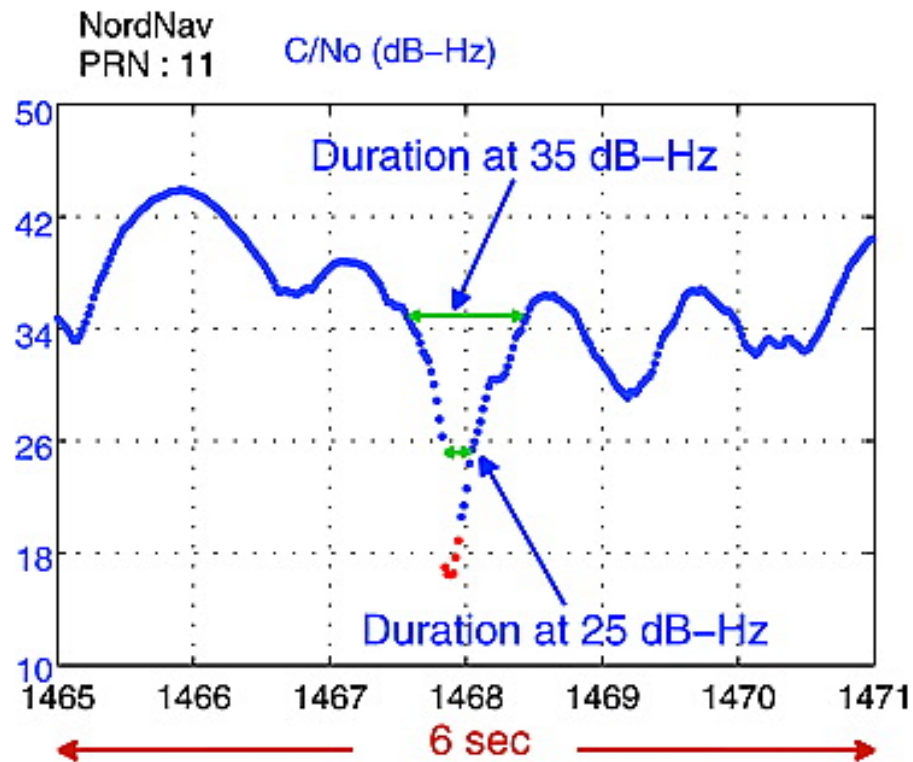


Figure 2.4: Definition of fading duration. Fading duration is obtained at each 50 Hz C/N_0 data point of every deep fade identified. The fading durations at lower absolute C/N_0 values are shorter.

2.4 Fading Duration Model

This section discusses properties of fading duration which is one of two important characteristics of deep signal fading that directly affect GPS navigation and aviation receiver design. Depending on the duration of deep fading, a possible strategy of a receiver to reduce the impact of scintillation would vary. If a signal outage is brief, “coasting” of tracking loops of a receiver can be a very useful strategy. Coasting is defined here to be a period of time over which the receiver can keep its tracking loops close enough to the correct value that the receiver can immediately reestablish tracking the signal when the power level is restored above the tracking threshold

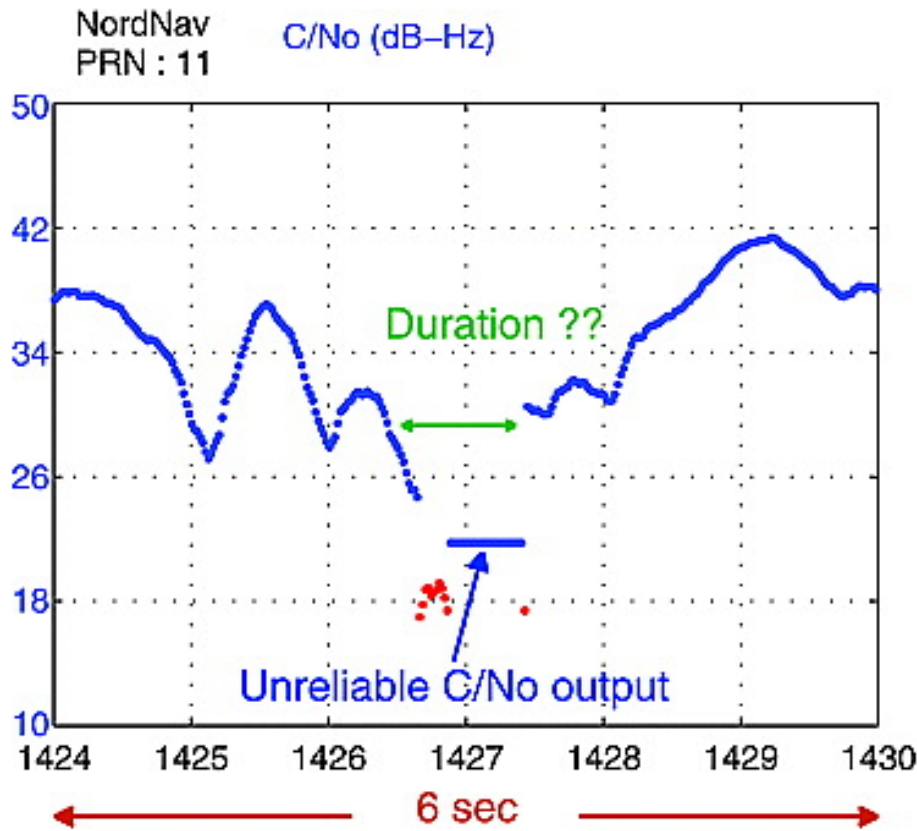


Figure 2.5: Examples of unreliable C/N_0 outputs from the NordNav receiver. These unreliable durations are not included in the statistics of this study.

of the receiver. The accuracy of the expected tracking information degrades as the coasting time increases. If the fading duration is long, a receiver may still be able to coast with the help of a high-grade Inertial Measurement Unit (IMU). However, this solution may be prohibitively expensive for most users.

The fading duration in this paper is defined as time to recover the previous C/N_0 value when deep signal fading occurs. According to this definition, fading duration is not a single number for a single fade but is obtained at each 50 Hz C/N_0 data point. Figure 2.4 shows fading durations at 25 dB-Hz and 35 dB-Hz as examples. The fading duration at 35 dB-Hz is about 1 s and the fading duration at 25 dB-Hz is about 0.2

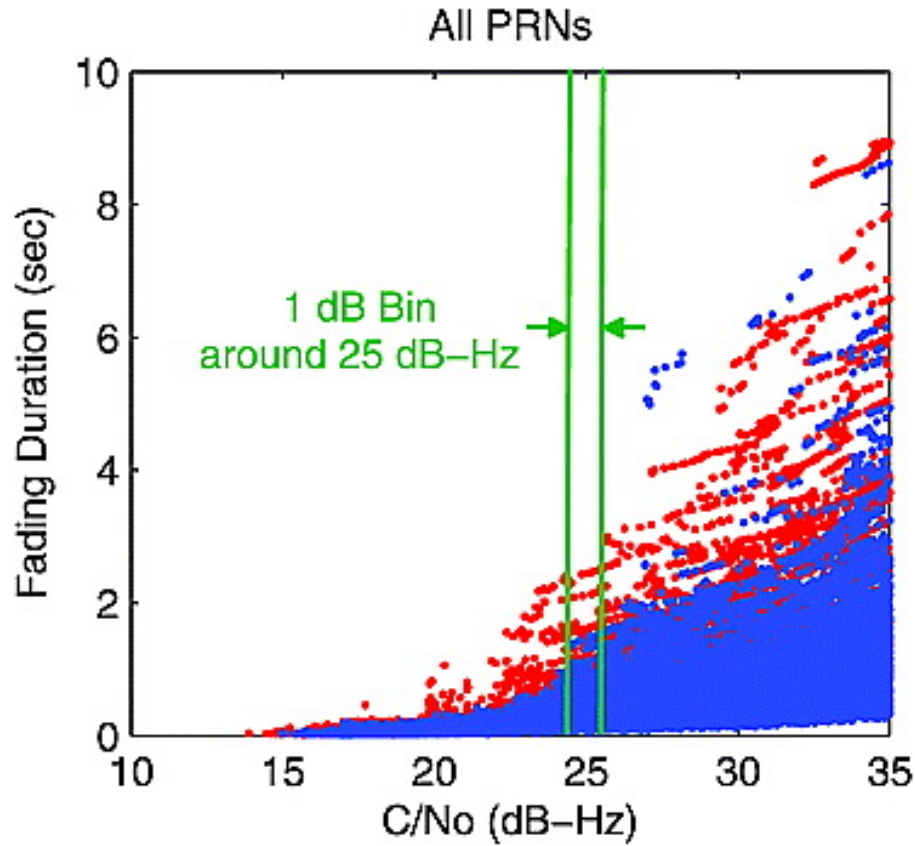


Figure 2.6: Fading durations obtained at all C/N_0 data points of deep fades. Only reliable data points (blue points) are considered for statistics.

s in this example. Note that these C/N_0 values are absolute C/N_0 values and not a relative depth of fade. This approach was chosen because a receiver's tracking loop performance depends on the absolute C/N_0 level.

Ideally, the fading duration could be obtained at every 50 Hz data point of every deep fade. Unfortunately, the actual response of the NordNav software receiver is not always ideal. For example, the NordNav receiver sometimes outputs unreliable C/N_0 values as seen in Figure 2.5. Consecutive constant C/N_0 outputs indicate the NordNav receiver does not process C/N_0 correctly. The fading duration is not well

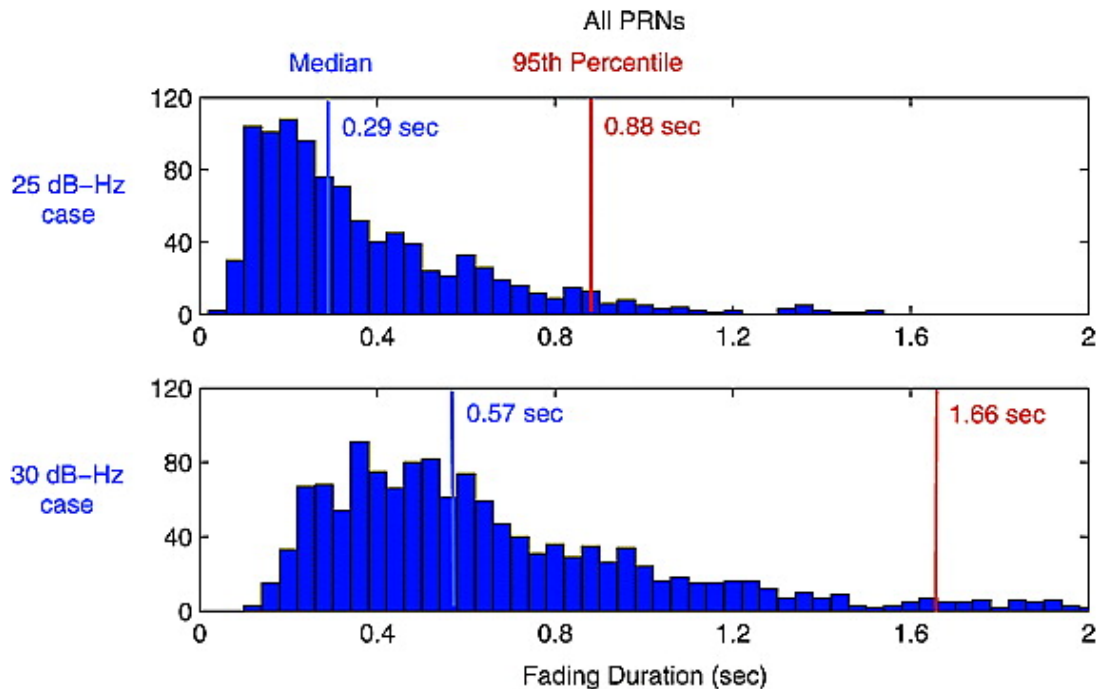


Figure 2.7: Histograms of fading durations at 25 dB-Hz and 30 dB-Hz. Medians and 95th percentiles of fading durations are obtained from the histograms.

defined in this case. Since these unreliable data points do not describe the physics of the ionosphere, they have to be separated from the reliable C/N_0 outputs to obtain meaningful statistics of fading duration for this data set.

Fading durations at all C/N_0 outputs for all satellites during the worst 45 min scintillation are plotted in Figure 2.6. The blue data points in Figure 2.6 represent fading durations at reliable C/N_0 outputs and the red points represent fading durations at unreliable C/N_0 outputs. The number of reliable data points is 18,502 which is 78% of the total number of data points.

Now the statistics of fading duration at each C/N_0 value for this data set can be obtained. The top histogram of Figure 2.7 is generated using only reliable data points within 1 dB around a C/N_0 of 25 dB-Hz from data in Figure 2.6. Figure

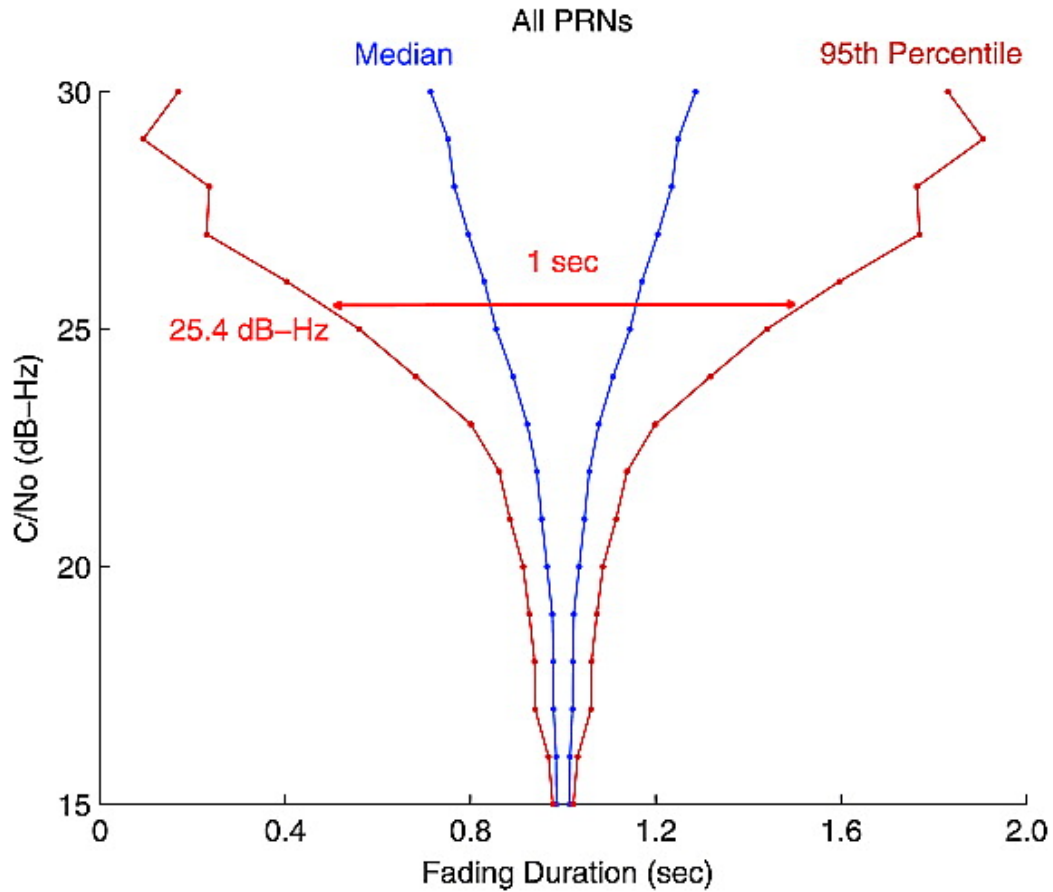


Figure 2.8: Empirical fading duration model. This model shows a median (blue) and a 95th percentile (red) of fading duration at each C/N_0 value. The model imitates the shape of fading time series. Hence, the median curves (blue) resemble a sharper fading and the 95th percentile curves (red) resemble a wider fading. However, the actual shape of fading in general is not symmetrical as shown in this figure.

2.7 (top) shows that the median of fading duration at 25 dB-Hz was 0.29 s and the 95th percentile was 0.88 s. When 1 dB around 30 dB-Hz is considered, the bottom histogram of Figure 2.7 is generated. In this case, the median and 95th percentile of fading duration were longer than the 25 dB-Hz case as expected from Figure 2.4 (p. 23).

Median and 95th percentile values were calculated at other C/N_0 values from 15

dB-Hz to 30 dB-Hz as well to develop an empirical fading duration model shown in Figure 2.8. Statistics of fading durations are obtained at each integer value of C/N_0 and linearly interpolated. A horizontal distance between two median curves (blue curves) or two 95th percentile curves (red curves) at a certain C/N_0 represents a median or 95th percentile of fading duration at the C/N_0 . Note that this model has information on fading duration only at each C/N_0 value but the model does not have information about the actual shape of fading. In Figure 2.8, it is shown as being symmetrical although this will not be true in general.

There are several ways to interpret this model. If a receiver loses carrier tracking lock at 25.4 dB-Hz, for example, the receiver can expect the signal to return to the same level of C/N_0 after 1 s in 95% of the deep fades. Another point of view is that if a receiver can coast for 1 s, if that receiver was also able to track down to at least 25.4 dB-Hz, it would have successfully handled 95% of the deep fades in this data set. There is a relationship between a receiver's sensitivity and required coasting time. If a receiver is more sensitive, in other words if a receiver can track signal at lower C/N_0 , the required coasting time would be smaller for the same level of functionality.

This fading duration model is generated from a limited number of data points from the previous solar maximum. It is observed that the 95th percentile of fading duration at 28 dB-Hz is slightly smaller than the 27 dB-Hz case, which is not intuitive. This result is due to the limited number of samples. In addition, this sampling derives from a single period of scintillation at a single location. It is believed to be loosely representative of severe scintillation and that much more often a user would encounter less severe effects. Nevertheless, it is acknowledged that longer and deeper fades are possible. Platform motion, in particular, can potentially lead to much longer fades under the scenario that platform motion is exactly lined up with motions of the

satellite and the electron density irregularity.

Another important point to consider is the uncertainty of the C/N_0 levels. As mentioned in Section 2.3 (p. 21), the C/N_0 level of the Ascension Island data is 8-10 dB lower than the C/N_0 level from a current receiver. If current receiver technology is taken into account, the vertical axis of the fading duration model could be adjusted from 15-30 dB-Hz to 25-40 dB-Hz. The fading duration model of Figure 2.8 is still meaningful as a conservative model when one does not consider any benefit from technology improvement since 2001.

2.5 Time Between Deep Fades

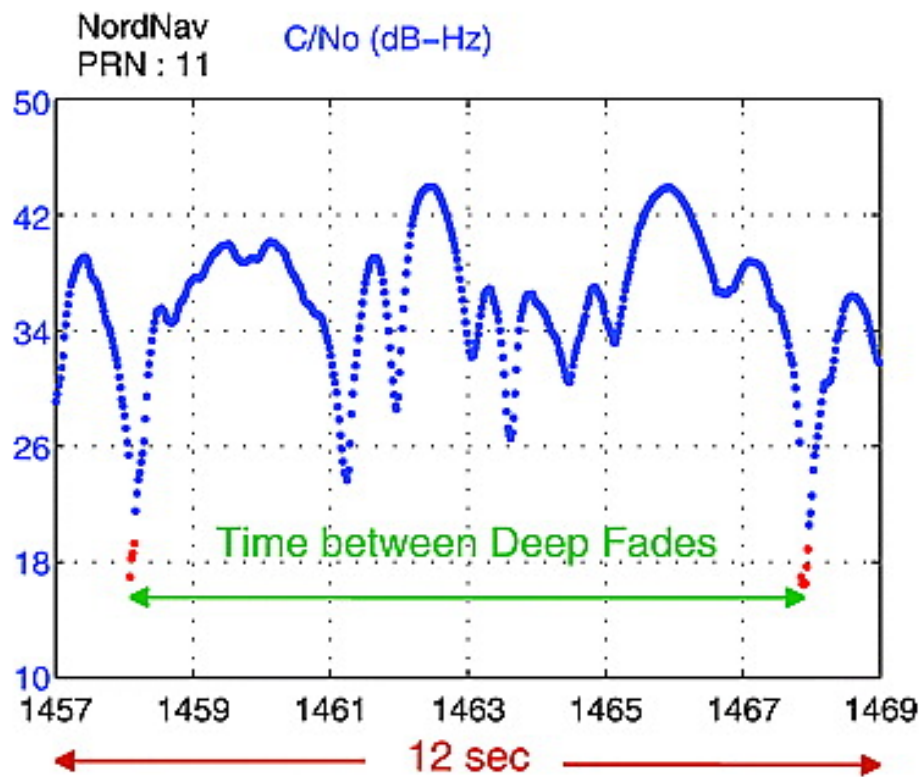


Figure 2.9: Definition of time between deep fades.

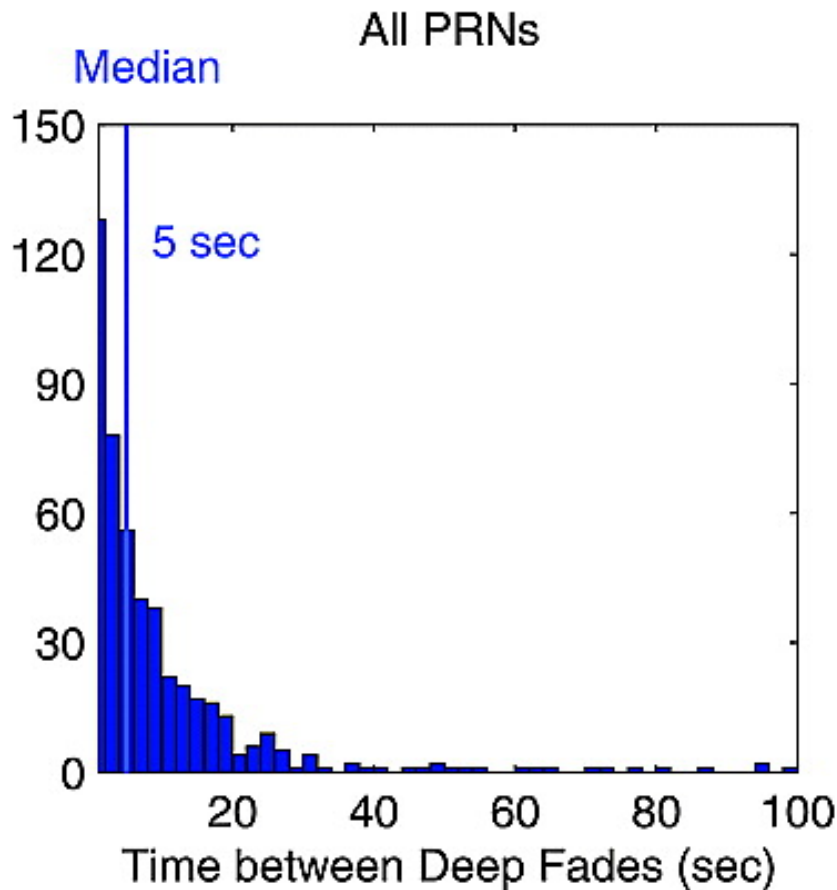


Figure 2.10: Histogram of time between deep fades during strong scintillation. The median time between deep fades during the 45 min of strong scintillation is only 5 s.

Another important characteristic of fading is the time between deep fades because it is related to the effective carrier smoothing time of the aviation receiver. An aviation receiver using GPS and WAAS smoothes its code measurements with less noisy carrier measurements using a Hatch filter [Hatch, 1982] with a 100 s time constant. In theory, the measurement noise can be reduced as much as a factor of 10 with this carrier smoothing technique. In practice, the reduction is found to be closer to half that value because the multipath error is correlated in time such that the smoothing effectiveness is reduced [Murphy *et al.*, 2005]. With a 100 s time constant, the Hatch

filter needs to continuously operate for a couple of hundred seconds without cycle slip to converge to its floor level. If a receiver loses carrier lock frequently within the 100 s smoothing period, the Hatch filter is frequently reset and cannot reduce code noise to the desired level.

The definition of time between deep fades of this paper is the time between minimum C/N_0 values of two consecutive deep fades as shown in Figure 2.9. The histogram in Figure 2.10 is obtained using time between deep fades of all satellite channels during the strong scintillation. This histogram shows that time between deep fades is very short and the median is only 5.3 s which is far shorter than the 100 s smoothing time constant of aviation receivers. Five seconds of smoothing reduces measurement noise less than 10%.

A receiver with the desired coasting capability may track enough satellites even during strong scintillation. However, the high measurement noise due to frequent resetting of the Hatch filter is also a problem. The Hatch filter must be reset whenever a cycle slip occurs. In order to guarantee aviation integrity, ambiguous carrier information while in a deep fade cannot be used upon reacquisition for carrier smoothing purposes. The very frequent deep fades observed in this research indicate that the availability of precision approach of aircraft may be significantly impacted during strong scintillation in the equatorial region.

2.6 Effects of Different Definitions of Deep Fading

Deep fading in this chapter so far has meant a signal fading in which the minimum C/N_0 is less than 20 dB-Hz in the Ascension Island data. This definition is well suited to the aviation receiver for the Brazil campaign because it is likely to lose carrier lock

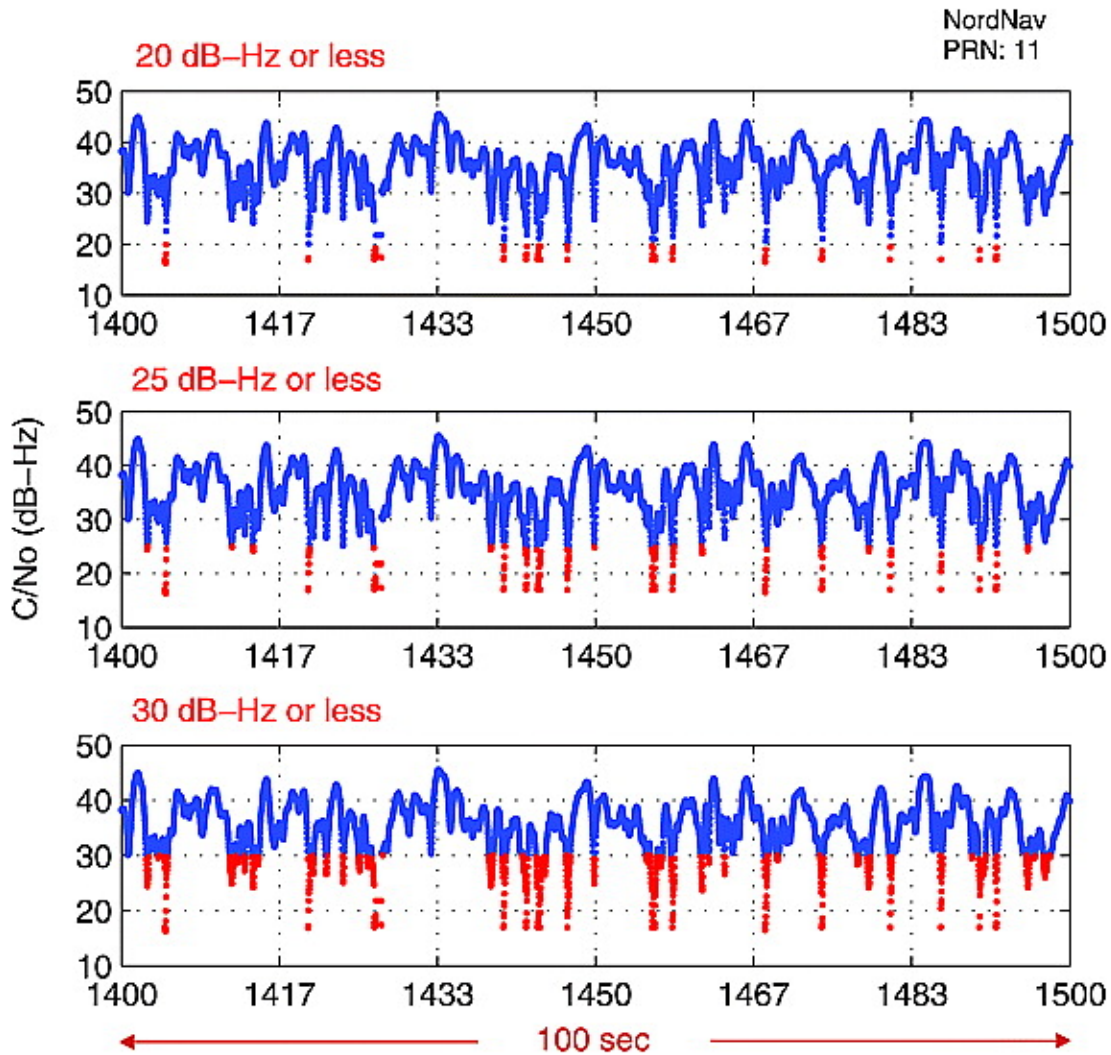


Figure 2.11: Comparison of different definitions of deep fading. When applying higher thresholds, more signal fluctuations are considered to be deep fading.

in this situation as discussed in Section 2.3 (p. 21). However, other receivers could lose carrier lock at higher C/N_0 . Signal fades that are less deep could also be harmful to those receivers.

Figure 2.11 presents deep fades in red according to three different definitions. Figure 2.11 (top) is the same as previously defined which has minimum C/N_0 of 20

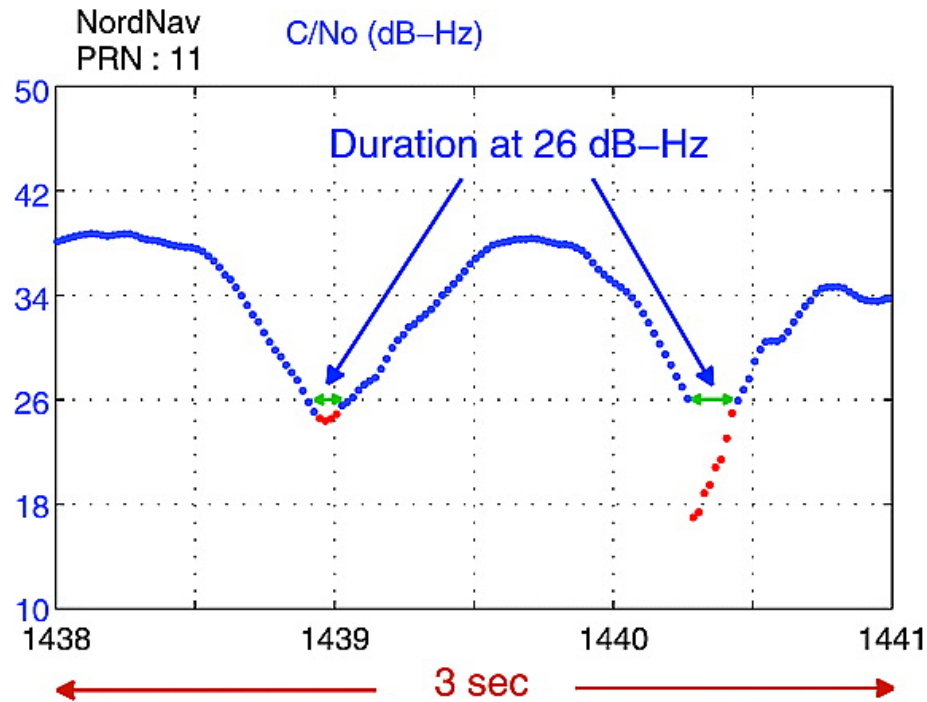


Figure 2.12: Effect of shallower fading on observed statistics. The shorter duration of the shallower fading on the left at the same C/N_0 level yields less conservative statistics for fading durations.

dB-Hz or below (Figure 2.3, p. 21). Figure 2.11 (middle) shows deep fading in which the defined fading has minimum C/N_0 of 25 dB-Hz or below. Figure 2.11 (middle) contains more deep fades shown in red. Figure 2.11 (bottom) contains even more deep fades because the deep fading in Figure 2.11 (bottom) is defined as a minimum C/N_0 of 30 dB-Hz or below. Remember that C/N_0 values here are all absolute values. This was chosen because a receiver's tracking loop performance is related to absolute C/N_0 , not relative C/N_0 drop. Hence, lower absolute C/N_0 value here indicates deeper signal fading.

If the minimum C/N_0 of 25 dB-Hz or below is defined as deep fading as in Figure 2.11 (middle), the first fade of Figure 2.12 is now considered as a deep fade. It

was not included in the statistics of the fading duration model (Figure 2.8, p. 27) because Figure 2.8 only considered fades with minimum C/N_0 of 20 dB-Hz or below. Including shallower fades in the analysis creates less conservative statistics for fading duration. Shallower fades usually have shorter fading durations for the same C/N_0 as shown in Figure 2.12. Hence, mean and 95th percentile values at the same C/N_0 would be smaller and consequently the fading duration model of Figure 2.8 would become sharper when shallower fades are taken into account. This provides a less conservative guideline for required coasting time.

However, the time between deep fades becomes even shorter when including shallower fades into the analysis. The median time between deep fades is 4.3 s when a minimum C/N_0 of 25 dB-Hz or below is considered to be deep fading. This is slightly shorter than the 5.3 s of 20 dB-Hz or below case presented in Figure 2.10 (p. 30). If a minimum of 30 dB-Hz or below is considered as in Figure 2.11 (bottom), the median time between deep fades decreases to only 2.7 s.

Consequently, the fading duration model of Figure 2.8 (p. 27) remains a conservative representation of the data. An aviation receiver losing lock at 20 dB-Hz would have experienced very brief signal outages (0.2 s in 95% cases) under the strong scintillation of solar maximum. The time between deep fades does not change significantly if a receiver can maintain carrier lock down to 25 dB-Hz, but if a receiver loses carrier lock above 25 dB-Hz, the time between deep fades becomes even shorter. However, measurement noise levels after 5.3 s of smoothing or 2.7 s of smoothing would not be significantly different. Both smoothing times are already very short compared to the filter warm-up time.

2.7 Summary

Tracking at least four satellites is a basic requirement for GPS navigation. A receiver that loses too many satellites due to the influence of scintillation cannot meet this goal. In order to develop a strategy to minimize the impact of scintillation, the characteristics of GPS signal fades under strong scintillation are investigated. This chapter developed an empirical fading duration model based on real scintillation data from the previous solar maximum. The fading duration model of this chapter is comparable with other research [El-Arini *et al.*, 2003] which reports about 0.2 s fading duration at 20 dB fading in Naha, Japan on 20 March 2002, although their approach to define and calculate fading duration is different from this work. Given the very short fading duration under scintillation, the coasting of a receiver's tracking loops during brief outages can be an effective strategy for immediate retracking of the lost channels. Coasting for less than 1 s without the help of an IMU is not a challenging task for a conventional receiver. The fading duration model in Figure 2.8 (p. 27) provides aviation receiver manufacturers with a guideline for coasting time depending on a receiver's tracking loop threshold.

In addition to the number of tracked satellites, measurement noise level is also an important parameter for determining operational availability of GPS aviation. The benefit of conventional carrier smoothing to reduce noise will be significantly impacted due to the very frequent deep fades as observed during the strong scintillation period analyzed here. Hence, the frequent deep fades during scintillation are worrisome for the approach guidance of aircraft. This effect will be further investigated in the following chapters.

Chapter 3

Impact of Ionospheric Scintillation on GPS Aviation Availability

3.1 Overview

The GPS signal environment under strong scintillation has been discussed in the previous chapter. In this chapter, the impact of the observed signal environment on the availability of GPS aviation is analyzed in detail. As explained, strong amplitude scintillation causes deep and frequent GPS signal fading. Since GPS receivers can lose carrier tracking lock at deep signal fading and the lost channel cannot be used for the position calculation until reacquired, ionospheric scintillation is a major concern for GPS aviation in the equatorial area for several hours after local sunset during solar maxima. In addition, frequent signal fading causes frequent reset of the carrier smoothing filter in aviation receivers. This leads to higher noise levels on the pseudorange measurements.

The effects from satellite loss due to deep fading (Section 3.2.1) and shortened

carrier smoothing time due to frequent fading (Section 3.2.2) are discussed in this chapter. These effects are considered in the availability study. Specifically, the operational availability of vertical navigation (Section 3.3.2) and horizontal navigation (Section 3.3.3) under the observed strong scintillation period of the past solar maximum are analyzed.

3.2 Ionospheric Scintillation and GPS Aviation

This section explains how deep and frequent signal fading affects aviation availability. Satellite loss due to deep fading adversely affects satellite geometry and significantly decreases aviation availability. High noise levels affecting pseudorange estimates due to shortened carrier smoothing time caused by frequent fades further reduce the availability. The effects from satellite loss and shortened carrier smoothing time discussed in this section will be considered in the availability analysis of Section 3.3 (p. 43). The importance of the fast reacquisition capability of a receiver is also discussed in this section.

3.2.1 Simultaneous Loss of Satellites and Reacquisition Time

The Ascension Island data show that when strong scintillation occurs, almost all satellites in view could suffer from deep signal fades. If a receiver loses many satellites simultaneously under this condition, the availability of GPS aviation would be significantly impacted. However, as Figure 3.1 illustrates, deep signal fades of different satellites do not usually happen at the exact same time. Hence, if a receiver can reacquire a lost satellite before it loses other satellites, it can avoid simultaneous losses and consequently reduce the impact of scintillation on GPS aviation.

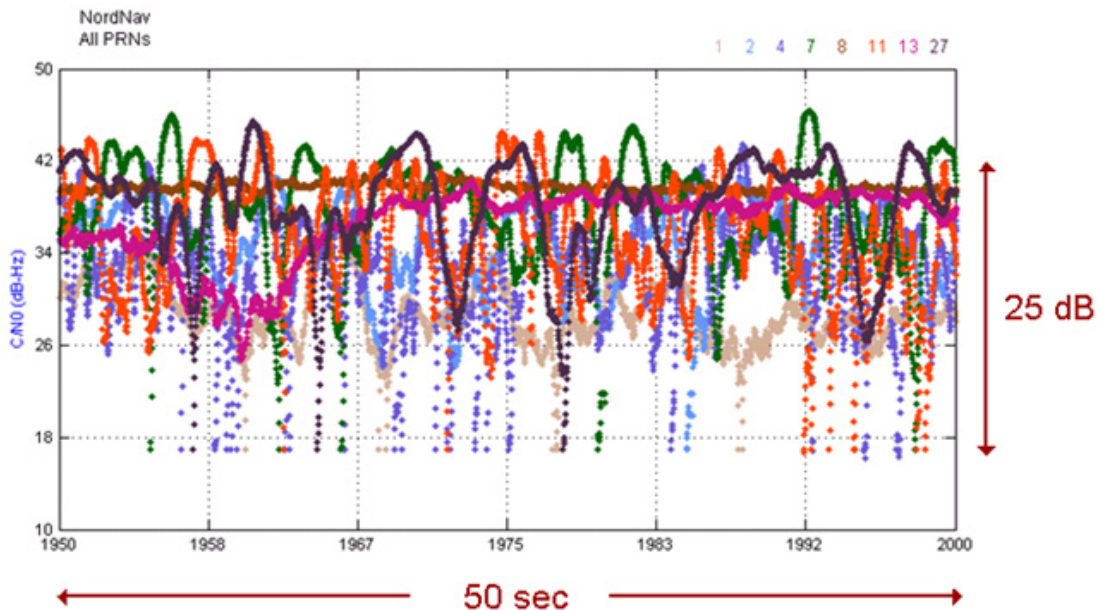


Figure 3.1: Example of C/N_0 outputs of all satellites in view during strong scintillation of the past solar maximum. Different colors represent different satellites. This data was collected at Ascension Island in 2001 and processed using a NordNav commercial software receiver. Detailed information of the data set is given in Section 2.2.1 (p. 17).

In fact, the WAAS MOPS [RTCA, 2006] specifies the recovery time of the lost channel after the reintroduction of signal, which is called “reacquisition time” in the MOPS. The current WAAS MOPS states, “For satellite signal outages of 30 seconds or less when the remaining satellites provide a GDOP of 6 or less, the equipment shall reacquire the satellite within 20 seconds from the time the signal is reintroduced. This requirement applies to a satellite with the minimum signal power in the presence of interfering signals as described in Appendix C [RTCA, 2006].” This means that a satellite lost after deep signal fading could have its reintroduction into the position solution delayed for up to 20 s. As mentioned in Section 1.3.2 (p. 10), the MOPS does not have any specific performance requirement under scintillation. The requirement

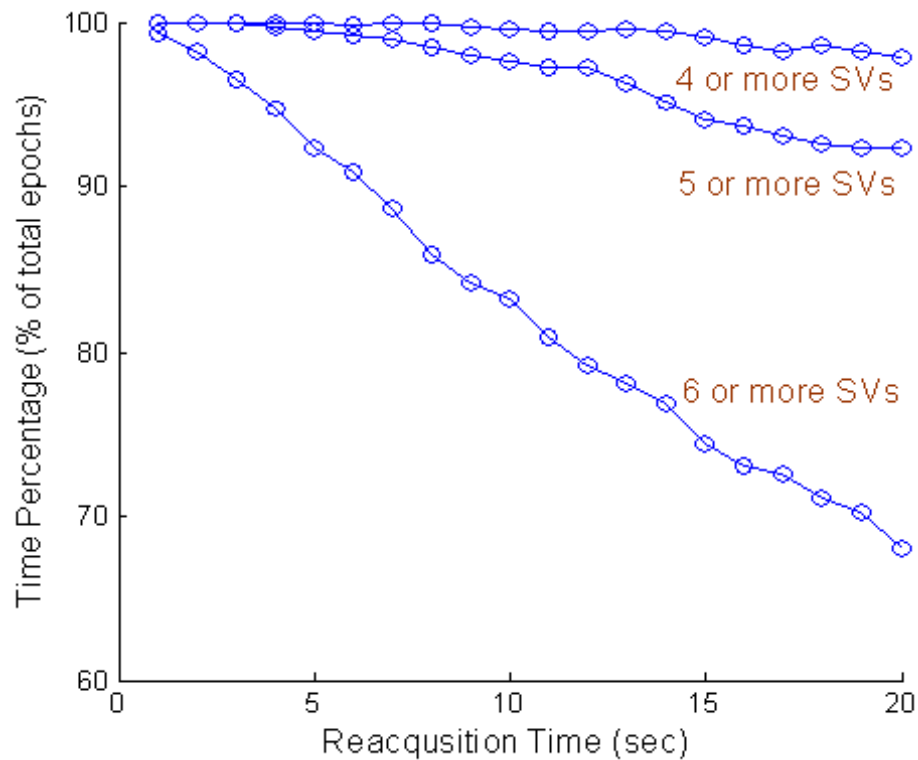


Figure 3.2: Number of simultaneously tracked satellites depending on various reacquisition times during the worst 45 min of the Ascension Island campaign. Shorter reacquisition time results in more satellites tracked.

of a reacquisition time considers the RF Interference (RFI) condition. Under an RFI, signal outages can be much longer than the outages under scintillation, which is usually less than 1 s. Hence, the requirement considers the condition of “signal outages of 30 seconds or less” and mandates a “20 second” limit for reacquisition.

The effect of the 20 s reacquisition time under strong scintillation is shown in Figure 3.2. A 20 s reacquisition time here means a 20 s loss of satellite tracking after the deep signal fading ends. If a 20 s reacquisition time is always assumed during the worst 45 min scintillation of the Ascension Island campaign, four or more satellites are tracked only 97.9% of the time. Five or more tracked satellites occurs only 92.3%

of the time and six or more satellites only 68.1%. Note that a receiver has to track at least four satellites with good geometry to navigate using GPS. The low percentages of sufficient number of satellites tracked may not provide enough availability of GPS aviation during times of expected strong scintillation.

Although WAAS MOPS allows up to 20 s reacquisition time, a receiver can perform much better under scintillation using a simple coasting strategy. The idea of coasting of tracking loops, which enables fast reacquisition of a lost satellite, has been introduced in Section 2.4 (p. 23). Given the very short duration of fading (about 0.2 s at the threshold of an aviation receiver) observed during the past solar maximum, simple coasting without an IMU is technically possible for a conventional receiver. Therefore, a receiver's reacquisition time can be much shorter than the 20 s requirement. (During the Brazil campaign, a certified WAAS receiver already demonstrated its fast reacquisition capability. This will be discussed in detail in Section 6.3, p. 105.)

The benefit of a shorter reacquisition time under scintillation is clearly demonstrated in Figure 3.2. If a receiver can always reacquire the lost channel within 2 s, for example, a receiver always tracks five or more satellites during the same strong scintillation period and tracks six or more satellites 98.3% of the time. Hence, in the availability study in Section 3.3 (p. 43), the reacquisition time of a receiver will be considered as an important parameter.

3.2.2 Frequent Signal Fading and Shortened Carrier Smoothing Time

As briefly introduced in Section 2.5 (p. 29), aviation receivers use Hatch filters [Hatch, 1982] to reduce the effect of the noise level of code measurements. The

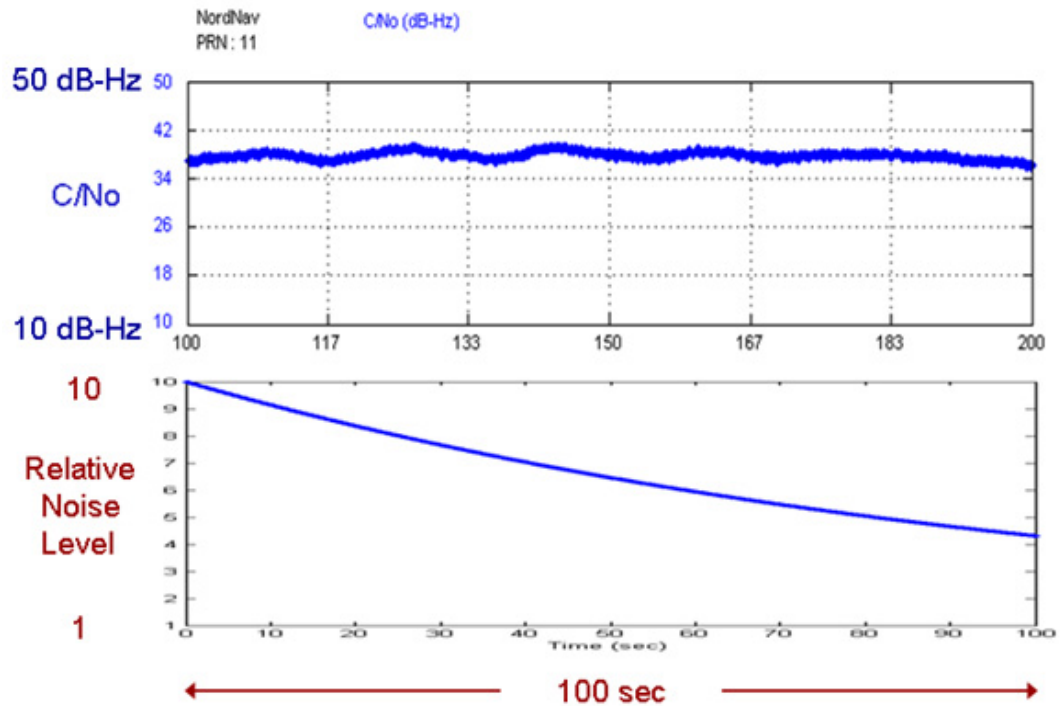


Figure 3.3: Decreasing code noise by Hatch filtering under a nominal condition without scintillation. Carrier tracking lock is assumed to be established at 0 s. C/N_0 remains nearly constant over 100 s.

WAAS MOPS specifies a smoothing time constant of 100 s. The MOPS also specifies noise performance for a fully converged filter, but does not specify a noise model for shorter smoothing times. In this study, it is conservatively assumed that the noise is uncorrelated from one second to the next.

Under a nominal condition as in Figure 3.3, the code noise exponentially decreases [Walter *et al.*, 2004] with a 100 s time constant using Hatch filtering and converges to floor level after a couple of hundred seconds. The relative noise level of code measurements with respect to the fully converged value is modeled as $1 + 9e^{-\frac{\Delta t}{100}}$, where Δt is the carrier smoothing time after establishing carrier lock. This model implies that the noise level is reduced by a factor of 10 after filter converging. However,

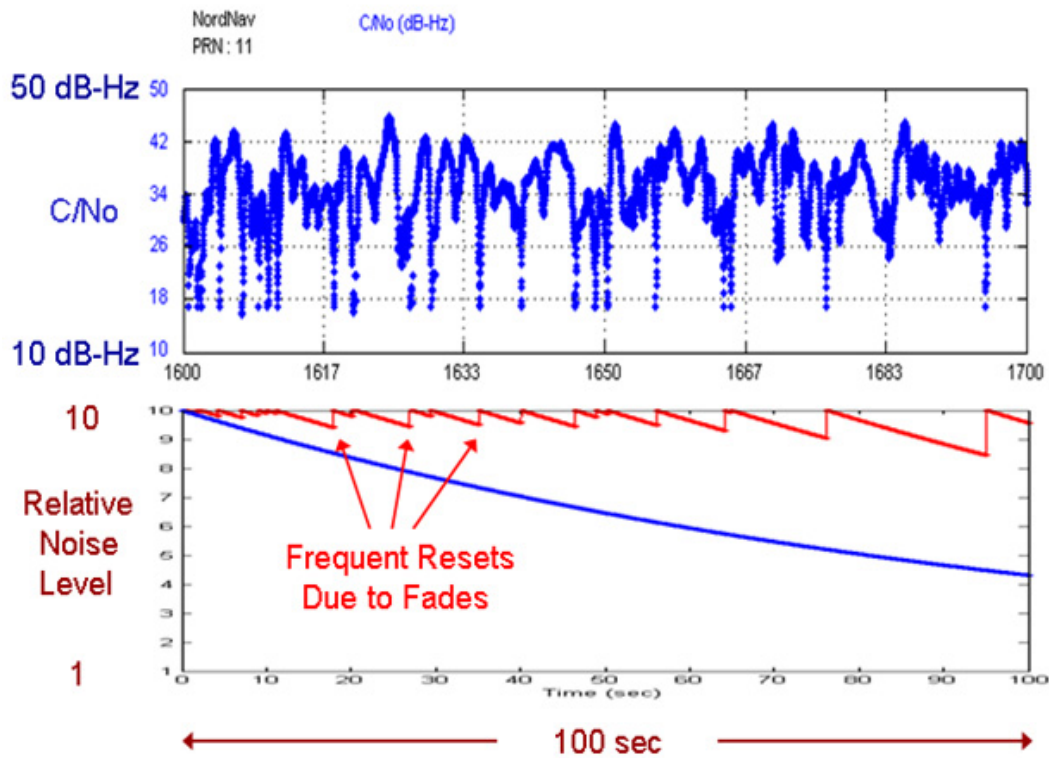


Figure 3.4: Frequent reset of Hatch filter and high code noise level under strong scintillation. For illustration purposes, a receiver is assumed to reestablish carrier lock promptly after loss of lock. High noise level (in red) under frequent fades adversely affects the availability of GPS aviation.

the Hatch filter has been shown to actually reduce noise level by a factor of only 2-5 depending on satellite elevations (based on empirical data) [Murphy *et al.*, 2005]. Hence, the Hatch filter model in this study is conservative because after reestablishing carrier lock, the relative noise level is assumed to be 10 times larger than the floor value rather than 2-5 times larger. Once the filter is converged, the relative noise remains at the floor level until the receiver loses lock again.

However, if strong scintillation is present, a receiver frequently loses lock and tries to reacquire the lost channel. After reacquiring the channel, the Hatch filter is reset and starts to smooth code measurements from the beginning. When the Hatch filter

is reset, the effect of the noise level on the code measurements is modeled as 10 times higher than the floor level as in Figure 3.4. Figure 2.10 (p. 30) showed that the median time between deep fades during the worst 45 min scintillation was only about 5 s which is very short compared to the 100 s smoothing time constant. After this study, El-Arini [2009] reported about 9 s median time between fades at 25 dB fading in Naha, Japan on 20 March 2002 (8:30 P.M. – 11:00 P.M., local time).

For the availability analysis of Section 3.3, the relative noise level of code measurements is modeled as $1 + 9e^{-\frac{\Delta t}{100}}$, where Δt is time since the filter reset, as in Figures 3.3 and 3.4. The code noise and multipath model for the availability analysis is multiplied by this relative noise level factor. This multiplication factor starts from 10 when smoothing time, Δt , is zero and converges to 1 if a receiver does not lose lock for a couple of hundred seconds. However, strong scintillation causes frequent loss of lock and prevents the Hatch filter from converging as in Figure 3.4. This higher noise level due to frequent loss of lock reduces aviation availability. A GPS/SBAS availability study with the consideration of the Hatch filter model under strong scintillation has not been previously performed.

3.3 Operational Availability During a Strong Scintillation Period

This section discusses how the availability analysis of GPS aviation under scintillation is performed in this study based on the real scintillation data. This study provides hypothetical availability results of the Localizer Performance with Vertical guidance (LPV)-200 [Cabler and DeCleene, 2002], which is a form of vertical navigation, and the Required Navigation Performance (RNP)-0.1 [Kelly and Davis, 1994], which is a

form of horizontal navigation, for a single user at Ascension Island during the worst 45 min of strong scintillation (Section 2.2.1, p. 17). Reacquisition time and shortened carrier smoothing time (discussed in Sections 3.2.1 and 3.2.2) are modeled in the simulation. The availability results are presented as availability contours considering different reacquisition times and probabilities of loss of lock at deep fade.

3.3.1 Availability Analysis Procedure

Figure 3.5 illustrates the procedure to analyze aviation availability (specifically, the availability of LPV-200) under scintillation. GPS avionics calculate the confidence bound of its position solution at each epoch based on several parameters which are satellite clock and ephemeris error, code noise and multipath, troposphere error, and satellite geometry. This confidence bound, usually called the “protection level,” ensures that the true position is within this bound with very high probability (99.99999%). If vertical and horizontal protection levels are smaller than the vertical and horizontal alert limits of LPV-200 (35 m and 40 m, respectively), LPV-200 service is “available” for this epoch. If protection levels are greater than the alert limits, in other words, if the true position is not protected within a small-enough bound with very high confidence, GPS avionics must raise a flag and LPV-200 service must not be available for the epoch in order to guarantee navigation safety (usually called “integrity”).

Without compromising the integrity, ionospheric scintillation reduces the availability in two ways. First, deep signal fades caused by scintillation can break a receiver’s carrier tracking lock. Since the lost satellite channels cannot be used for position calculation, satellite geometry (the number and the distribution of satellites in view) is impacted during outage periods. This effect is critical especially when multiple

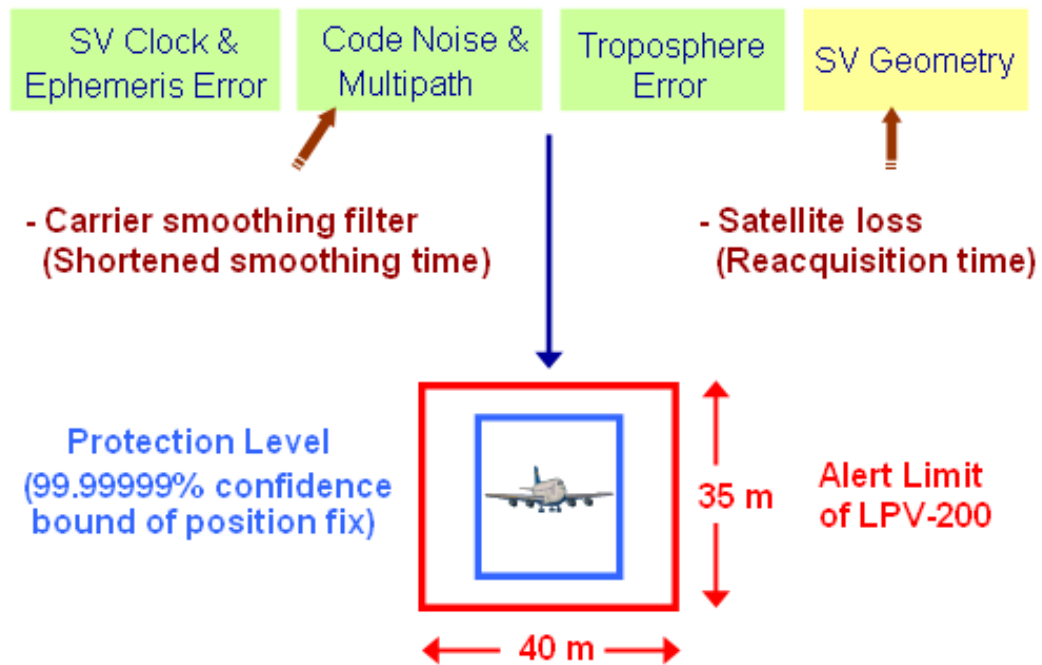


Figure 3.5: Availability analysis procedure. 1 m user range accuracy, iono-free dual frequency code noise and multipath model, troposphere model from the WAAS MOPS, and a real satellite constellation are used for the availability analysis. Satellite loss due to deep signal fading changes satellite geometry. Shortened carrier smoothing time due to frequent fades increase code noise and multipath.

satellites are lost simultaneously. The duration of each satellite loss determines the probability of simultaneous losses. The outage duration depends on the receiver's reacquisition time. Longer reacquisition time results in worse satellite geometry and lower aviation availability (Section 3.2.1, p. 37).

Another availability reduction is from shortened carrier smoothing time which leads to high code noise level. Ideally, a GPS aviation receiver should maintain its carrier tracking lock for a couple of hundred seconds to reduce the noise level of pseudorange measurements to the floor level by a carrier smoothing filter. Frequent loss of lock (discussed in Section 3.2.2, p. 40) reduces effective lock time and increases

the noise level of pseudorange measurements. The satellite loss and the increased noise level due to scintillation can increase protection levels over alert limits and consequently reduce the availability.

The Matlab Algorithm Availability Simulation Tool (MAAST) [Jan *et al.*, 2009] was modified for this work to incorporate scintillation effects such as the loss of lock after deep fades and the shortened carrier smoothing time of a smoothing filter. For satellite clock and ephemeris errors, 1 m User Range Accuracy (URA) is assumed. The troposphere error model is from the WAAS MOPS. For purposes of comparison, the satellite geometries are assumed to be the same as the satellite constellation of the observed worst-case scintillation period from the campaign at Ascension Island in 2001 (Section 2.2.1, p. 17). Because this research is considering the future situation where aircraft will be equipped with dual frequency GPS avionics, the iono-free dual frequency code noise and multipath model is used for this analysis. However, the possible availability benefit depending on the correlation level between L1 and L5 deep fades (will be discussed in Chapter 5, p. 82) is not taken into consideration. Instead, 100% correlation of deep fades between L1 and L5 channels is assumed. In other words, a receiver is assumed to lose its L5 channel as well whenever it loses its L1 channel after deep fading. Since the correlation level of deep fades between L1 and L5 frequencies is not yet known from real data, this most conservative approach is taken. (As of April 2010, only one GPS satellite broadcasts an L5 test signal [Gao *et al.*, 2009b; Gunawardena *et al.*, 2009] and there is no GPS L5 strong scintillation data available.)

The protection levels are calculated every second for the worst 45 min of strong scintillation. Operational availability of a single user at Ascension Island during the same period is obtained. Since the simulation utilizes 1 m URA and the iono-free

dual frequency model, the availability results in Sections 3.3.2 (p. 47) and 3.3.3 (p. 54) are valid under a future GNSS Evolutionary Architecture Study (GEAS) configuration which can provide aviation integrity worldwide. Among the three architectures discussed in [Walter *et al.*, 2008], the GNSS Integrity Channel (GIC) architecture is assumed in this study, which means that the integrity information is assumed to be provided by separate WAAS-like channels.

3.3.2 Availability of Vertical Navigation (LPV-200)

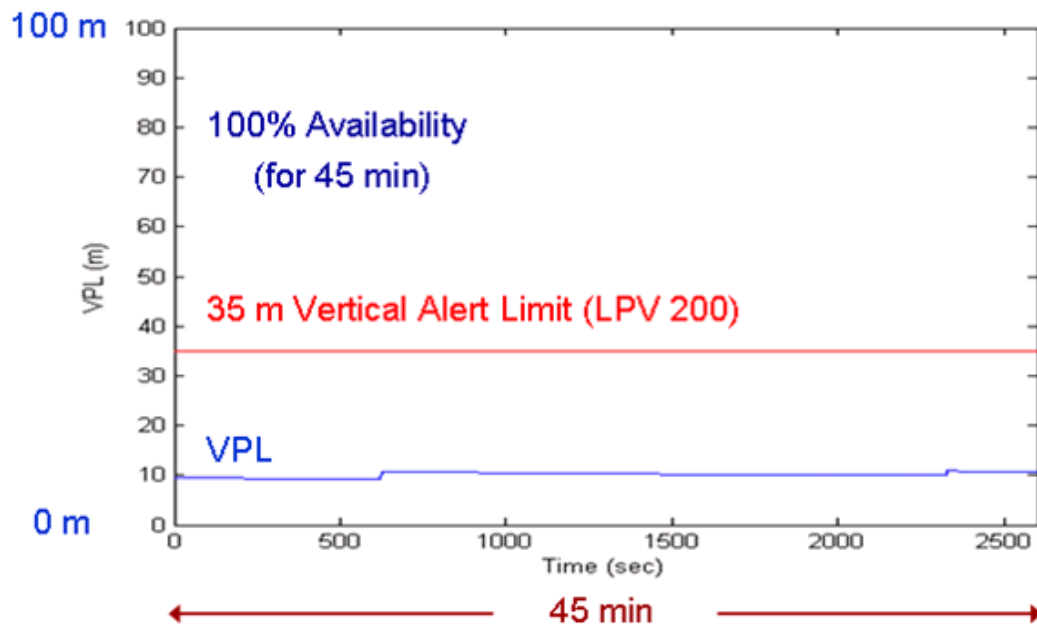


Figure 3.6: Simulated vertical protection level without considering scintillation effects. The actual satellite geometry during the 45 min of strong scintillation at Ascension Island on 18 March 2001 was used for the VPL calculation.

Figure 3.6 shows the simulated Vertical Protection Level (VPL) during the worst 45 min scintillation. The VPL of Figure 3.6 is obtained with the actual satellite geometry of the strong scintillation period, but scintillation effects such as satellite

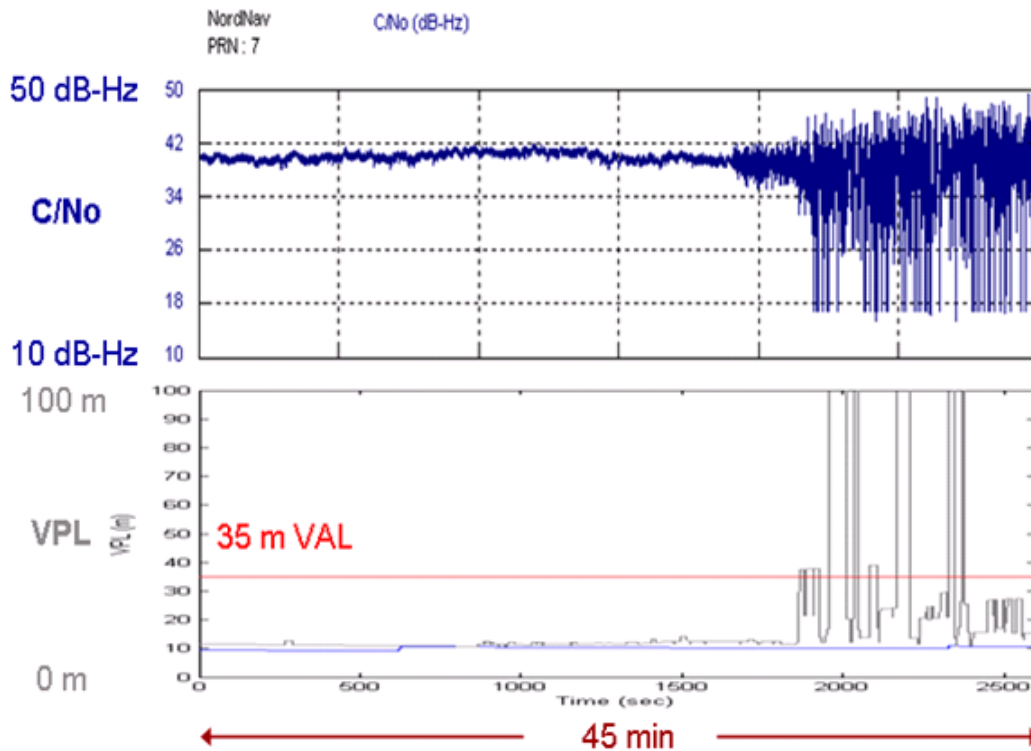


Figure 3.7: C/N_0 and vertical protection level during the worst 45 min scintillation considering satellite outages only. The longest allowable reacquisition time under the WAAS MOPS (20 s) is always assumed for VPL calculation. The effect of shortened carrier smoothing time is not yet considered.

loss and shortened carrier smoothing time are not yet considered. This best case VPL, simulated without accounting for any scintillation effects, is always below the 35 m Vertical Alert Limit (VAL) of LPV-200, so the availability of LPV-200 during this period without scintillation effects would have been 100%. (As explained in Section 1.2.1 (p. 3) GPS and GIC can guide aircraft down to a 200 ft decision height in LPV-200.)

However, if strong scintillation occurs, the VPL increases significantly as Figure 3.7 (bottom) demonstrates. As shown, deep and frequent signal fades of PRN 7 in Figure 3.7 (top) have a dramatic negative effect on VPL. Only the effect of satellite

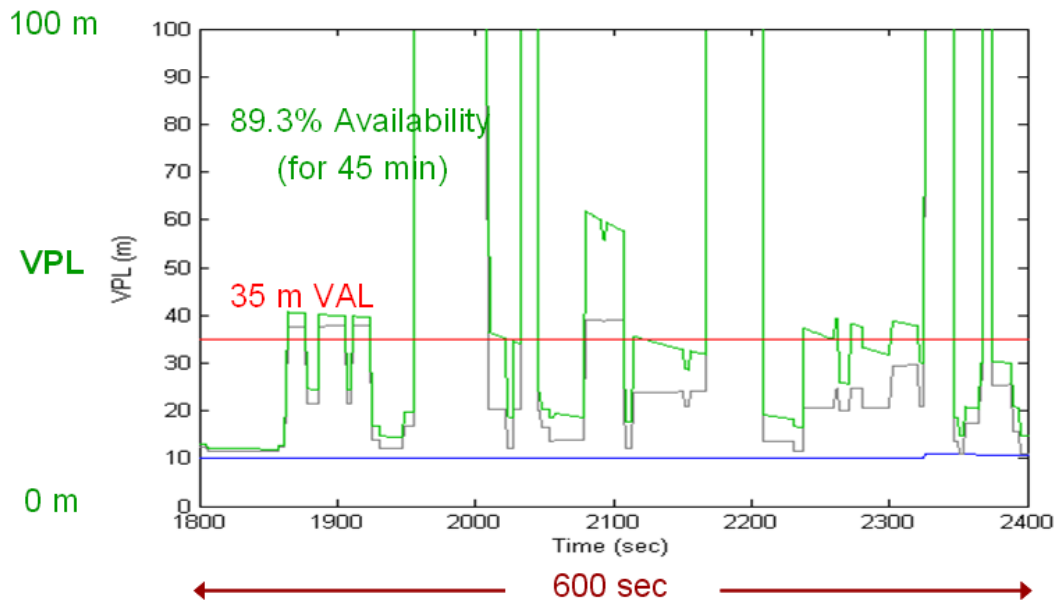


Figure 3.8: Impact of shortened carrier smoothing times due to frequent fades (600 s example from the 45 min data). The gray VPL curve was obtained after considering satellite outages only, but the green VPL curve considers effects from both satellite outages and shortened carrier smoothing times. A 20 s reacquisition time is assumed as in Figure 3.7.

loss is considered to calculate the VPL of Figure 3.7. The effect of shortened carrier smoothing time due to frequent fades is not yet considered.

When the effect of shortened carrier smoothing times due to frequent fades is also considered, the VPL values are further increased as shown in the green curve of Figure 3.8. Availability during the 45 min is only 89.3% in this case for the green curve. The gray VPL curve of Figure 3.8, which is a zoomed-in plot from Figure 3.7, is also shown to illustrate the impact of the shortened carrier smoothing times of the Hatch filters on top of the impact of satellite outages in Figure 3.7.

Although shortened smoothing times increase the VPL further, the poor satellite geometry causes the high VPL spikes over 100 m in Figures 3.7 and 3.8. Hence, the impact of satellite geometry itself is most critical during strong scintillation. As

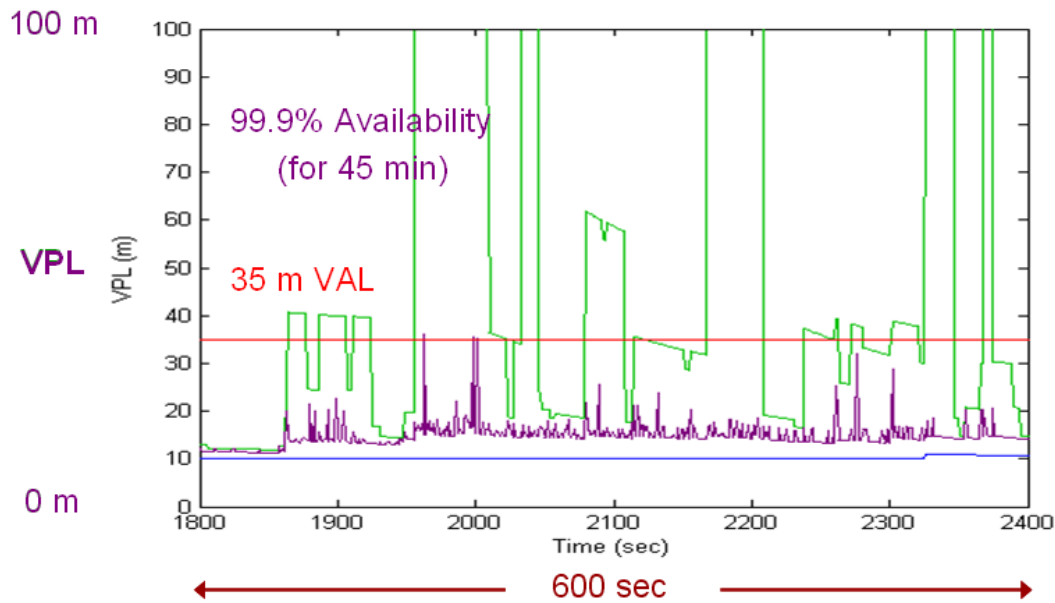


Figure 3.9: Availability benefit of a shorter reacquisition time (1 s vs. 20 s). The green VPL curve assumes 20 s reacquisition time (the WAAS MOPS limit) and the purple VPL curve assumes 1 s reacquisition time. The figure shows the clear availability benefit of a shorter reacquisition time for a receiver (600 s example from the 45 min data).

shown in Figure 3.2 (p. 39), the number of simultaneously tracked satellites is strongly dependent on a receiver's reacquisition time. The VPL values of Figures 3.7 and 3.8 are obtained with the most conservative assumption of a 20 s reacquisition time which allows 20 s loss of a satellite after deep fading. This is an allowable but pessimistic scenario under the current WAAS MOPS.

However, if a receiver can reacquire a lost channel quickly, for example within 1 s, it can achieve 99.9% availability for the same time period (Figure 3.9). The purple VPL curve of Figure 3.9 shows the case of 1 s reacquisition time. Note that this 99.9% availability is obtained after considering the effects from both satellite loss and shortened smoothing times based on the real scintillation data. If a 150 s time window of precision approach is considered, there could be continuity breaks due to

high VPL spikes for a maximum of two approaches during these 45 min.

This result demonstrates a clear availability benefit from a shorter reacquisition time under scintillation. The effect of satellite geometry is dominant for the availability during strong scintillation at least with the GPS constellation of 2001. Shorter reacquisition time reduces the chance of simultaneous loss of satellites and therefore provides better satellite geometry. Better satellite geometry results in higher availability even with the effect of the shortened carrier smoothing time of the Hatch filters.

The future constellations of GPS and Galileo (the European satellite navigation system under development) are expected to alleviate the effect of loss of multiple satellites. For example, four satellites lost is critical if a receiver has only eight satellites in the sky, but it can be manageable if there are 16 satellites in the sky. However, the geometry of the electron density irregularities should also be considered in this case. If the irregularities cover almost all of the sky as in Figure 2.1 (p. 18), 14 out of 16 satellites could be affected by scintillation. In this case, the benefit of dual constellations may not be fully realized if signal fades of different satellite channels are highly correlated. Correlation of signal fades between different satellites and its impact on the availability will be discussed in greater detail in Chapter 4 (p. 58).

The dependency of availability on a receiver's reacquisition time is presented in Figure 3.10. According to this figure, less than 1 s reacquisition time is required to achieve more than 99.9% availability during the strong scintillation period. The availability result of Figure 3.10 is based on a conservative assumption that a receiver loses lock with 100% probability whenever deep signal fading occurs.

Tracking loop performances of various receivers are very different depending on their designs and dynamic environments. The NordNav commercial software receiver

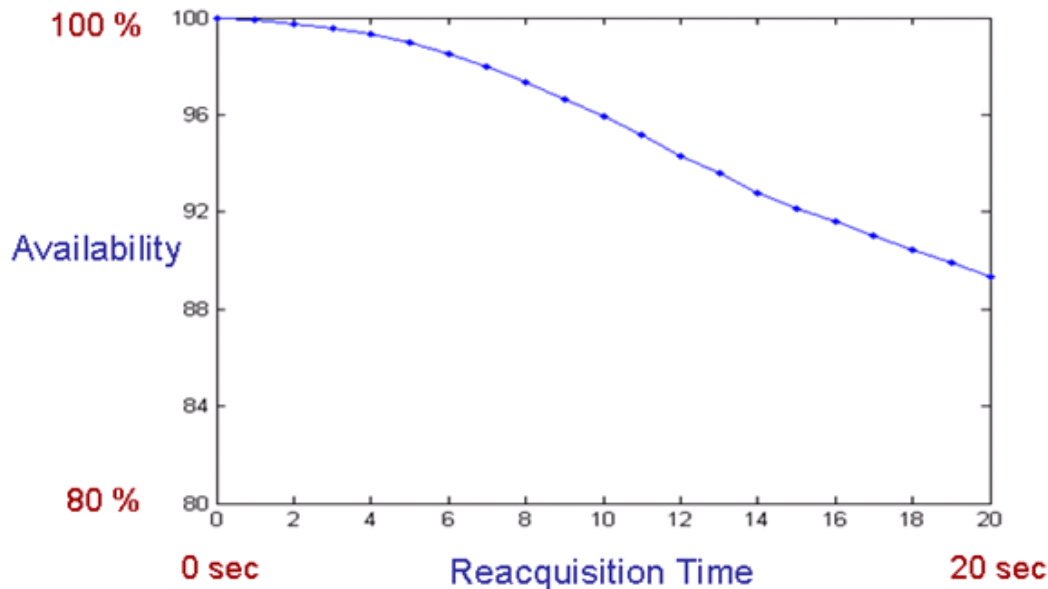


Figure 3.10: Availability vs. reacquisition time. Operational availability for vertical navigation (LPV-200) during the 45 min is shown as a function of reacquisition time. Less than 1 s reacquisition time is required to have more than 99.9% availability. A receiver is assumed to lose its lock with 100% probability at every deep fade.

with narrow tracking loop bandwidth used for this research loses lock at around 17-19 dB-Hz but typical receivers require 26-30 dB-Hz to maintain tracking lock [Kintner *et al.*, 2007]. The certified aviation receiver used for the Brazil campaign (Section 2.2.2, p. 20) also tracked signals down to around 28-30 dB-Hz. Since an aviation receiver must track high vehicle dynamics, it cannot use a very narrow tracking loop bandwidth like a terrestrial software receiver can when it tracks stationary data. For Figures 3.7 through 3.10, it was conservatively assumed that a receiver loses lock at 30 dB-Hz with 100% probability.

Because of the uncertainties from the sensitivity of a receiver, C/N_0 improvement from current technology, and actual fading depth, the exact probability of loss of lock of an aviation receiver at the 30 dB-Hz threshold is not obtainable from the given data.

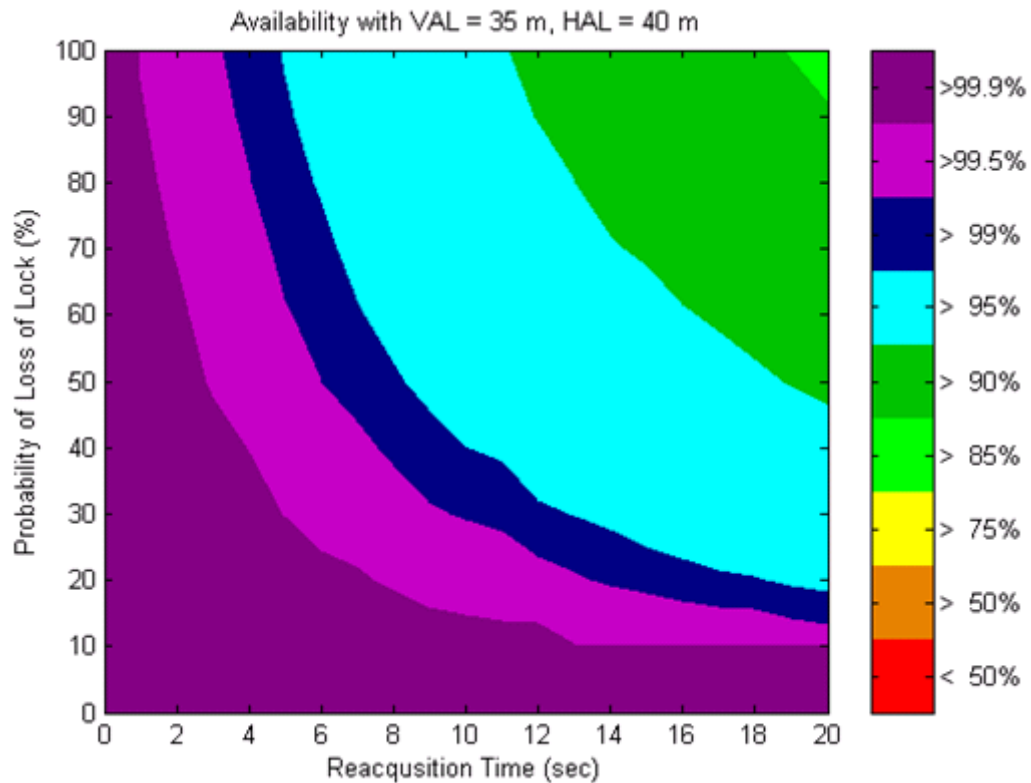


Figure 3.11: Availability contour for vertical navigation (LPV-200) during the worst 45 min scintillation. The color represents operational availability at every combination of probability of loss of lock and reacquisition time. 35 m vertical alert limit and 40 m horizontal alert limit for LPV-200 are used for the simulation.

Alternatively, the most conservative scenario (100% probability of loss of lock) was assumed for Figures 3.7 through 3.10. The simulation can be repeated with different probabilities of loss of lock (e.g., every 10%, from 0% to 100%). Another dimension of the simulation space can be the reacquisition times (e.g., every second, from 0 s to 20 s). Figure 3.11 shows the availability results in this simulation space. This plot confirms the intuitive result that shorter reacquisition time and lower probability of loss of lock at deep fade result in better availability. (“Deep fade” was defined in Section 2.3, p. 21.) In addition to this qualitative expression, the plot quantitatively

shows availability levels during the worst 45 min according to different probabilities of loss of lock and reacquisition times.

3.3.3 Availability of Horizontal Navigation (RNP-0.1)

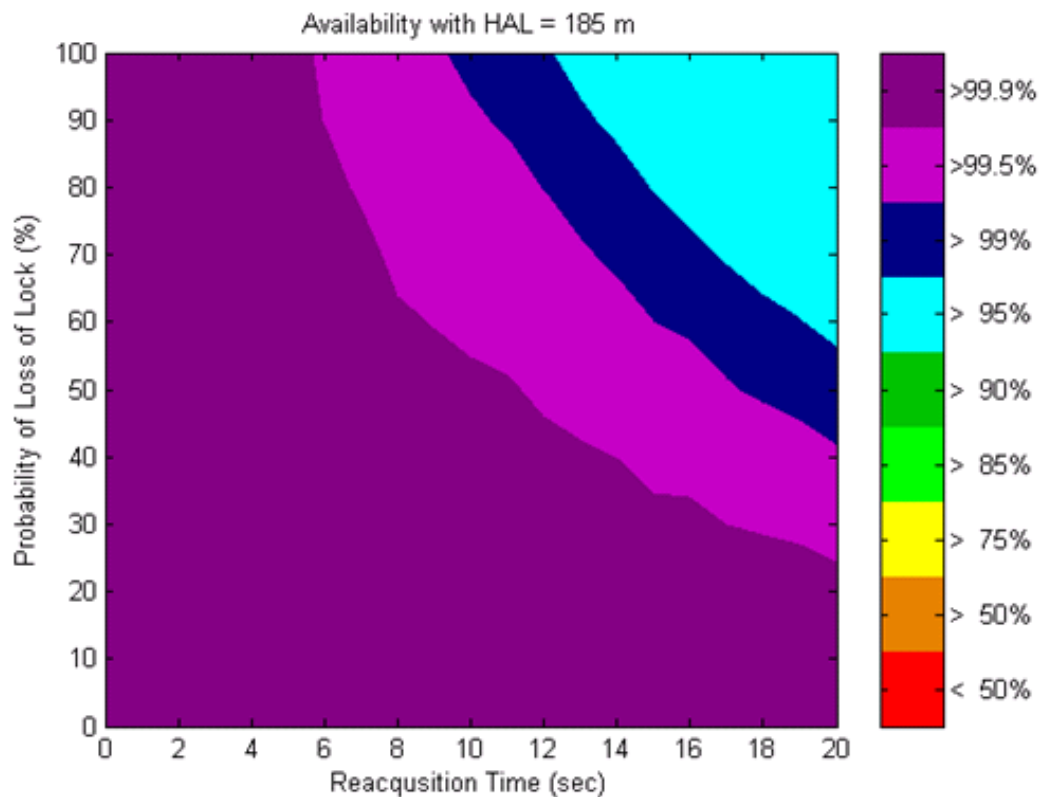


Figure 3.12: Availability contour for horizontal navigation (RNP-0.1) during the worst 45 min scintillation. The color represents operational availability at every combination of probability of loss of lock and reacquisition time. 185 m horizontal alert limit for RNP-0.1 is used for the simulation.

The availability contour for LPV-200 (Figure 3.11) is useful to illustrate operational availabilities during the strong scintillation period according to two parameters, i.e., probability of loss of lock at deep fade and reacquisition time of a receiver after loss of lock. Similarly, the availability contour for horizontal navigation (RNP-0.1) is

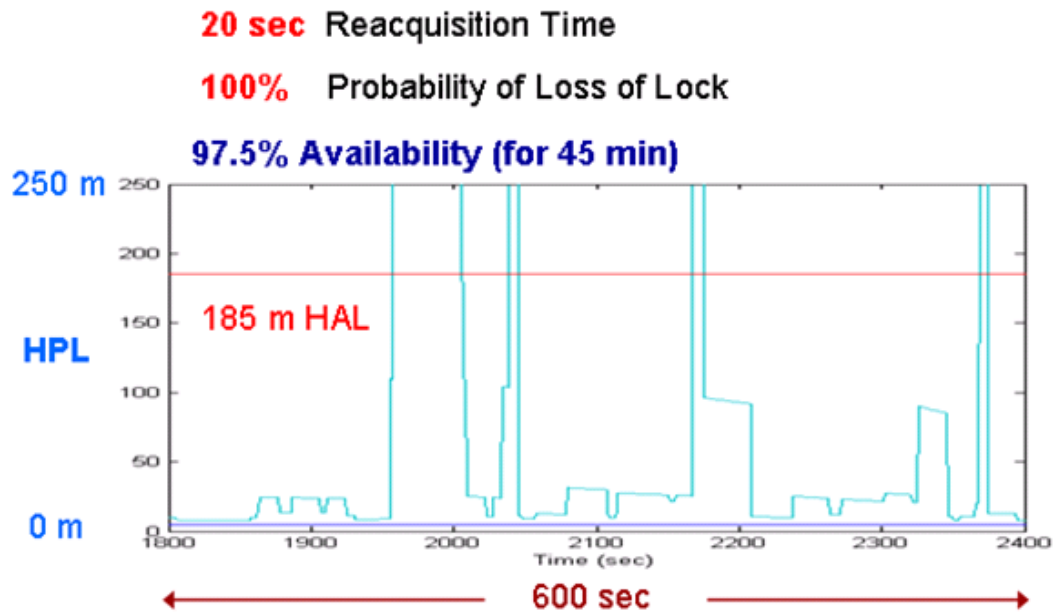


Figure 3.13: Horizontal protection level during strong scintillation (600 s example from the 45 min data). Even with the most conservative assumptions about reacquisition time and probability of loss of lock, the operational availability of RNP-0.1 during the 45 min is 97.5%.

generated as seen in Figure 3.12. A 185 m (0.1 nautical miles) Horizontal Alert Limit (HAL) for RNP-0.1 is used for this analysis. Compared to the 40 m HAL for LPV-200, RNP-0.1 service is for a less stringent phase of flight such as en route. Since it is horizontal navigation, there is no vertical alert limit for RNP-0.1. Other procedures to simulate the availability are the same as in the LPV-200 case (Figure 3.5, p. 45).

The availability of RNP-0.1 is considerably better than the availability of LPV-200 as expected. Even with the worst case assumption of 20 s reacquisition time and 100% probability of loss of lock at deep fade, a 97.5% availability is achieved as seen in Figure 3.13. The high Horizontal Protection Level (HPL) spikes exceeding HAL are due to very poor satellite geometry. Many satellites are lost simultaneously if a receiver takes 20 s to reacquire each lost channel. As a result, the receiver cannot

always track the minimum of four satellites required to form a position solution. When this occurs, the HPL becomes infinite. However, if a receiver reacquires a lost channel within 4 s, it always tracks more than or equal to four satellites and achieves 100% availability even with the most conservative assumption of 100% probability of loss of lock at deep fade. Note that increased noise level due to shortened carrier smoothing time is not critical for horizontal navigation, but satellite geometry is paramount. Hence, short reacquisition capability to guarantee a good geometry is highly desired to provide high availability during strong scintillation.

3.4 Summary

This chapter analyzed the impact of observed strong scintillation on operational availabilities of vertical navigation (LPV-200) and horizontal navigation (RNP-0.1) of aircraft. Seven out of eight satellites were affected by scintillation during the worst 45 min, which represents a very stressing environment. The achievable availability level was illustrated as a function of the reacquisition time of a receiver and the probability of loss of lock at deep fade. The results show that a generic aviation receiver just complying with the 20 s reacquisition time limit of the current WAAS MOPS would provide very low availabilities for LPV-200 and RNP-0.1 during the worst 45 min. However, if a receiver could reestablish tracking the lost satellite within 4 s, 100% availability of RNP-0.1 could have been attainable even with the most conservative assumption of 100% probability of loss of lock at deep fade. Due to the much tighter VAL (35 m) and HAL (40 m) of LPV-200, a 1 s reacquisition time was required to provide 99.9% availability of LPV-200, if 100% probability of loss of lock at deep fade is assumed.

The method proposed in this chapter to analyze the operational availability of GPS aviation under scintillation is useful to investigate the impact of strong scintillation on GPS aviation. This approach is very different from the previous availability study [Conker *et al.*, 2003] which showed the global trend of scintillation impact on GPS aviation. In particular, the effect of shortened carrier smoothing time under scintillation is first studied by the present work. However, this method relies on an observed data set, so the potential impact of even stronger scintillation than the previous observations is still not answered. The following chapters will overcome this limitation and provide a better picture of the impact of scintillation on GPS aviation.

Chapter 4

Satellite-to-Satellite Correlation of GPS Signal Fades Under Strong Ionospheric Scintillation

4.1 Overview

If electron density irregularities cover almost all of the sky as observed during the previous solar maximum, a GPS receiver may not track enough satellites to form a position solution. An important question that has not been satisfactorily answered is the probability of simultaneous loss of multiple satellites under strong scintillations. Although almost all satellites can be affected by scintillation over the same time-frame, the probability of simultaneous loss of multiple satellites is expected to be low because deep fades of different satellite channels do not necessarily overlap at the exact same epoch (e.g., Figure 3.1, p. 38).

In order to investigate the probability of simultaneous loss, this chapter proposes

a metric to measure the correlation level of two fading channels from the perspective of GPS aviation (Section 4.2). Using this metric, the satellite-to-satellite correlation of deep fades is studied based on real scintillation data (Section 4.3). In addition, this chapter proposes a way to generate correlated fading processes with arbitrary correlation coefficients (Section 4.4). This fading process model enables one to study the impact of scintillation on aviation availability under arbitrary fading rates and arbitrary correlation levels between satellite channels. Hence, the study is no longer limited by the available scintillation data sets. Using this fading process model, the availability of LPV-200 under many severe scintillation scenarios is analyzed in Section 4.5.

4.2 Deep GPS Signal Fades and Correlation Coefficients

Although amplitude fading can occur very frequently under strong scintillation, most of the C/N_0 fluctuations due to scintillation in Figure 4.1 (bottom), for example, are not problematic for GPS aviation as the receiver is able to maintain its tracking lock. However, the deep signal fades (marked in red) causing loss of carrier tracking lock of a receiver are of real concern. Hence, the GPS aviation researchers' primary interest is not how a signal fluctuates, but whether a receiver loses lock due to deep fading.

Although a receiver may lose a few satellites simultaneously, it can still provide position solutions if it tracks at least four satellites with good geometry. Hence, it is important to know how often deep fades, which cause loss of lock, of multiple satellites occur simultaneously. In other words, the correlation of deep fades between satellite channels under scintillation should be well understood. The impact of scintillation on

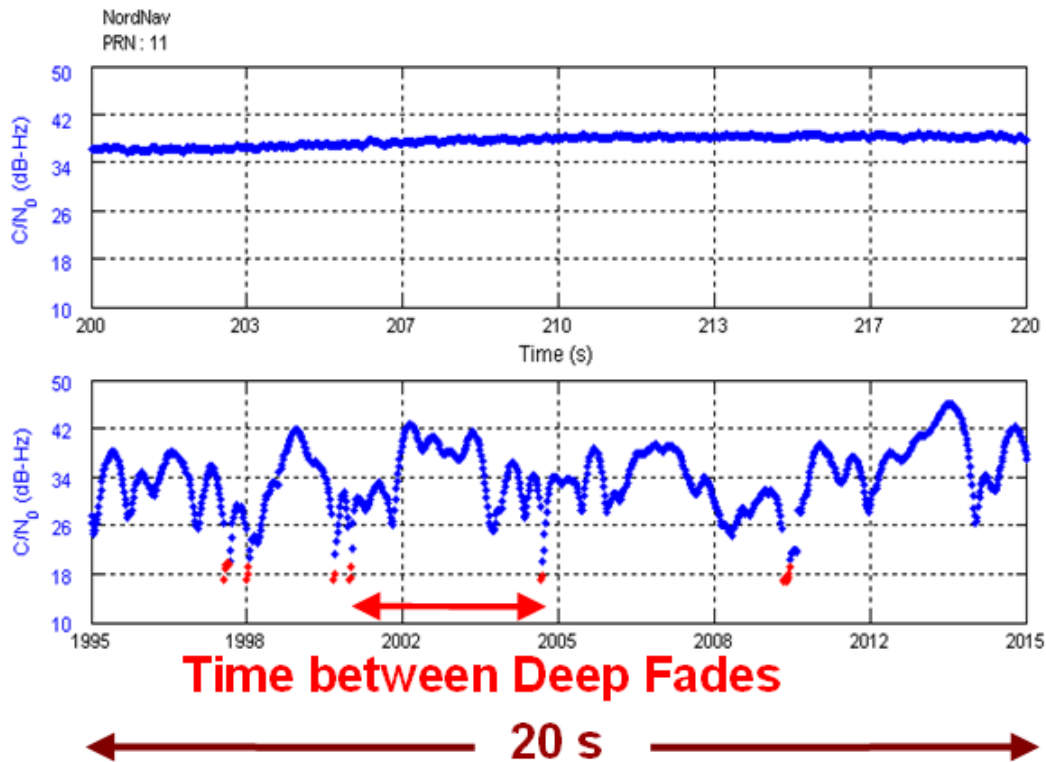


Figure 4.1: Comparison of 50 Hz C/N_0 outputs of nominal (top) and scintillation (bottom) cases. This is a 20 s example from the data collected at Ascension Island during the past solar maximum (2001). Samples from deep fadings (20 dB-Hz or below) are marked in red.

GPS aviation can be mitigated by the geometric diversity of GPS satellites depending on the correlation level.

A high correlation of deep fades here means that the deep fades of different satellite channels occur simultaneously with a high probability. This interpretation of correlation is exactly what interests GPS aviation researchers. However, the conventional definition of the sample correlation coefficient of Equation (4.1) does not provide any information with respect to how often two channels fade simultaneously.

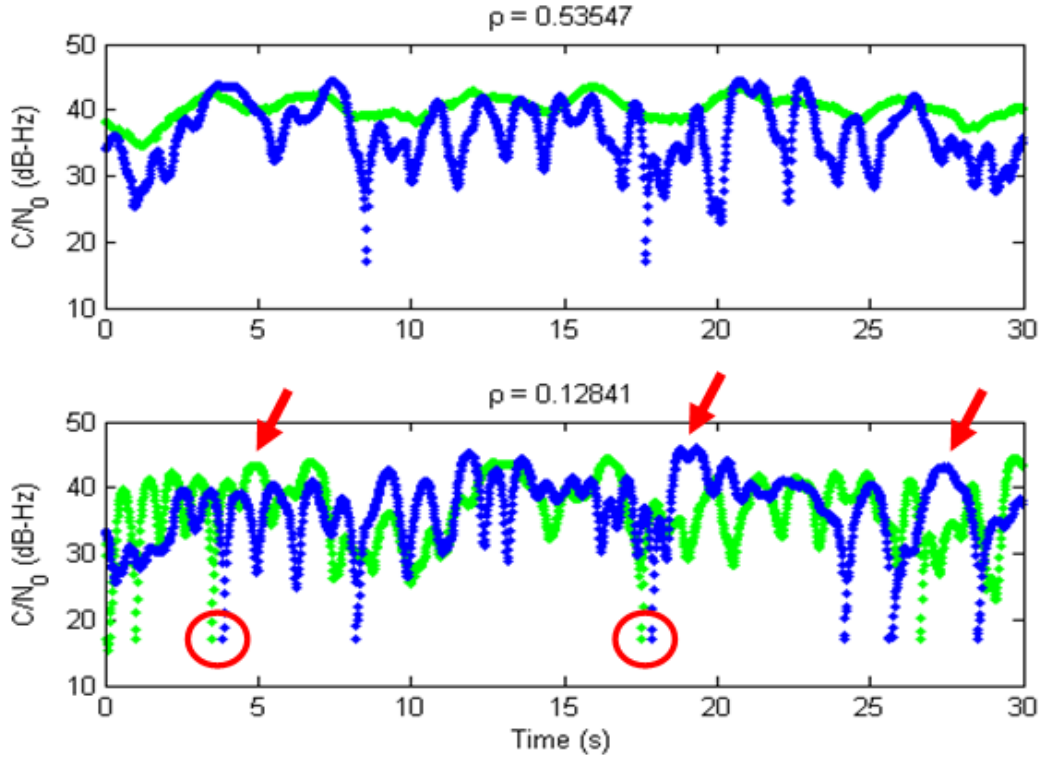


Figure 4.2: Weakness of the conventional sample correlation coefficient. The bottom plot with simultaneous deep fades (red circles) is more problematic for GPS aviation than the top plot. However, the bottom plot has a lower correlation coefficient because of the opposite trends of the two C/N_0 time series (red arrows).

$$\hat{\rho} = \frac{\sum_i (x_i - \bar{x})(y_i - \bar{y})}{\sqrt{\sum_i (x_i - \bar{x})^2} \sqrt{\sum_i (y_i - \bar{y})^2}} \quad (4.1)$$

Figure 4.2 illustrates a weakness in this definition of a sample correlation coefficient. The x_i and y_i of Equation (4.1) are the C/N_0 sample points in green and blue in Figure 4.2. The \bar{x} and \bar{y} are the mean values. In Figure 4.2 (top), only one C/N_0 time series (blue) experiences deep fading. Hence, the receiver would still be able to track the other channel (green) although one channel (blue) is lost for a brief period

of time after deep fading. Figure 4.2 (bottom) represents a more challenging scenario. In this case, two channels sometimes fade simultaneously (red circles). As a result, the receiver loses two channels together during these outages.

Obviously, the bottom plot represents a worse scenario for GPS navigation, but it has a lower sample correlation coefficient (0.13) than the other case (0.54) when the correlation coefficient of Equation (4.1) is applied. This is because the definition of Equation (4.1) merely evaluates the similarity of the trends of two time series. The green series of Figure 4.2 (top) follows the general trend of the blue series. Consequently, the correlation coefficient of the top figure is high. However, the green series of Figure 4.2 (bottom) sometimes goes up while the blue series goes down and vice versa (red arrows), which significantly reduces its sample correlation coefficient. Again, GPS aviation researchers are interested in how often deep fades of different channels occur simultaneously. Deep fades are very brief and C/N_0 sample points during deep fades are few in number. Therefore, the sample points during deep fades have little influence on the sample correlation coefficient obtained by Equation (4.1), which is dominated by the large number of sample points out of deep fades, which are not of primary interest.

Figure 4.2 clearly demonstrates the weakness of the conventional definition of sample correlation coefficient for the study of scintillation impact on GPS aviation. This section suggests an alternative definition of a sample correlation coefficient as Equation (4.2). (T is an observation time window.)

$$\hat{\rho}(T) = \frac{\text{Number of simultaneous deep fades between channel 1 and 2}}{\sqrt{\text{Number of deep fades of channel 1}} \sqrt{\text{Number of deep fades of channel 2}}} \quad (4.2)$$

The sample correlation coefficient of Equation (4.2) exactly describes how often both

channels fade simultaneously, by definition. This correlation coefficient varies between 0 and 1. The mathematical background of this correlation coefficient will be provided in Section 4.4 (p. 70). The correlation study of this work follows this definition of correlation coefficient.

4.3 Satellite-to-Satellite Correlation Under Strong Scintillation

4.3.1 Satellite-to-Satellite Correlation During a Past Solar Maximum Period

As Conker *et al.* [2003] mentioned, a realistic estimate of the probability of simultaneous loss of multiple satellites is needed for evaluating scintillation impact on GPS aviation. A quantitative study about the probability of simultaneous loss of satellites is possible using the correlation coefficient proposed in Section 4.2. If the sample correlation coefficient of Equation (4.2) is applied to study satellite-to-satellite correlation of deep fades, it can be interpreted as Equation (4.3). (T is an observation time window.)

$$\hat{\rho}(T) = \frac{\text{Number of simultaneous deep fades between satellite 1 and 2}}{\sqrt{\text{Number of deep fades of satellite 1}}\sqrt{\text{Number of deep fades of satellite 2}}} \quad (4.3)$$

Following this interpretation, the sample correlation coefficients during the most severe scintillation period of the campaign at Ascension Island (Section 2.2.1, p. 17) are shown in Figure 4.3.

Among the nine day data from Ascension Island, the worst 45 min scintillation

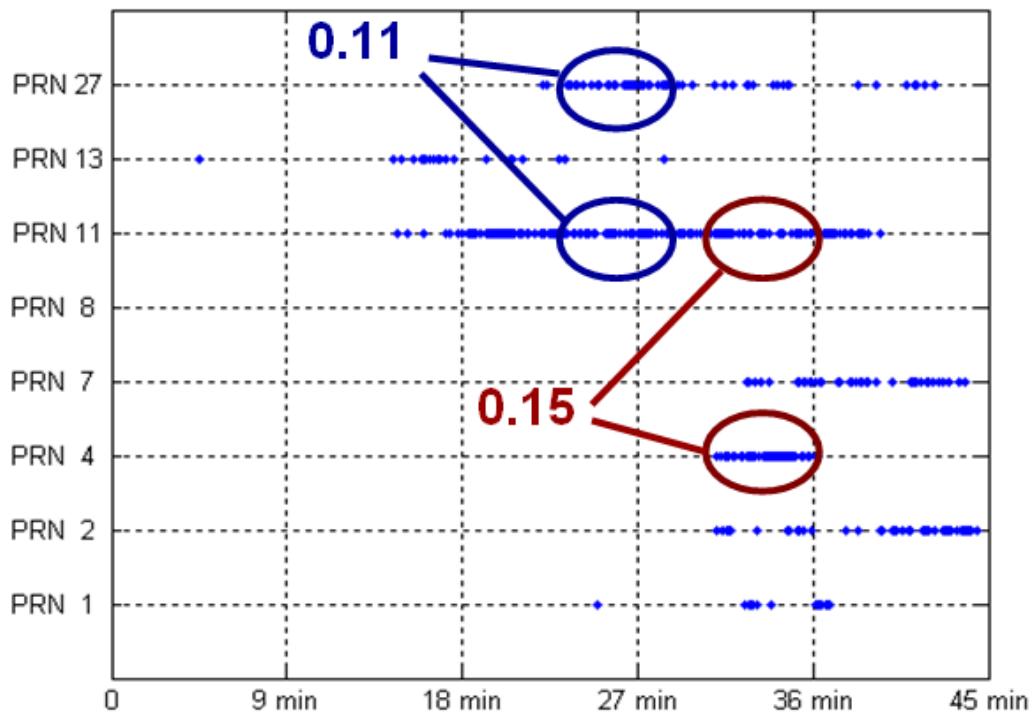


Figure 4.3: Correlation of deep fades between two satellite channels following the definition of Equation (4.3) during a strong scintillation period of the previous solar maximum. (The observation time window, T , is 300 s.) The blue points represent the instances of deep fades at the corresponding satellite channels. Seven satellites were fading during the worst 45 min scintillation at Ascension Island, but the maximum correlation coefficient during the worst 300 s (in ellipses) was only 0.15, which was between PRN 4 and PRN 11.

was selected for Figure 4.3. During the worst 45 min, seven satellites out of eight experienced frequent deep fades (Figure 2.1, p. 18), which implies that electron density irregularities covered almost all portions of the sky. However, the worst-case correlation coefficient between PRN 4 and PRN 11 was only 0.15 during the worst 300 s, and the worst-case correlation coefficient between PRN 11 and PRN 27 was only 0.11. Therefore, although seven satellites were affected by scintillation, the correlation of deep fades between different satellites was very low, which means that the probability of the simultaneous deep fades of multiple satellites was very low.

The correlation coefficient of deep fades is estimated by assuming that the fades of different satellites are “simultaneous” if they are within a 0.5 s range. This is believed to be a conservative estimation because the fading duration at 20 dB-Hz threshold in the Ascension Island data is about 0.2 s (95%) based on the fading duration model in Figure 2.8 (p. 27). El-Arini *et al.* [2003] also observed about 0.2 s fading duration at 20 dB fading in Naha, Japan. If signal fades within 0.2 s are considered to be “simultaneous,” the sample correlation coefficients would be even lower than the coefficients in Figure 4.3.

Note that this worst 45 min scintillation with seven affected satellites is not a common observation even in the equatorial area during solar maxima. For example, El-Arini *et al.* [2003] reported a maximum of four affected satellites under scintillation during the campaign in Naha, Japan, which is also located in the equatorial anomaly region where strong scintillation is highly expected. In addition to the intensity of scintillation, the number of satellites affected by scintillation is also a very important factor for GPS aviation. Hence, seven satellites under lower scintillation intensity, for example, may be more problematic for GPS aviation than three satellites with much higher scintillation intensity.

This section has shown that the correlation of deep signal fades was very low even though almost all satellite channels experienced deep fading. However, the “correlation of loss of lock” of a receiver is not exactly the same as the “correlation of deep fades.” Even under the same signal environment, the correlation of loss of lock can be very different depending on a receiver’s reacquisition capability. For example, if deep fades of two satellite channels are 2 s apart, a receiver does not experience a overlapping loss of lock if it can reestablish tracking the lost channel within 2 s. If it takes longer than 2 s, the receiver experiences overlapping loss of two

Table 4.1: Correlation coefficients of loss of lock between two satellite channels during the worst 300 s at Ascension Island depending on a receiver’s reacquisition time.

Satellite Pair	Reacquisition Time				
	1 s	2 s	3 s	4 s	5 s
PRN 4 & 11	0.18	0.30	0.34	0.38	0.45
PRN 11 & 27	0.18	0.38	0.47	0.53	0.57

satellites. Therefore, the reacquisition time of the lost channel after the reintroduction of signal should also be considered to properly measure the correlation of loss of lock of a receiver. When the sample correlation coefficient of Equation (4.2) (p. 62) is applied to study satellite-to-satellite correlation of loss of lock, it can be interpreted as Equation (4.4).

$$\hat{\rho}(T) = \frac{\text{Number of overlapping losses of lock between satellite 1 and 2}}{\sqrt{\text{Number of losses of lock of satellite 1}}\sqrt{\text{Number of losses of lock of satellite 2}}} \quad (4.4)$$

If a receiver’s reacquisition time is t , the loss of lock of satellite channel 1 and 2 within t results in an overlapping loss. With this interpretation, the sample correlation coefficients between two satellite channels are obtained in Table 4.1. As expected, longer reacquisition times result in higher correlation coefficients of loss of lock.

The difference between the correlation coefficients of deep fades (Figure 4.3) and the correlation coefficients of loss of lock (Table 4.1) should be emphasized. The correlation coefficient of deep fades in Figure 4.3 (p. 64) describes the correlation level of “signal environment” between two satellite channels. The signal environment itself is independent of a receiver’s algorithm and performance. Hence, the reacquisition capability of a receiver was not considered to calculate the correlation coefficients in Figure 4.3. On the other hand, the correlation coefficient of loss of lock in Table 4.1

is affected by a receiver's reacquisition capability on top of the correlation of signal environment. Consequently, it better describes the effective correlation of satellite channels experienced by a receiver.

4.3.2 Correlation of Closely-Spaced Satellites During a Strong Scintillation Period of Solar Minimum

Electron density irregularities can cover large portions of the sky during solar maxima, but GPS signals from different satellites pass through different irregularities on their way to a receiver. Hence, there is no strong physical reason to expect high probability of simultaneous fades between different satellite channels unless two satellites are located very close to each other. In fact, some GPS satellites (e.g., on-orbit spares) are located close to each other in the same orbital plane. The Ascension Island data set does not have scintillation of closely-spaced satellites, but the scintillation of closely-spaced satellites was observed during a Brazil campaign (Section 2.2.2, p. 20). The Brazil data were collected at Sao Jose dos Campos for 36 days (December 2005 – January 2006) during solar minimum using a certified WAAS receiver. Although it was a solar minimum period, strong scintillation with a scintillation index (S_4 index) of about 1.0 was observed on the worst scintillation day (25 December 2005).

Red dots in Figure 4.4 show the locations of loss of satellites during 5 hours (18:00 – 23:00, local time) on 25 December 2005. A certified aviation receiver is at the center of Figure 4.4. The outer circle represents 6 degree elevation and the center point represents 90 degree elevation. The receiver lost carrier tracking lock on low elevation satellites, but loss of low elevation satellites is normal. (The low elevation here means an elevation below 5 degree mask angle.) Scintillation caused

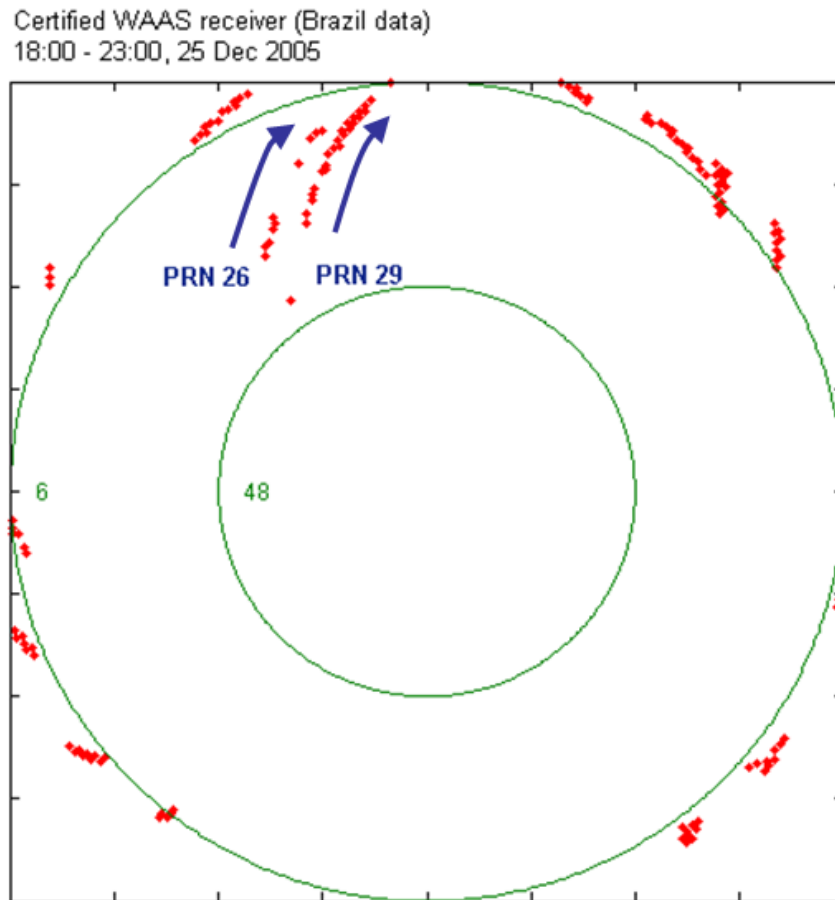


Figure 4.4: Locations of loss of satellites (red dots) during 5 hours on 25 December 2005 at Sao Jose dos Campos, Brazil. Two closely-spaced satellites (PRN 26 and PRN 29) experienced loss of lock for about an hour, but there was no case of simultaneous loss of these two satellites. The data were collected by a stationary aviation receiver located at the center of this figure. The green lines represent elevation angle contours.

loss of higher elevation satellites (PRN 26, PRN 29) as well. These two closely-spaced satellites passed through the northern part of the sky at the same time and experienced loss of lock in the same time-frame for about an hour (22:00 – 23:00, local time). Hence, we can imagine that electron density irregularities were developed on the northern part of the sky during this period. Since the lock status of each satellite channel of the certified aviation receiver is known, the sample correlation coefficient

between two satellite channels can be obtained by Equation (4.4) (p. 66).

These Brazil data were collected at 1 Hz rate and the lock status of the certified receiver was also reported at every second. Interestingly enough, there was not even a single case of simultaneous loss of these two closely-spaced satellites during this one hour period of strong scintillation. Therefore, the sample correlation coefficient obtained by Equation (4.4) is zero during this period. Note that the zero correlation of loss of lock during this period is obtained from the actual response of the certified aviation receiver. The correlation coefficient could be higher if the ionospheric pierce points of the satellites were moving along the same magnetic meridian because of the field-aligned nature of the irregularities causing scintillation at low latitudes. However, the likelihood of this worst-case movement of multiple satellites is expected to be low. Hence, closely-spaced satellites do not necessarily result in the high probability of simultaneous loss.

This section reports very low correlation between closely-spaced satellites on the worst scintillation day of the 36 day campaign in Brazil. However, the Brazil data were collected during solar minimum, so the data do not contain the very frequent deep fades as observed during the past solar maximum. Therefore, the correlation between closely-spaced satellites under very frequent deep fades can be much higher than this observation, which should be carefully studied with extensive data during the next solar maximum (around 2013).

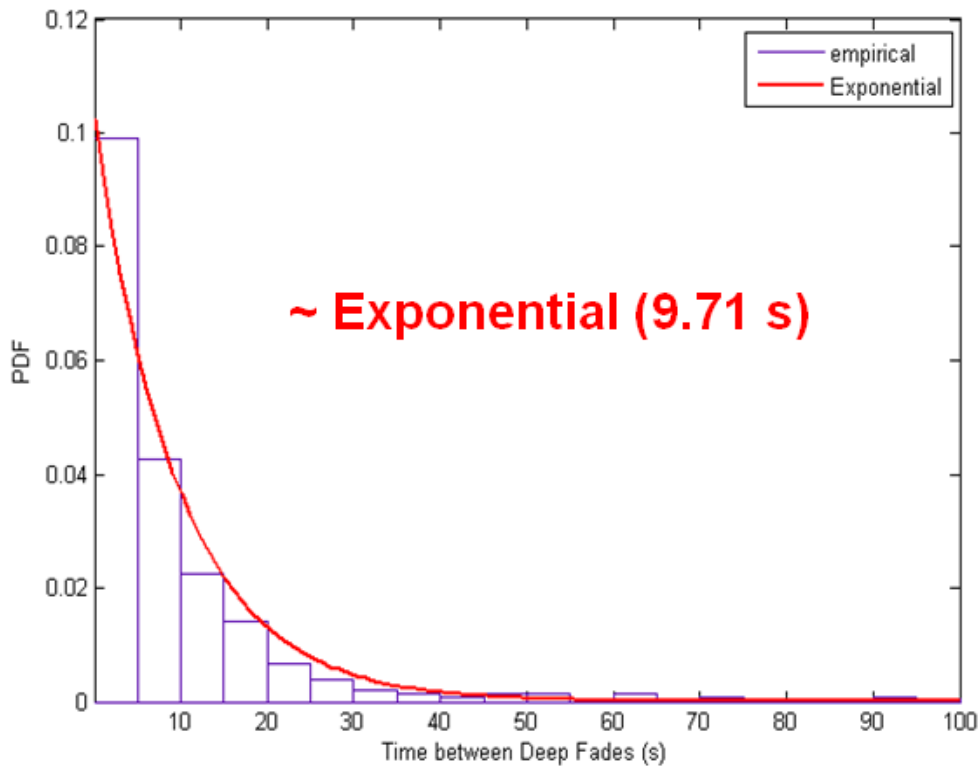


Figure 4.5: Empirical probability density function of time between deep fades during the worst 45 min scintillation at Ascension Island. The time between deep fades approximately follows the exponential distribution with a mean of 9.71 s.

4.4 A Method to Generate Correlated Fading Processes

This section proposes a method to simulate correlated fading channels with an arbitrary correlation coefficient (Equations (4.3) and (4.4)) between two channels. With this correlated fading process model and the observed correlation coefficients in Section 4.3 (p. 63), the availability of LPV-200 under severe scintillation scenarios will be evaluated in Section 4.5 (p. 76). Furthermore, this section provides a mathematical justification of the proposed correlation coefficient in Section 4.2 (p. 59).

In order to develop a method to generate correlated fading processes, this section first studies the statistics of the time between deep fades during the worst 45 min scintillation at Ascension Island. (The definition of time between deep fades is given in Figure 4.1, p. 60.) The empirical Probability Density Function (PDF) of the time between deep fades during the worst 45 min is shown in Figure 4.5. An interesting observation is that the distribution of time between deep fades during the worst 45 min approximately follows an exponential distribution. This data set contains very frequent deep fades. (The median time between deep fades was about 5 s during this worst 45 min, and the mean time between deep fades was about 10 s.)

If less frequent fades are included in the analysis, the distribution in Figure 4.5 would have a fatter tail, and the distribution may not be well modeled by an exponential distribution. However, an empirical PDF with a thinner tail than the actual distribution can provide a conservative representation of the statistics of the time between deep fades for the availability analysis in Section 4.5 (p. 76). Hence, the actual distribution can still be conservatively modeled by an exponential distribution with a thinner tail. In order to provide a conservative model for the availability study in Section 4.5, the worst 45 min data with the most frequent deep fades are selected. In addition, sample points with more than 100 s time between deep fades are discarded for obtaining the empirical PDF. Note that the empirical PDF in Figure 4.5 does not represent nominally observed scintillation of solar maxima. It represents very frequent deep fades which are not typically observed even during solar maxima. The author is not aware of an observed situation with more frequent deep fades under scintillation than Figure 4.5.

An important implication of the exponentially-distributed time between deep fades is that the corresponding counting process of the number of deep fades is a Poisson

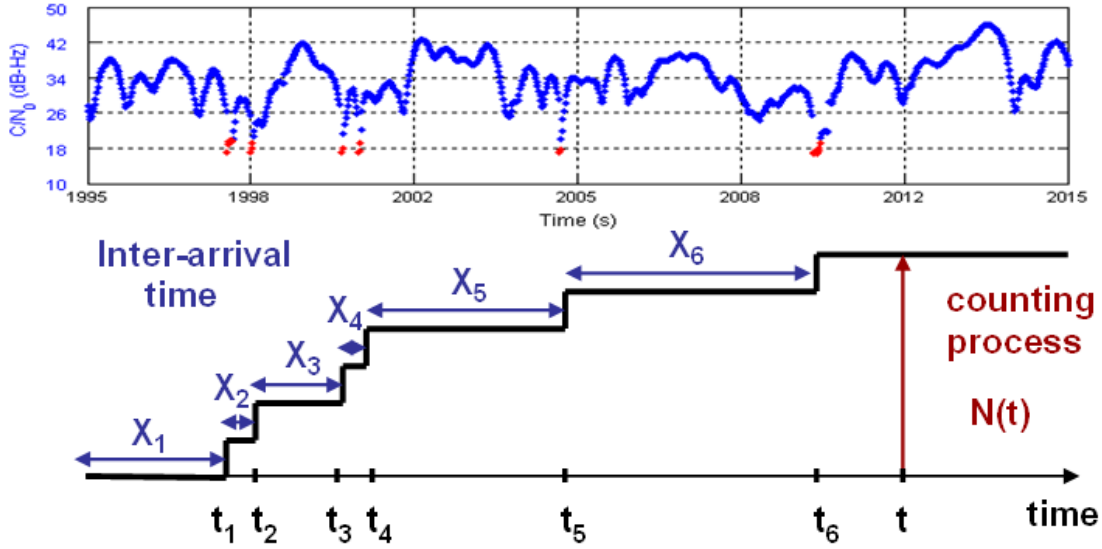


Figure 4.6: Modeling a fading process (a counting process of the number of deep fades) as a Poisson process. The inter-arrival time (time between deep fades), X_i , follows an exponential distribution if, and only if, the counting process of the number of arrivals (number of deep fades), $\{N(t), t \geq 0\}$, is a Poisson process. The arrival times, t_i , represent the instances of deep fades indicated in red on the top plot.

process [Gallager, 1996]. Figure 4.6 illustrates this relationship. The time between deep fades corresponds to an inter-arrival time of a generic arrival process. Since the inter-arrival time (or the time between deep fades) follows the exponential distribution with a mean of 9.71 s, the counting process of the number of arrivals (or the number of deep fades) is the Poisson process of rate $\frac{1}{9.71\text{s}}$. The counting process, $\{N(t), t \geq 0\}$, can have zero and positive integer values for each nonnegative real number t .

The Poisson process has many interesting properties. For instance, if the $\{N(t), t \geq 0\}$ of Figure 4.6 is a Poisson process of rate λ , the $N(t)$ for a given time t is a Poisson random variable with a mean and variance λt . If two independent Poisson processes of rates λ_1 and λ_2 are combined together, the resulting process is still a Poisson process of added rate, $\lambda_1 + \lambda_2$ [Gallager, 1996]. Using this property, two correlated Poisson

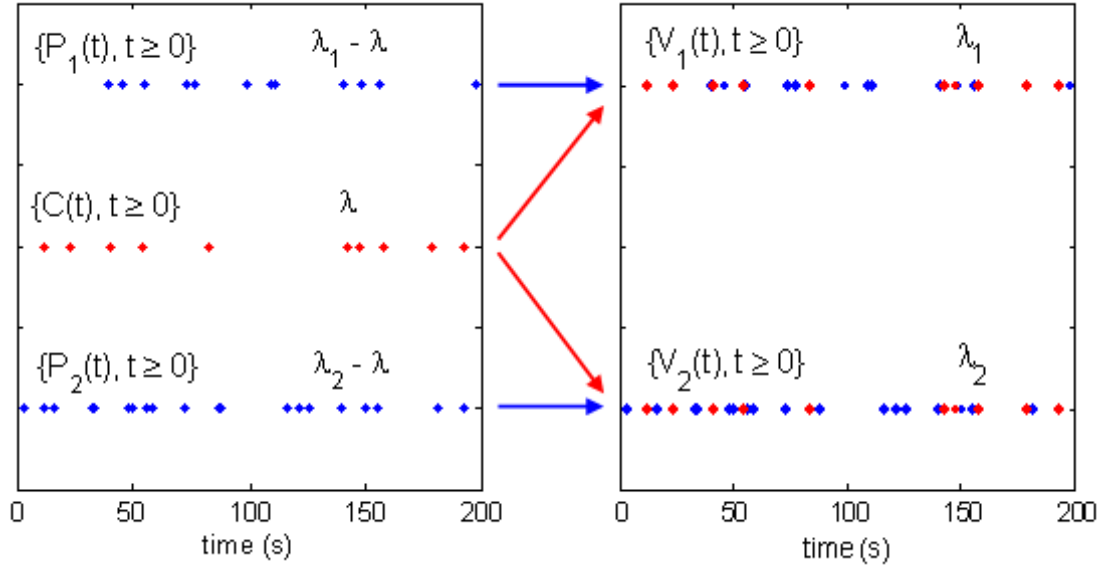


Figure 4.7: Generation of two correlated Poisson processes of rates λ_1 and λ_2 from three independent Poisson processes of rates $\lambda_1 - \lambda$, λ , and $\lambda_2 - \lambda$. A common Poisson process of rate λ (the red Poisson process in the middle) is combined with two independent Poisson processes of rates $\lambda_1 - \lambda$ and $\lambda_2 - \lambda$ to generate two correlated Poisson processes of rates λ_1 and λ_2 .

processes can be generated from three independent Poisson processes (Figure 4.7).

In Figure 4.7, the common Poisson process of rate λ (the red Poisson process) is combined with two independent Poisson processes of rates $\lambda_1 - \lambda$ and $\lambda_2 - \lambda$. The result is two correlated Poisson processes of rates λ_1 and λ_2 . Let the common Poisson process be $\{C(t), t \geq 0\}$ and the two correlated Poisson processes be $\{V_1(t), t \geq 0\}$ and $\{V_2(t), t \geq 0\}$. Since the covariance between $V_1(t)$ and $V_2(t)$ for a given t is the same as the variance of $C(t)$ for the given t (see the Appendix B, p. 121, for proof), the correlation coefficient between $V_1(t)$ and $V_2(t)$ for the given t is obtained as Equation (4.5). Note that $C(t)$, $V_1(t)$, and $V_2(t)$ for a given t are Poisson random variables with means and variances of λt , $\lambda_1 t$, and $\lambda_2 t$, respectively, because $\{C(t), t \geq 0\}$, $\{V_1(t), t \geq 0\}$, and $\{V_2(t), t \geq 0\}$ are Poisson processes of rates λ , λ_1 , and λ_2 ,

respectively.

$$\rho = \frac{\text{Cov}[V_1(t), V_2(t)]}{\sqrt{\text{Var}[V_1(t)]}\sqrt{\text{Var}[V_2(t)]}} = \frac{\text{Var}[C(t)]}{\sqrt{\text{Var}[V_1(t)]}\sqrt{\text{Var}[V_2(t)]}} = \frac{\lambda t}{\sqrt{\lambda_1 t}\sqrt{\lambda_2 t}} = \frac{\lambda}{\sqrt{\lambda_1}\sqrt{\lambda_2}} \quad (4.5)$$

The physical interpretation of λt is the expected number of arrivals of a Poisson process of rate λ during an interval t . Hence, if a fading process is modeled as a Poisson process of rate λ , for example, λt is interpreted as the expected number of deep fades during an interval t . The common Poisson process, $\{C(t), t \geq 0\}$, in Figure 4.7 models the instances of simultaneous deep fades between two satellite channels. The correlated Poisson processes, $\{V_1(t), t \geq 0\}$ and $\{V_2(t), t \geq 0\}$, model the instances of the correlated deep fades of the satellite 1 and satellite 2 channels, respectively. Therefore, the correlation coefficient of Equation (4.5) can be interpreted as follows, if correlated fading processes are modeled as correlated Poisson processes.

$$\begin{aligned} \rho &= \frac{\lambda t}{\sqrt{\lambda_1 t}\sqrt{\lambda_2 t}} \\ &= \frac{\text{Expected number of simultaneous deep fades during } t}{\sqrt{\text{Expected number of deep fades of satellite 1 during } t} \times \frac{1}{\sqrt{\text{Expected number of deep fades of satellite 2 during } t}}} \times \quad (4.6) \end{aligned}$$

This correlation coefficient exactly describes how often satellite 1 and satellite 2 channels experience deep fades simultaneously; hence, this is a proper metric to measure the probability of simultaneous deep fades between two channels.

Once the time series of the signal intensity of two satellite channels are given, the “sample” correlation coefficient, $\hat{\rho}$, of deep fades during an observation time window

T can be estimated using Equation (4.7).

$$\hat{\rho}(T) = \frac{\text{Number of simultaneous deep fades between satellite 1 and 2}}{\sqrt{\text{Number of deep fades of satellite 1}}\sqrt{\text{Number of deep fades of satellite 2}}} \quad (4.7)$$

Once the lock status of two satellite channels of a receiver during an observation time window T is given, the sample correlation coefficient of loss of lock can be similarly estimated from Equation (4.8).

$$\hat{\rho}(T) = \frac{\text{Number of overlapping losses of lock between satellite 1 and 2}}{\sqrt{\text{Number of losses of lock of satellite 1}}\sqrt{\text{Number of losses of lock of satellite 2}}} \quad (4.8)$$

Note that Equations (4.7) and (4.8) are the same as Equations (4.3) and (4.4), respectively, which were used to study the satellite-to-satellite correlation based on the real scintillation data in Section 4.3 (p. 63). Therefore, the definition of the sample correlation coefficient in Section 4.3 is mathematically justified in this section. This definition of a correlation coefficient is mathematically derived from the statistical observation and makes good physical sense.

Furthermore, Figure 4.7 (p. 73) illustrates a way to generate two correlated fading processes with an arbitrary correlation coefficient. The rate of deep fades (the number of deep fades of a satellite channel per unit time) is known from the worst 45 min data (i.e., $\lambda_1 = \lambda_2 = \frac{1}{9.71}$). Hence, we can obtain λ for an arbitrary correlation coefficient, ρ , from Equation (4.5) (p. 74).

$$\lambda = \rho\sqrt{\lambda_1}\sqrt{\lambda_2} = \frac{\rho}{9.71} \quad (4.9)$$

Once λ is obtained for a given correlation coefficient, ρ , three independent Poisson processes, $\{P_1(t), t \geq 0\}$, $\{C(t), t \geq 0\}$, and $\{P_2(t), t \geq 0\}$ in Figure 4.7 of rates

$\lambda_1 - \lambda$, λ , and $\lambda_2 - \lambda$, respectively, can be generated. Finally, the correlated fading processes, $\{V_1(t), t \geq 0\}$ and $\{V_2(t), t \geq 0\}$, of rates λ_1 and λ_2 , respectively, with the correlation coefficient ρ are obtained by combining these three Poisson processes (Figure 4.7).

4.5 Availability Analysis of LPV-200 Under Severe Scintillation Scenarios

The procedure to simulate operational availability of LPV-200 under scintillation was discussed in Section 3.3.1 (p. 44), but it was based on the observed scintillation data from the past solar maximum. Although the availability study in Section 3.3.1 is valuable to analyze the availability impact during observed scintillation periods, the same method cannot be used for simulating the availability under an arbitrary scintillation condition which can be more severe than the previous observations. Now a method to simulate fading channels with any fading rates and correlation coefficients is available from Section 4.4, and therefore this limitation can be overcome.

Figure 4.8 explains how the fading process model is applied to the availability simulation. Compared to the procedure in Figure 3.5 (p. 45), the instances of loss of lock are generated by the fading process model. Hence, severe scintillation scenarios can be incorporated in the availability study. (In Figure 3.5, the instances of loss of lock were obtained from the real scintillation data.) Other settings for the availability simulation such as the carrier smoothing filter model remain the same. Since the reacquisition time of a receiver is an important parameter for aviation availability under scintillation (e.g., Figure 3.10, p. 52), the parametric study of this section considers the reacquisition time as well as the satellite-to-satellite correlation.

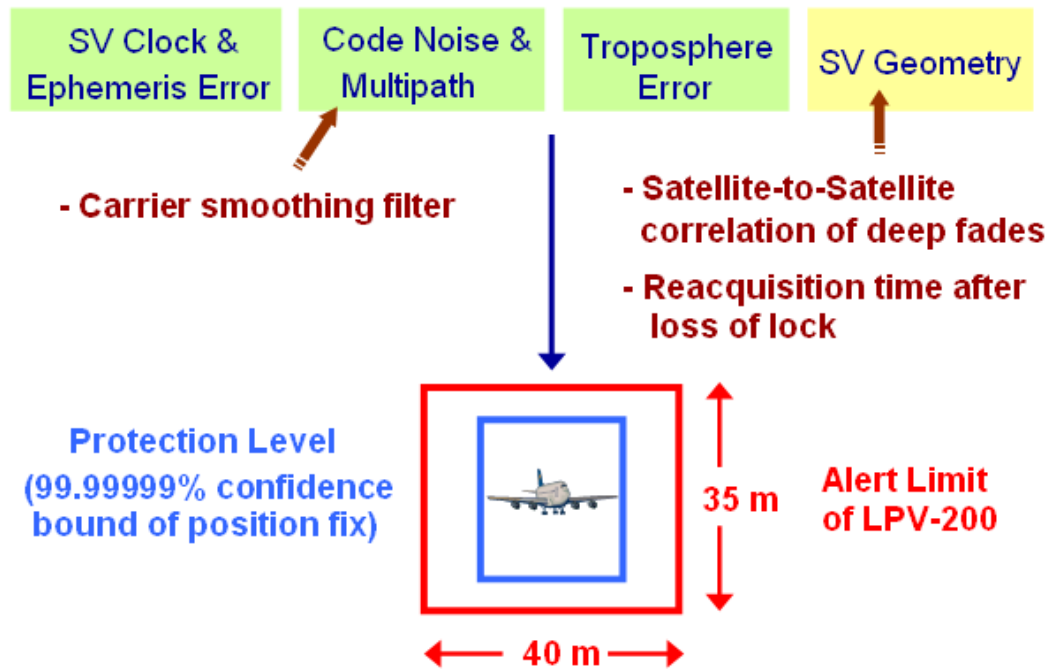


Figure 4.8: Procedure to simulate the availability of LPV-200 under severe scintillation scenarios. The satellite geometry is impacted by the loss of lock after deep fading. (The instances of loss of lock are modeled by correlated Poisson processes considering satellite-to-satellite correlation of deep fades. The duration of loss of lock is determined by a receiver’s reacquisition time.) Frequent loss of lock increases code noise and multipath level in pseudorange measurements. (A carrier smoothing filter model is used to consider this effect as in Figure 3.5.)

Remember that the correlation coefficient of deep fades and the correlation coefficient of loss of lock were distinguished in Section 4.3.1 (p. 65). Since the availability study of this section requires generating a correlated fading environment before considering a receiver’s reacquisition time, the observed correlation coefficients of deep fades (Figure 4.3, p. 64) are used for generating the correlated fading channels. Then, the effect of a receiver’s reacquisition time is parametrically studied.

The operational availabilities of LPV-200 under 45 min severe scintillation scenarios are presented in Figure 4.9 with two parameters: the correlation coefficient

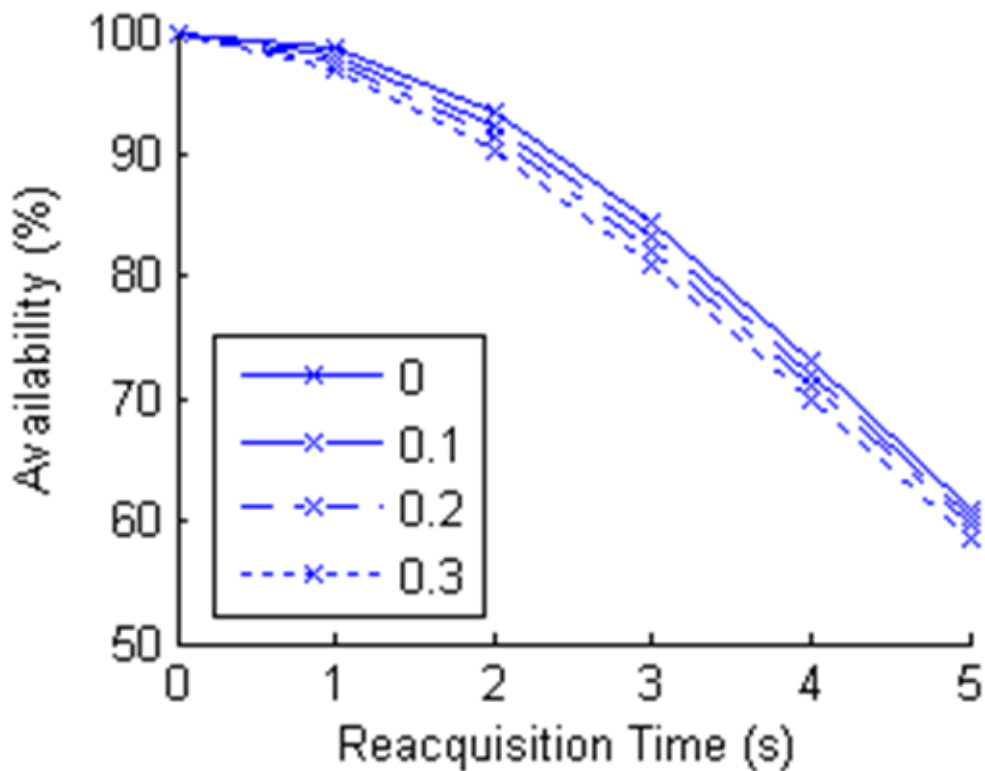


Figure 4.9: Availability of LPV-200 under severe scintillation scenarios with various satellite-to-satellite correlation coefficients of deep fades (0, 0.1, 0.2, and 0.3). The availability result is more sensitive to a receiver’s reacquisition time than the correlation level. A 1 s reacquisition time provides more than 95% availability in these correlation levels.

between two satellite channels and the reacquisition time of a receiver. Under the severe scintillation scenarios, all eight satellite channels are assumed to be affected by the very frequent deep fades observed in Ascension Island for the whole 45 min period. (In the real data, seven satellites were affected only during portions of the 45 min.) Even further, the deep fades of four satellite pairs are assumed to be correlated for the whole 45 min. (In the real data, the most correlated satellite pair experienced simultaneous deep fades with the correlation coefficient of 0.15 for the worst 300 s only.) Although adjacent satellites are more likely to be lost simultaneously under

scintillation, the simultaneously lost satellite pairs (i.e., 4 pairs from the 8 satellites in view) in the analysis of this section are selected in a way to maximize their separations. Since the simultaneous loss of distant satellites reduces the availability more than the simultaneous loss of adjacent satellites, this approach is more conservative than the physically expected situation.

After generating correlated fading processes with a correlation coefficient (every 0.1, from 0 to 0.3) by the method proposed in Section 4.4 (p. 70), a receiver's reacquisition time (every 1 s, from 0 s to 5 s) is applied for the availability calculation. Although the maximum observed correlation coefficient of deep fades in the Ascension Island data was 0.15 (Figure 4.3, p. 64), the simulation considers four different correlation coefficients (0, 0.1, 0.2, and 0.3) for the sensitivity study. As shown in Figure 4.9, the satellite-to-satellite correlation of deep fades has less impact on the availabilities than the reacquisition time of a receiver. With a 1 s reacquisition time, more than 95% availability is expected even under the severe scintillation scenarios with a correlation coefficient of 0.3.

It should be emphasized that the severe scintillation scenarios generated in this section represent much worse conditions than any observation in the literature. In these scenarios, every satellite channel always experiences very frequent deep fades, and four satellite pairs are always lost simultaneously with a given correlation coefficient. In addition, 100% probability of loss of lock under deep fades is assumed. In other words, a receiver is assumed to lose its carrier tracking lock at every single deep fade with a 100% probability. (In Figure 3.11, p. 53, 0% – 100% probabilities of loss of lock were considered, but the most conservative assumption is chosen in this section.) This study focuses on the effect of amplitude fading due to scintillation and does not explicitly consider phase jitter which has been emphasized in [Kintner *et al.*, 2009;

Humphreys *et al.*, 2009]. The amount of phase jitter affects the probability of loss of lock in the 28-30 dB-Hz threshold range of the aviation receiver. Instead, this study conservatively assumes that the receiver loses lock at 30 dB-Hz with 100% probability. Further, a receiver is assumed to lose its L5 channel whenever it loses its L1 channel (100% correlation of loss of lock between L1 and L5 channels).

Even with these severe scintillation scenarios and the conservative steps throughout the analysis, the results show that a 1 s reacquisition time can provide more than 95% availability of LPV-200. Therefore, a fast reacquisition after a brief outage can be a very effective strategy to provide higher availability under the given geometric diversity of satellites and the observed low satellite-to-satellite correlation of deep fades.

4.6 Summary

The correlation of signal fades between satellite channels must be studied to better assess the operational availability of GPS aviation under strong ionospheric scintillation. Although a few researchers have tried to investigate the correlation between fading channels, an appropriate metric to measure the correlation level for GPS aviation applications has not been previously applied. This chapter proposes a better definition of correlation coefficient, which describes the probability of simultaneous deep fades (and the probability of simultaneous loss of lock) between channels.

Using this correlation metric, the satellite-to-satellite correlation was evaluated based on real scintillation data from the past solar maximum. The result quantitatively confirms that the correlation of deep fades between two satellite channels was very low (less than 15% correlation) even during the worst-case scintillation of

the campaign at Ascension Island. It was also observed that the correlation between closely-spaced satellites was low as well during the Brazil campaign. Hence, notable availability benefit from the geometric diversity of satellites is attainable during strong scintillation. If a future GNSS receiver tracks both GPS and Galileo (the European GNSS under development), the number of satellites in view would be approximately doubled. Considering the low satellite-to-satellite correlation, this improved geometry from dual constellations will further increase the aviation availability significantly.

Although the signal environment under scintillation demonstrated low satellite-to-satellite correlation of deep fades, it was shown that the effective correlation experienced by a receiver (i.e., the correlation of loss of lock) can be much higher depending on a receiver's reacquisition capability. Using the correlated fading process model proposed in this chapter, the availability of LPV-200 under severe scintillation scenarios was analyzed with the consideration of a receiver's reacquisition time. The result confirmed that the reacquisition time is the most sensitive parameter for the availability during scintillation under the given satellite geometry.

Chapter 5

Future Dual Frequency GPS Aviation Under Strong Ionospheric Scintillation

5.1 Overview

The previous chapter has discussed the low satellite-to-satellite correlation of deep fades during strong scintillation. Future dual frequency avionics will track a new L5 signal in addition to the current L1 signal for civil aviation. Hence, the correlation between the L1 and L5 channels (frequency-to-frequency correlation) also needs to be studied for better estimating the availability of future dual frequency GPS aviation under strong scintillation. Since L5 strong scintillation data are not available until the next solar maximum (around 2013), this chapter simulates correlated L1/L5 fading processes using the method proposed in Section 4.4 (p. 70) for the availability study.

Section 5.2 performs an availability analysis of LPV-200 under simulated severe

scintillation periods which are much worse than the observed strong scintillation. A new VPL equation is proposed for dual frequency aviation under scintillation. The effect of frequency-to-frequency correlation between the L1 and L5 channels is parametrically studied. After the availability study, the sensitivity of the availability results to the fading rate of the L5 channel is evaluated in Section 5.3.1. Since sudden large changes in ionospheric delay are expected to occur simultaneously with strong scintillation in the equatorial area, large ionospheric gradients must be bounded during a single frequency loss for guaranteeing aviation integrity. The sensitivity of the availability results to the maximum bounded ionospheric gradient is evaluated in Section 5.3.2. Using the newly-proposed method to generate fading processes with both frequency-to-frequency correlation and satellite-to-satellite correlation, the impact of low satellite-to-satellite correlation is analyzed in Section 5.3.3.

5.2 Availability Analysis of Future Dual Frequency GPS Aviation Under Ionospheric Scintillation

This section analyzes the availability of future dual frequency GPS aviation under severe scintillation scenarios. The availability analyses of Chapters 3 and 4 did not fully consider the possible availability benefit from the new L5 signal. Instead, Chapters 3 and 4 assumed the most conservative scenario of 100% correlation of deep fades between L1 and L5 channels under scintillation. In other words, L1 and L5 channels were assumed to be lost simultaneously with a 100% probability under scintillation. This assumption is very conservative, of course. For example, El-Arini *et al.* [2009] reported the correlation coefficient of 0.7 between L1 and L2 channels based on early GPS scintillation data collected in 1989 (L5 strong scintillation data are not

yet available). Although the definition of correlation coefficient in this research is different from the definition used in [El-Arini *et al.*, 2009], the 100% correlation is an extremely conservative assumption. If deep fades of the L1 and L5 channels do not always occur simultaneously, a receiver can take benefit from a backup channel when one frequency is briefly lost. This section relaxes the assumption of 100% frequency-to-frequency correlation and assesses the possible benefit from future dual frequency aviation depending on the correlation level between L1 and L5 channels.

5.2.1 Availability Analysis Procedure

Figure 5.1 illustrates the procedure to analyze the availability of future dual frequency aviation under severe scintillation scenarios. As in Figures 3.5 (p. 45) and 4.8 (p. 77), the carrier smoothing filter model and the iono-free dual frequency code noise and multipath model are used for the analysis in this chapter. Unlike Figure 4.8 however, which considered the satellite-to-satellite correlation of deep fades, Figure 5.1 incorporates the frequency-to-frequency correlation of deep fades. Since the maximum satellite-to-satellite correlation observed during the strong scintillation at Ascension Island was only about 15% (Figure 4.3, p. 64), the satellite-to-satellite correlation is ignored in the first part of the analysis. Later, Section 5.3.3 (p. 97) will discuss the effect of the ignored satellite-to-satellite correlation on the availability results of this chapter.

Currently, only one GPS satellite is broadcasting an L5 test signal [Gao *et al.*, 2009b; Gunawardena *et al.*, 2009]. Hence, the actual correlation level of deep fades between L1 and L5 channels of a satellite during strong scintillation cannot be known until the next solar maximum (around 2013). However, Section 4.4 (p. 70) proposed a method to generate correlated fading processes with any correlation level between

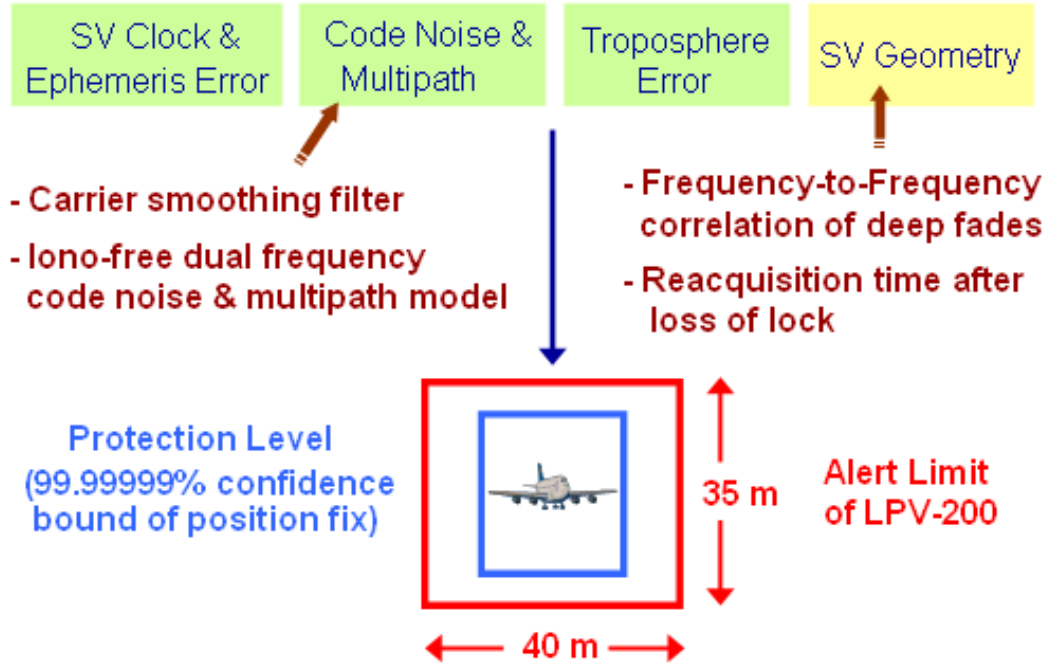


Figure 5.1: Availability simulation procedure considering frequency-to-frequency correlation. The correlated fading process model with frequency-to-frequency correlation is used to simulate the instances of loss of the L1 and L5 channels of each satellite. The low satellite-to-satellite correlation is ignored.

two channels. Although Section 4.5 (p. 76) generated fading processes with satellite-to-satellite correlation, the same method can be applied to generate fading processes with frequency-to-frequency correlation. In this case, $\{V_1(t), t \geq 0\}$ in Figure 4.7 (p. 73) can be interpreted as a fading process of the L1 channel and $\{V_2(t), t \geq 0\}$ can be interpreted as a fading process of the L5 channel. Once L1 and L5 scintillation data are available, the sample correlation coefficient of deep fades between the L1 and L5 channels can be obtained using Equation (5.1). (T is an observation time window.)

$$\hat{\rho}(T) = \frac{\text{Number of simultaneous deep fades between L1 and L5 channels}}{\sqrt{\text{Number of deep fades of L1 channel}} \sqrt{\text{Number of deep fades of L5 channel}}} \quad (5.1)$$

Note that the rate of L1 fading (the number of L1 deep fades per unit time; equivalently, the number of L1 losses of lock per unit time, if a receiver is conservatively assumed to lose lock at every deep fade), λ_{L1} , for the availability simulation of this chapter is obtained from the Ascension Island data (i.e., $\lambda_{L1} = \frac{1}{9.71\text{s}}$) as in Section 4.4. However, the rate of L5 fading is not yet known from real scintillation data. According to Fremouw *et al.* [1978], the amplitude scintillation index (S_4 index) of the L5 frequency (1.176 GHz) is expected to be larger than the S_4 index of the L1 frequency (1.575 GHz).

$$S_{4,L5} = S_{4,L1} \left(\frac{f_{L1}}{f_{L5}} \right)^{1.5} = 1.55 S_{4,L1} \quad (5.2)$$

However, Equation (5.2) does not relate the fading rates of the L1 and L5 channels. Although the signal fluctuations of the L5 channel could be worse than the L1 signal fluctuations, the higher power and better code structure of the L5 signal [Van Dierendonck and Hegarty, 2000] would reduce the chance of loss of lock of the L5 tracking channel. Section 5.2.2 will assume that the L5 fading rate (the number of L5 losses of lock per unit time) is the same as the L1 fading rate. Later, Section 5.3.1 (p. 94) will evaluate the effect of higher L5 fading rates on the availability results.

5.2.2 Availability Results Depending on Ionospheric Delay Estimation

In a future dual frequency operation, ionospheric delay can be directly measured by GPS avionics. Hence, the WAAS satellites do not need to broadcast ionospheric delay estimations for these users. This is a significant benefit over current single

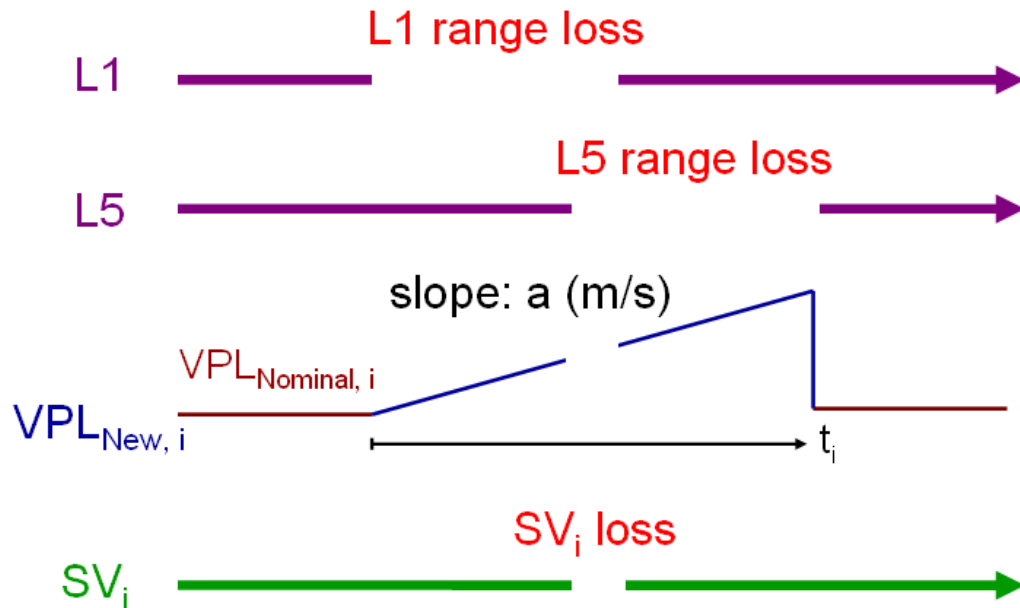


Figure 5.2: Inflation of vertical protection level while ionospheric delay cannot be directly measured. The horizontal axis indicates the time. The t_i is the elapsed time after a single frequency loss of a satellite i . The satellite i is lost when both frequencies are lost. During a single frequency loss, the pseudorange measurements from the other frequency can still be used for position calculations if the protection levels are properly inflated.

frequency aviation. Future GNSS Evolutionary Architecture Study (GEAS) architectures, which will enable worldwide LPV service, rely on this dual frequency upgrade of GPS satellites [Walter *et al.*, 2008; Hegarty and Chatre, 2008]. However, if one frequency is briefly lost due to deep fading, the ionospheric delay cannot be directly measured until both frequencies are tracked. Figure 5.2 illustrates this situation. If both frequencies from a satellite channel are lost, no pseudorange measurement is available from the satellite; hence, the satellite is excluded from the position calculation. If a receiver tracks only the L5 frequency while the L1 frequency is lost after deep fading, for example, pseudorange measurements from L5 are still available although ionospheric delay cannot be measured by a single frequency alone.

The uncertainty of the ionospheric delay error accumulates as the time advances after a single frequency loss. Hence, the protection levels (the confidence bound of the position solutions) must be properly inflated according to the elapsed time after a single frequency loss in order to provide protection from this unknown ionospheric delay error. The inflation of a new Vertical Protection Level (VPL) is conceptually illustrated in Figure 5.2. After a single frequency loss of a satellite i , the contribution to VPL from the satellite i increases with a certain slope, a , as a time, t_i , advances. Once the receiver is tracking again both frequencies of the satellite i , the new VPL drops to the nominal VPL value. The illustration of Figure 5.2 gives insight for understanding the mathematical formula of the newly-proposed VPL given in Equation (5.3).

$$\begin{aligned} \text{VPL}_{\text{New}} &= \text{VPL}_{\text{Nominal}} + \sum_{i=1}^N |S_{U,i} a t_i| \\ &= K_v \sqrt{\sum_{i=1}^N S_{U,i}^2 \sigma_i^2} + \sum_{i=1}^N |S_{U,i} a t_i| \end{aligned} \quad (5.3)$$

The expression for the nominal case VPL, $\text{VPL}_{\text{Nominal}} = K_v \sqrt{\sum_{i=1}^N S_{U,i}^2 \sigma_i^2}$, is given in p. J-1 of [RTCA, 2006]. As explained in [RTCA, 2006], $S_{U,i}$ is “the partial derivative of position error in the vertical direction with respect to the pseudorange error on the i^{th} satellite.” The σ_i^2 is the variance of model distribution that overbounds the true error distribution on the i^{th} satellite. Hence, $\sum_{i=1}^N S_{U,i}^2 \sigma_i^2$ is the “variance of model distribution that overbounds the true error distribution in the vertical axis.” $K_v = 5.33$ is chosen to provide 10^{-7} bound (99.99999% confidence bound) of signal-in-space error, which is required for LPV-200. The inflated VPL term, $\sum_{i=1}^N |S_{U,i} a t_i|$, is added to this nominal case VPL under a single frequency loss. The $a t_i$ is the deterministic model that overbounds the uncertainty of true ionospheric delay error

on the i^{th} satellite at a time, t_i , after a single frequency loss. Note that the time, t_i , is zero when the satellite i tracks both frequencies. The inflation rate, a , must be selected to overbound the uncertainty of true ionospheric delay error under a single frequency loss.

Depending on the selection of the inflation rate, a , three different approaches to bound the ionospheric delay error are evaluated in this section. Under each approach, availability results will be presented with two parameters: the correlation coefficient between L1 and L5 fading channels (every 0.1, from 0 to 1.0), and the reacquisition time of a receiver (every 1 s, from 0 s to 10 s).

The most conservative approach assumes $a = \infty$, which tends the contribution of satellite i to VPL, $|S_{U,i} a t_i|$, toward infinity when satellite i loses either frequency (i.e., when $t_i > 0$). In other words, a receiver does not trust range measurements from a satellite if the receiver loses either the L1 or L5 channel of the satellite because the ionospheric delay cannot be directly measured. Since a satellite is excluded from the position calculation whenever either frequency is lost in this extremely conservative approach, the aviation integrity is always guaranteed. However, the aviation availability would be very low under strong scintillation as shown in Figure 5.3. Even a 1 s reacquisition time cannot provide a high availability ($> 99\%$). As noted in Figure 5.3, a higher correlation between the L1 and L5 channels gives a better availability in this most conservative approach. (A higher frequency-to-frequency correlation means that deep fades of the L1 and L5 channels occur simultaneously with a higher probability.) This is because a receiver does not use range measurements for position calculations unless dual frequency measurements are available. Hence, if a receiver loses one frequency followed by the other, the total duration of the satellite loss would be extended. Therefore, it is better to lose both frequencies together instead of losing

one frequency after the other, if the fading rates of two frequency channels are fixed.

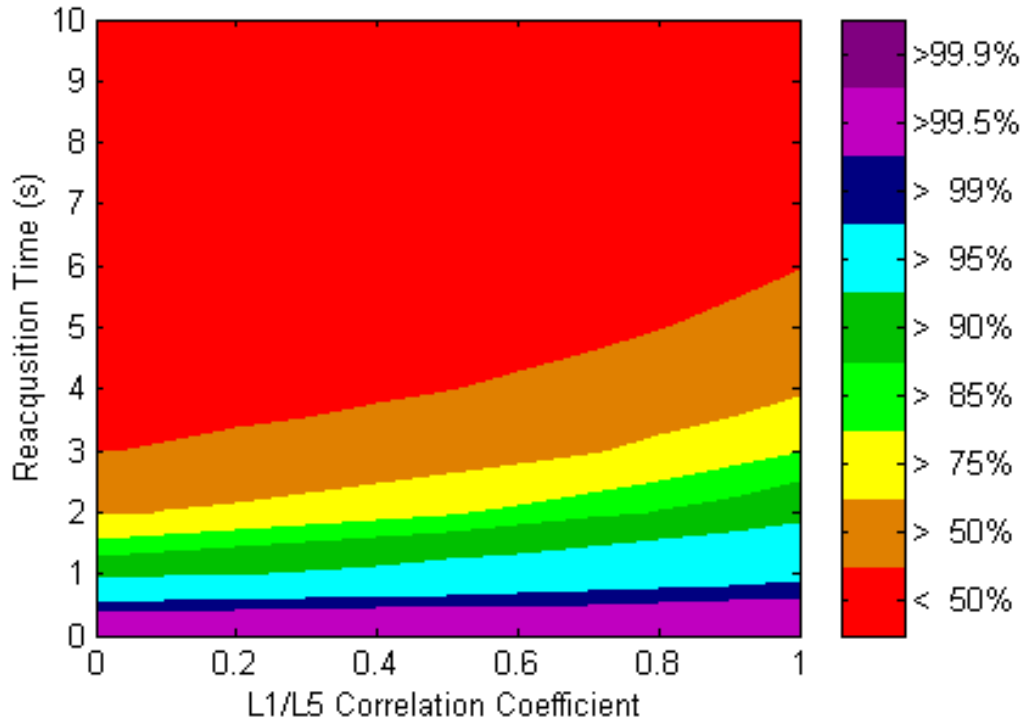


Figure 5.3: Availability contour of LPV-200 under severe scintillation scenarios and the most conservative approach ($a = \infty$) to bound the ionospheric delay error during a single frequency loss. The a is the inflation rate in Equation (5.3). A higher frequency-to-frequency correlation gives a better availability if the fading rates of the L1 and L5 channels are fixed.

Severe scintillation scenarios are generated for the availability analysis of Figure 5.3 as in Section 4.5 (p. 76). The only difference is that Figure 5.3 considers a frequency-to-frequency correlation as a parameter and ignores satellite-to-satellite correlation because it was very low even during strong scintillation periods (Figure 4.3, p. 64). In contrast, Figure 4.9 (p. 78) considered a satellite-to-satellite correlation as a parameter and assumed 100% correlation between the L1 and L5 channels. Note that the method to generate fading processes in Section 4.4 (p. 70) cannot incorporate both satellite-to-satellite correlation and frequency-to-frequency correlation at the

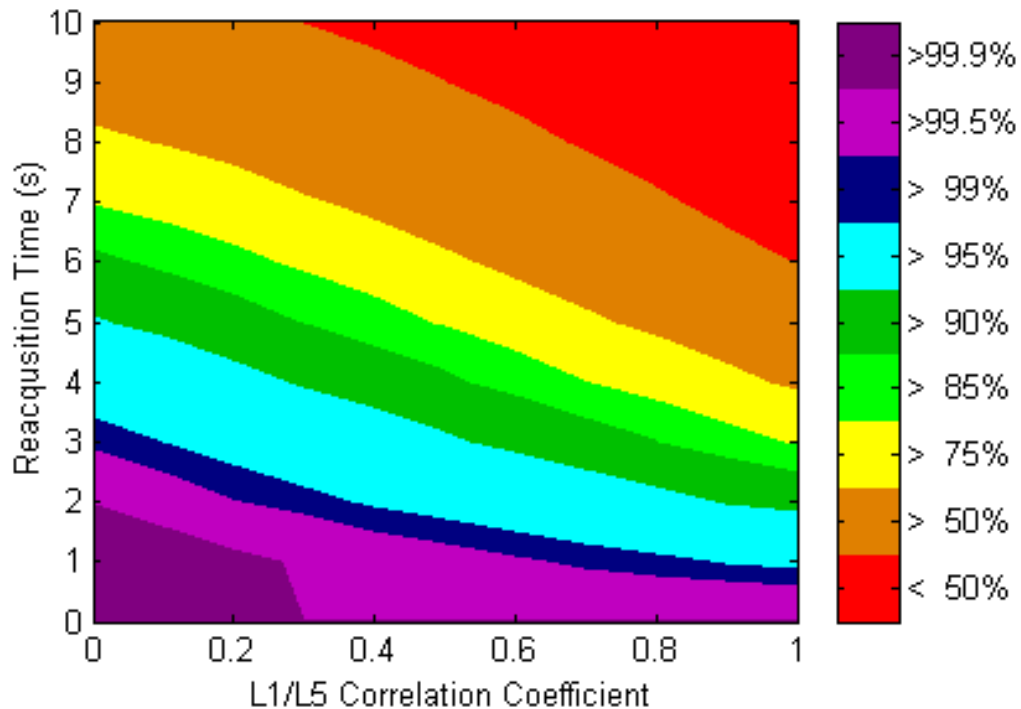


Figure 5.4: Availability contour of LPV-200 under severe scintillation scenarios and the most optimistic approach ($a = 0$, i.e., the ionospheric error does not grow with time.) to bound the ionospheric delay error during a single frequency loss.

same time. That is why each analysis has considered either the frequency-to-frequency correlation as a parameter or the satellite-to-satellite correlation as a parameter.

Another extreme approach is to assume $a = 0$. Since fading duration is very brief (Figure 2.8, p. 27), the ionospheric delay error may not grow significantly during this short period. Hence, a receiver may use the most recent ionospheric delay measurement during the brief period of single frequency loss. In this most optimistic approach, a receiver fully relies on the pseudorange measurements from a single frequency and the most recent ionospheric delay measurement when the other frequency is briefly lost. The availability of LPV-200 under this approach is presented in Figure 5.4. Now the receiver takes the full benefit from the backup frequency. (Hence,

a lower frequency-to-frequency correlation of deep fades provides a better availability.) Although the actual correlation level between the L1 and L5 channels should be validated during the next solar maximum, Figure 5.4 parametrically illustrates the expected availability levels depending on a correlation coefficient and a receiver's reacquisition time under severe scintillation. In this case, a 1 s reacquisition time provides more than 99% availability if the L1/L5 correlation is less than 80%.

Two extreme approaches for bounding the ionospheric delay error have been discussed. The most conservative approach is too conservative to provide high availability even if the integrity is perfectly guaranteed. The most optimistic approach gives high availability, but it may be too optimistic to guarantee the integrity. In the equatorial area, scintillation often accompanies depletions, i.e., regions of steep ionospheric gradient. Thus, sudden large changes in ionospheric delay are expected to occur simultaneously with strong scintillation. Hence, this expected steep ionospheric gradient should be properly bounded by a non-zero inflation rate, a (Figure 5.2, p. 87).

In the third approach, the steepest observed ionospheric gradient and the worst-case geometry of the gradient and the satellites are assumed for guaranteeing the integrity. According to Pullen *et al.* [2009], 425 mm/km was the largest observed gradient in slant ionospheric delay within the conterminous United States (CONUS). The worst-case combination of geometries is illustrated in Figure 5.5. If a satellite and a plane move in the same direction and if the steepest ionospheric gradient moves towards the plane, the relative speed of the Ionospheric Pierce Point (IPP) with respect to the ionospheric gradient could be as high as 950 m/s. As a result, the temporal pseudorange error can grow as fast as about 0.5 m/s. Hence, if $a = 0.5$ m/s is selected in Equation (5.3) (p. 88), the ionospheric delay error due to the maximum

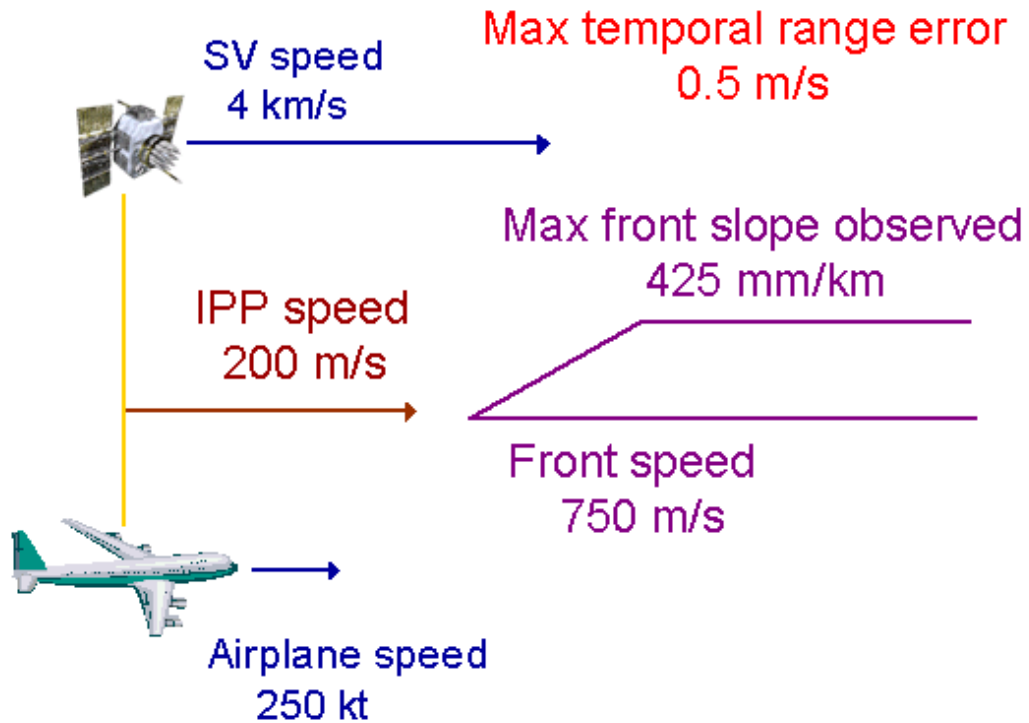


Figure 5.5: Maximum temporal pseudorange error (0.5 m/s) under the worst-case combination of the geometry of a plane, a GPS satellite, and the maximum ionospheric front slope observed in CONUS.

observed gradient under the worst-case geometries for all satellites in view will be properly bounded.

The availability contour with $a = 0.5$ m/s is shown in Figure 5.6. Compared to the most optimistic approach of Figure 5.4, there is not much difference in availabilities if a receiver reacquires the lost channel within 3 s. Therefore, a high availability with the required integrity would be attainable even under the severe scintillation scenarios if the new VPL equation in Equation (5.3) (p. 88) is applied and the inflation rate, a , is properly selected.

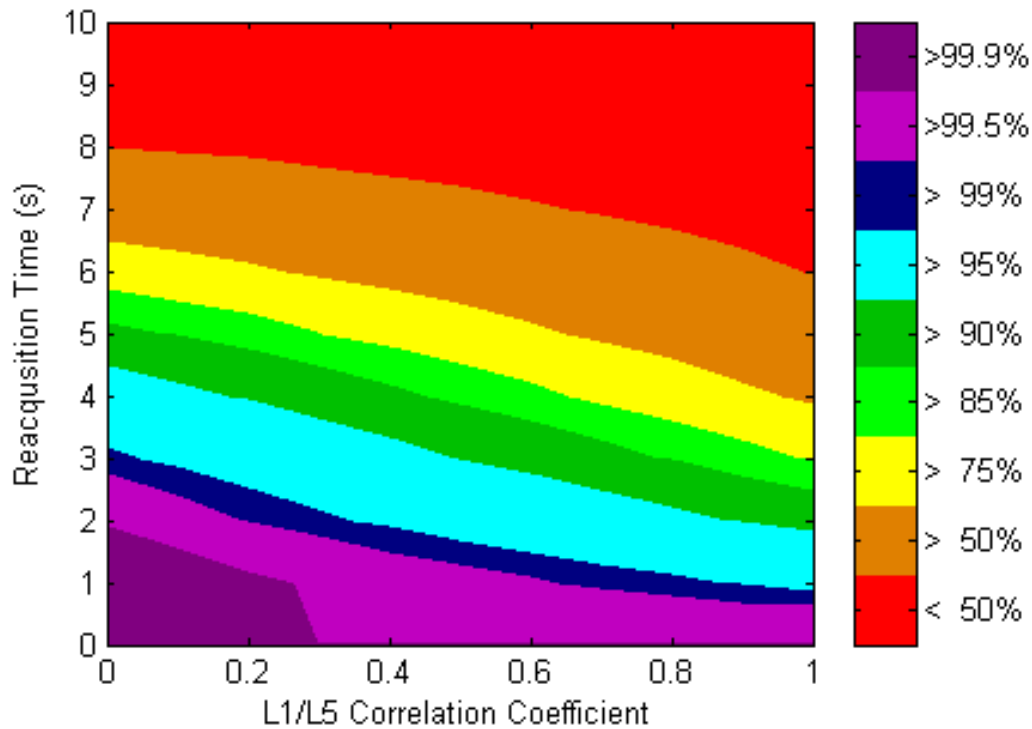


Figure 5.6: Availability contour of LPV-200 under severe scintillation scenarios and the maximum observed ionospheric gradient and the worst-case geometries. $a = 0.5$ m/s is selected to bound the maximum temporal pseudorange error.

5.3 Sensitivity Analysis of the Availability Results

5.3.1 Sensitivity to the Fading Rate of the L5 channel

The previous section assumed that the fading rate of the L5 channel would be the same as the fading rate of the L1 channel. As discussed in Section 5.2.1 (p. 86), this assumption is probable, but it is not yet supported by real scintillation data. Therefore, this section evaluates the sensitivity of the availability results of the previous section to the L5 fading rate.

As the L5 fading rate increases from $1/9.7$ deep fades per second to $1/7.0$, the expected availability slightly decreases (Figure 5.7). However, if a receiver can reacquire

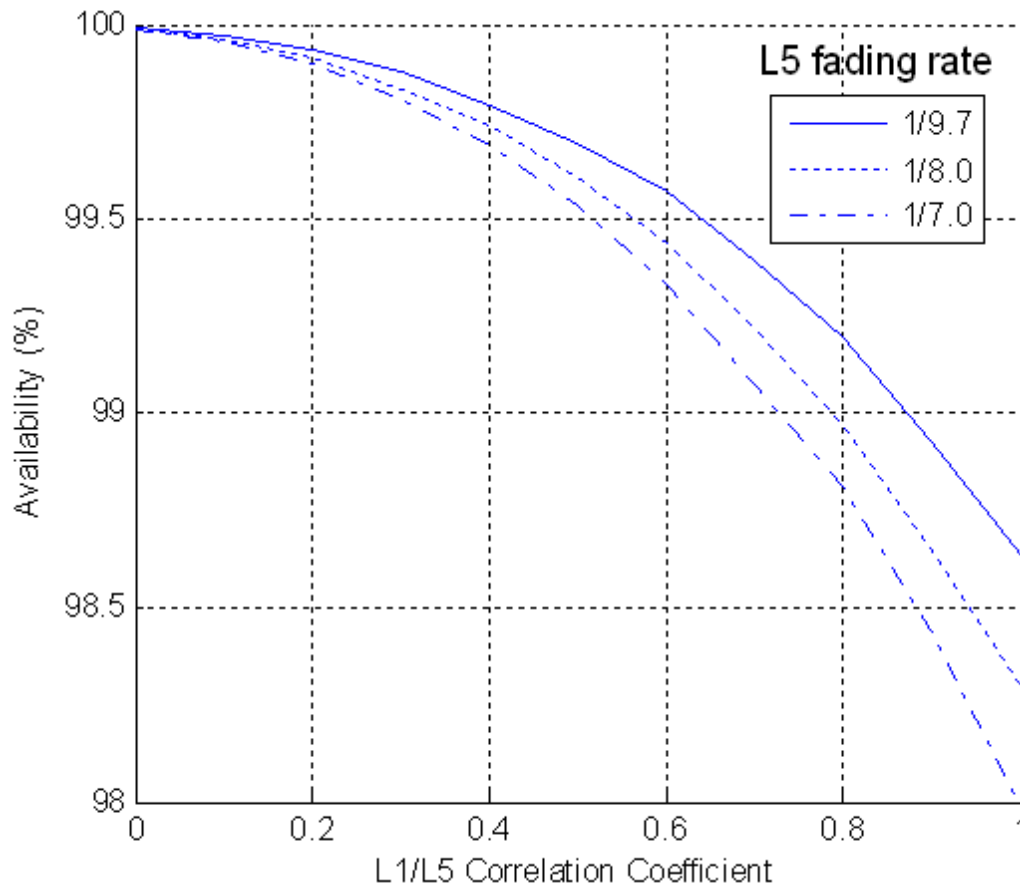


Figure 5.7: Availability of LPV-200 with various L5 fading rates (1/9.7, 1/8.0, and 1/7.0 deep fades per second). The L1 fading rate is fixed to 1/9.7 as observed during the strong scintillation of the previous solar maximum. Reacquisition time is assumed to be 1 s.

the lost channel within 1 s as in Figure 5.7, more than 98% availability is attainable even under the 100% correlation between L1 and L5 and the simulated severe scintillation scenarios. As in Figure 5.6, the new VPL of Equation (5.3) (p. 88) with $a = 0.5$ m/s is used for this analysis. Compared to Figure 5.6, it is evident that the reacquisition time is a much more sensitive parameter than the L5 fading rate.

5.3.2 Sensitivity to the Maximum Bounded Ionospheric Gradient

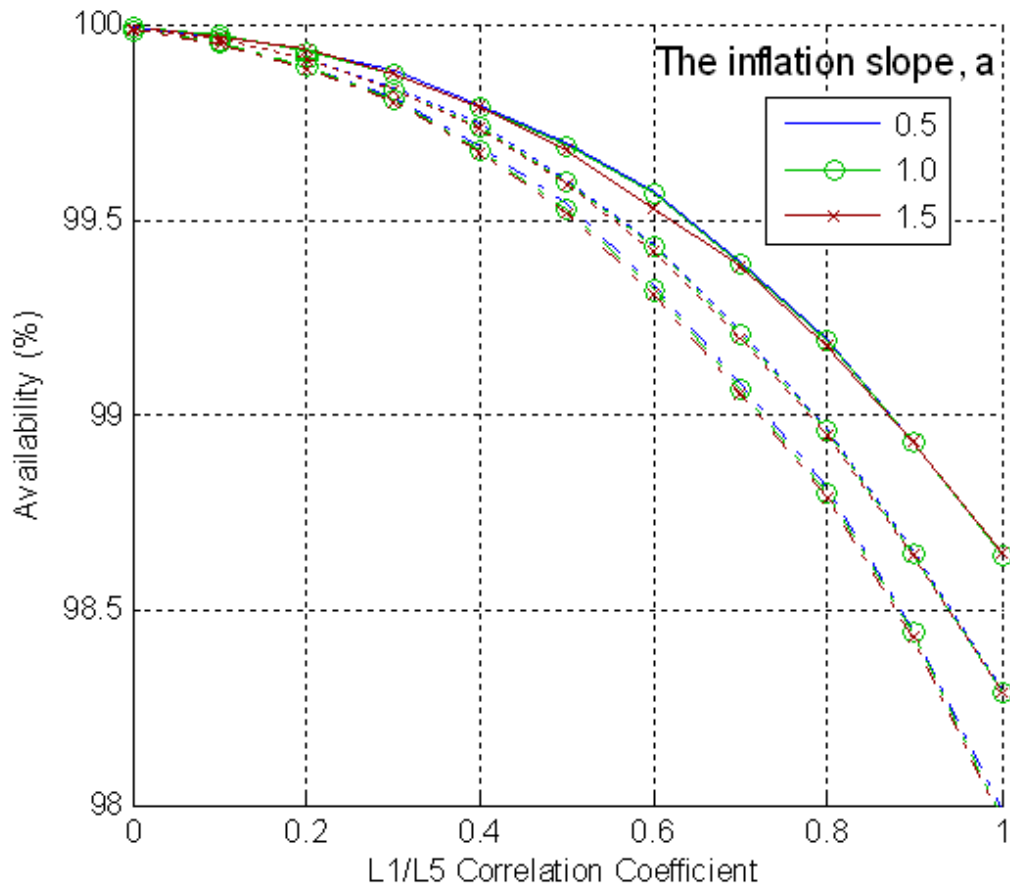


Figure 5.8: Availability of LPV-200 with various inflation rates, a , of the new VPL equation (0.5, 1.0, 1.5 m/s). As in Figure 5.7, three L5 fading rates (1/9.7, 1/8.0, and 1/7.0 deep fades per second) are considered for each value of a . Reacquisition time is assumed to be 1 s.

The sensitivity study of Figure 5.7 assumed that $a = 0.5$ m/s can bound the uncertainty of the ionospheric delay error during a single frequency loss. As explained in Figure 5.5 (p. 93), this is true for the steepest ionospheric gradient observed in CONUS and the worst-case geometry. However, an even steeper ionospheric gradient

may occur in the equatorial area during high solar activity, although it has not been reported in the literature. In order to provide more protection to the uncertainty, $a = 1.0$ m/s or even $a = 1.5$ m/s can be applied. If $a = 1.0$ m/s is used, for example, it can protect against a twice steeper ionospheric gradient (i.e., 850 mm/km) than the steepest observed gradient in CONUS.

The sensitivity of the availability results to the maximum bounded ionospheric gradient is studied with $a = 0.5$, 1.0, and 1.5 m/s (Figure 5.8). Interestingly, the availability result is not very sensitive to the maximum bounded gradient, if a receiver can reacquire a lost channel within 1 s. Even with $a = 1.5$ m/s, which can protect against a three times steeper ionospheric gradient than the steepest observed value and the worst-case geometry, the additional contribution of a satellite to VPL, which is $a t_i$ in Equation (5.3) (p. 88), grows up to 1.5 m. This value is not very significant compared to the VAL of LPV-200, which is 35 m. Hence, the importance of a short reacquisition time under strong scintillation is further emphasized.

5.3.3 Impact of Satellite-to-Satellite Correlation of Deep Fades

The method to generate correlated fading processes proposed in Section 4.4 (p. 70) is useful to simulate the instances of deep fades during arbitrary severe scintillation with any fading rate and correlation coefficient between two channels. However, the method cannot simulate doubly-correlated fading processes. Imagine two GPS satellites with L1 and L5 channels. The L1 channel of satellite 1 and the L1 channel of satellite 2 can be correlated (satellite-to-satellite correlation), for example. Similarly, the L1 and L5 channels of satellite 1 can also be correlated (frequency-to-frequency correlation). The method in Section 4.4 cannot consider both satellite-to-satellite

correlation and frequency-to-frequency correlation at the same time. Hence, the impact of satellite-to-satellite correlation itself has been studied with the conservative assumption of 100% correlation between frequencies as in Section 4.5 (p. 76). Later, the impact of frequency-to-frequency correlation is separately studied with the assumption of 0% correlation between satellites as in Section 5.2 (p. 83). Although the satellite-to-satellite correlation was ignored during the frequency-to-frequency correlation study in this chapter, it was justified because the level of observed satellite-to-satellite correlation during strong scintillation was very low (Figure 4.3, p. 64).

However, it will be still informative to study whether or not the effect of satellite-to-satellite correlation on the availability results of this chapter is really negligible. A new method to generate doubly-correlated fading processes is proposed and explained in Appendix C (p. 123). This method can consider both satellite-to-satellite correlation and frequency-to-frequency correlation simultaneously. A caveat of this method is that the summation of the satellite-to-satellite correlation coefficient and the frequency-to-frequency correlation coefficient cannot be greater than 1. Hence, if a satellite-to-satellite correlation coefficient of 0.15 is assumed as observed during the past solar maximum, a frequency-to-frequency correlation coefficient cannot be larger than 0.85. This section assumes the satellite-to-satellite correlation coefficient of 0.15 and evaluates the availability of LPV-200 for frequency-to-frequency correlation coefficients from 0 to 0.80 (every 0.10).

As shown in Figure 5.9, the availability contour does not present a significant difference from the availability contour in Figure 5.6 (p. 94) which ignored the effect of satellite-to-satellite correlation. Therefore, the 15% satellite-to-satellite correlation observed during the past solar maximum does not significantly impact the availability of LPV-200. The effect of frequency-to-frequency correlation is more important, and

the effect of a receiver's reacquisition time is paramount.

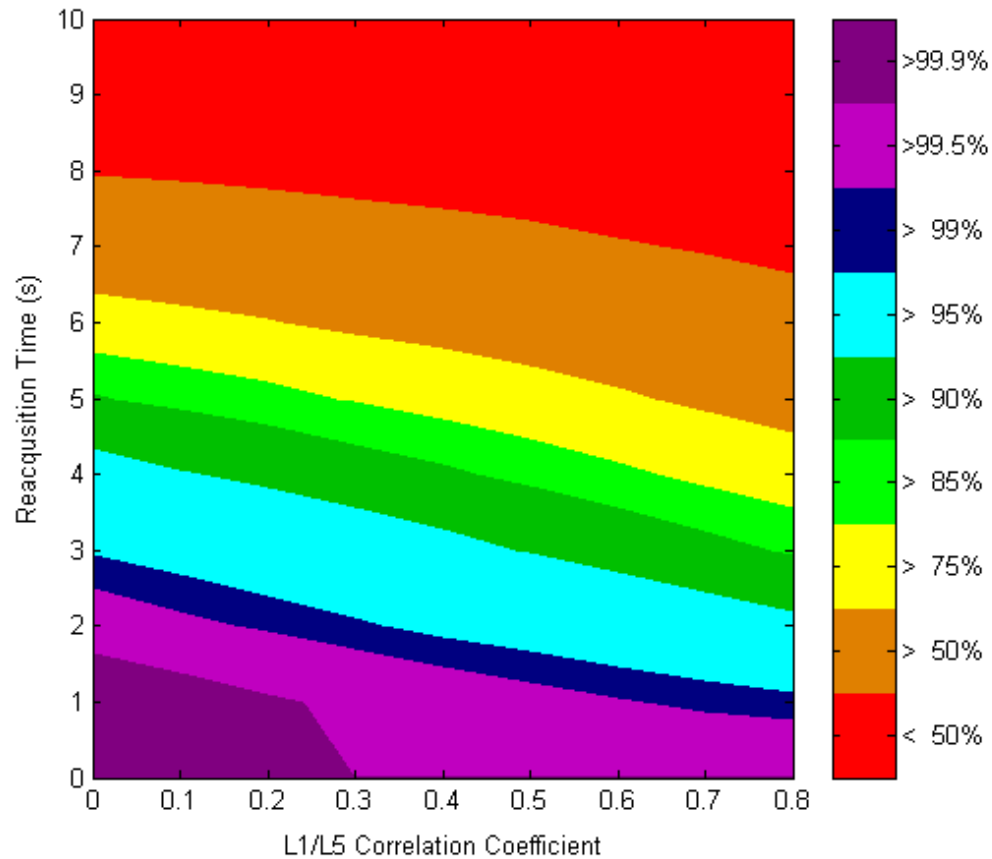


Figure 5.9: Availability contour of LPV-200 with the consideration of both satellite-to-satellite correlation (15% correlation) and frequency-to-frequency correlation (every 10%, from 0% to 80%). The 15% satellite-to-satellite correlation does not noticeably change the availability result from Figure 5.6.

As emphasized in Section 4.5 (p. 79), the severe scintillation scenarios simulated for the availability study in this chapter are much worse than the real observations during the past solar maximum. Figure 5.10 compares the instances of loss of lock during the observed strong scintillation period and the simulated severe scintillation

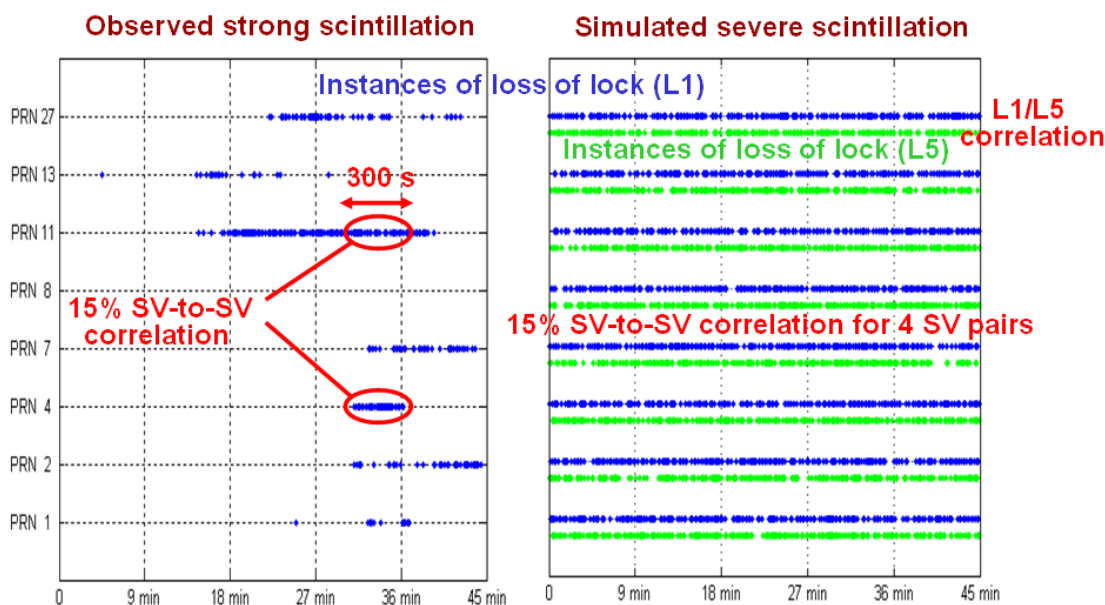


Figure 5.10: Comparison between the observed strong scintillation and the simulated severe scintillation. Each dot indicates the instance of loss of lock of the corresponding channel (a blue dot for the L1 channel and a green dot for the L5 channel). During the simulated scintillation, a receiver loses lock on L1 and L5 very frequently for the whole 45 min.

period. During the real scintillation from the past solar maximum, seven GPS satellites lost lock for fractions of 45 min. However, during the simulated scintillation used for the availability analysis, all eight satellites frequently lose lock for the whole 45 min, which is much worse than the real scintillation. Although the real scintillation data was recorded by an L1-only receiver, correlated L1 and L5 channels are generated for the dual frequency simulation. In addition to this frequency-to-frequency correlation, 15% satellite-to-satellite correlation is applied using the method in Appendix C (p. 123) for the four satellite pairs during the whole 45 min. (The satellite pairs are conservatively selected to maximize their separations as in Section 4.5, p. 76.) In the real scintillation, the 15% correlation occurred during the worst 300 s

only. Other conservative assumptions in Section 4.5, such as 100% probability of loss of lock at deep fades, are carried over for the availability study in this chapter.

Even with this severe scintillation scenario and the conservative steps throughout the analysis, more than 99% availability of LPV-200 is achievable if a receiver can reacquire the lost channel within 1 s and the L1/L5 correlation coefficient is less than 0.8 (Figure 5.9, p. 99). Remember that a 1 s reacquisition time could provide more than 99.9% availability of LPV-200 during the worst 45 min scintillation even with the assumption of 100% correlation between the L1 and L5 channels (Figure 3.9, p. 50). This difference in the availability results (99% availability vs. 99.9% availability) is due to the fact that the severe scintillation scenario of this chapter is much worse than the observed scintillation as explained in Figure 5.10 (p. 100).

5.4 Summary

The expected availability benefit from future dual frequency aviation was parametrically studied in this chapter. In order to guarantee aviation integrity during a single frequency loss, the uncertainty of ionospheric delay error must be properly bounded. A new VPL equation to protect against the ionospheric delay error was proposed, and three different approaches to bound the uncertainty were compared. Two extreme approaches (i.e., the inflation rate $a = \infty$ or $a = 0$ in Equation (5.3), p. 88) are either too conservative or too optimistic. By a proper selection of the inflation rate, high availability of LPV-200 is attainable while still guaranteeing integrity.

If the L5 fading rate is higher than the worst-case L1 fading rate observed at Ascension Island, the availability would be slightly reduced. However, the L5 fading

rate is not a very sensitive parameter, especially when the sensitivity to the reacquisition time is compared. The sensitivity study showed that high availability is attainable even under the ionospheric gradient that is three times steeper than the steepest gradient observed in CONUS. The impact of the ignored satellite-to-satellite correlation is incorporated into the analysis via the proposed doubly-correlated fading process model. The result confirmed that the low satellite-to-satellite correlation during strong scintillation does not meaningfully change the availability results.

Chapter 6

Suggestion for Future Dual Frequency Aviation Receiver Performance Standards

6.1 Overview

Although a receiver may lose its carrier tracking lock frequently under strong scintillation, a high level of aviation availability is still achievable if the receiver has fast reacquisition capability after very brief outages. After summarizing the availability benefit of fast reacquisition in Section 6.2 and discussing the observed performance of a certified WAAS receiver during strong scintillation in Section 6.3, an additional requirement for future dual frequency aviation receiver performance standards is suggested in Section 6.4.

6.2 Benefit of Fast Reacquisition Capability Under Scintillation

The availability benefit of fast reacquisition capability after loss of lock under scintillation has been demonstrated in Chapters 2 through 5. Figure 3.2 (p. 39) showed that the number of simultaneously-tracked satellites under scintillation strongly depends on a receiver's reacquisition time. The expected availability level of LPV-200 during a strong scintillation period was also a strong function of the reacquisition time (Figure 3.10, p. 52). Figure 3.12 (p. 54) showed that a moderate reacquisition time of 4 s could provide 100% availability of RNP-0.1 (horizontal navigation) even with the conservative assumption of 100% probability of loss of lock at every deep fade. Hence, the focus of the study thereafter was on the availability of LPV-200 (vertical navigation) which has more stringent alert limits than the case of RNP-0.1.

The analyses of Chapters 4 and 5 relied on the simulated severe scintillation scenarios which are much worse than the real observations. The impact of satellite-to-satellite correlation with correlation coefficients below 0.3 on the availability of LPV-200 is not significantly different from the case of zero correlation between satellites (Figure 4.9, p. 78). The worst-case satellite-to-satellite correlation during the Ascension Island campaign was only about 0.15 for the worst 300 s (Figure 4.3, p. 64). Therefore, the satellite-to-satellite correlation was ignored for the analysis in Figure 5.6 (p. 94) which considered the frequency-to-frequency correlation only. Later, the assumption of zero satellite-to-satellite correlation was justified by the result in Figure 5.9 (p. 99). Figure 5.9 considered both the frequency-to-frequency correlation and the satellite-to-satellite correlation using the newly-proposed simulation method.

Figure 5.6 (p. 94) confirmed that a high availability (more than 99%) of LPV-200

can be achieved even under the severe scintillation scenarios and the conservative assumption of 100% probability of loss of lock at deep fade, if a future dual frequency aviation receiver can reacquire the lost channel within 1 s and the new VPL equation is applied. Note that the real scintillation is expected to be less severe than the simulated scintillation scenarios for Figure 5.6. Hence, the 99% availability would be a lower bound of the actual availability of LPV-200 during real scintillation. Remember that strong scintillation usually persists only for several hours after the local sunset in the equatorial area. The availability analyses in this research considered the worst 45 min of a day. Therefore, the 99% availability during the worst 45 min of a day implies that the average operational availability for 24 hours of solar maxima will be much higher than 99%.

6.3 Reacquisition Performance of a Certified Aviation Receiver

Now it becomes evident that fast reacquisition capability is paramount to guarantee high aviation availability during scintillation. However, the reacquisition time cannot be arbitrarily short. A reasonable suggestion for the reacquisition time limit under current receiver technology can be obtained by observing the performance of a certified aviation receiver during scintillation. (As mentioned in Section 3.2.1 (p. 37), the current WAAS MOPS specifies 20 s reacquisition time limit for signal outages of 30 s or less. However, the 20 s limit is not short enough to guarantee high availability during strong scintillation.)

A certified WAAS receiver was deployed during the Brazil campaign (Section 2.2.2, p. 20). Although the campaign was performed during a solar minimum period,

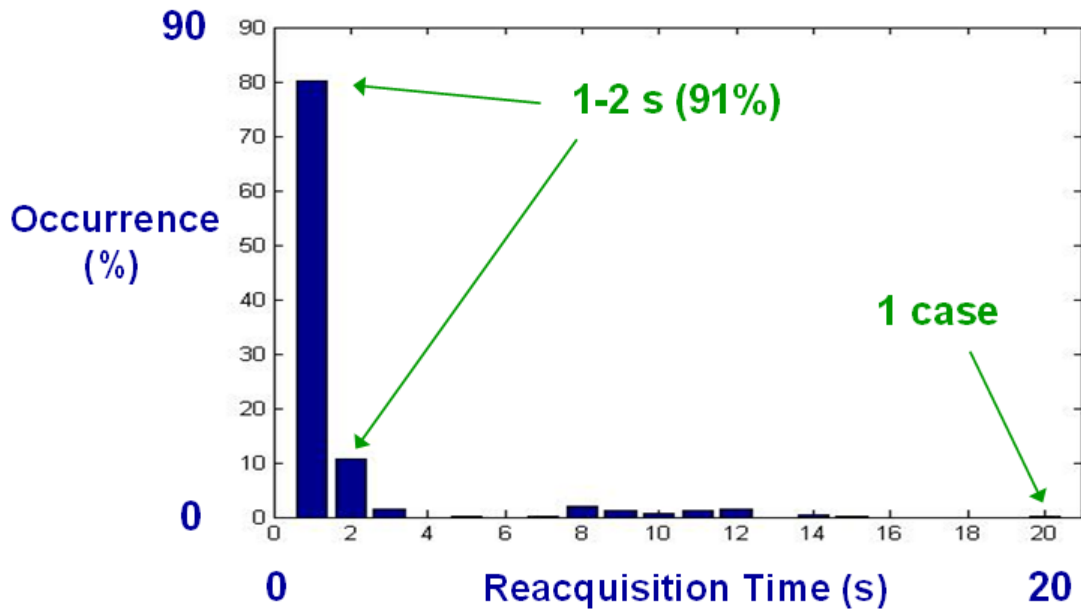


Figure 6.1: Observed reacquisition times of a certified WAAS receiver during the 36 day campaign in Brazil. The performance of the certified receiver was much better than the current requirement of a 20 s reacquisition time.

strong scintillation with S_4 index of about 1.0 was sometimes observed. During the 36 day campaign, the certified WAAS receiver always satisfied the 20 s reacquisition time limit of the WAAS MOPS. There was one case of 20 s loss of a satellite but the certified receiver reacquired the lost channels within 1–2 s for 91% of the cases (Figure 6.1). Hence, the certified aviation receiver was capable of performing much better than the WAAS MOPS requirement. This is mainly because the signal outages under scintillation are very brief. Although the MOPS requirement considers outages of 30 s or less, the observed fading duration at the expected tracking threshold of the aviation receiver was only about 0.2 s (95%).

The algorithm of the certified WAAS receiver might already be designed to manage short signal outages properly because it demonstrated fast reacquisition capability during the campaign. The idea of “coasting” was introduced in Section 2.4 (p. 23).

If the aviation receiver kept its tracking loops close enough to the correct value for 1 s, for example, it could immediately reestablish tracking the lost channel when the signal is reintroduced within that second. Therefore, a simple receiver algorithm coasting the tracking loop for 1 s before initiating full reacquisition mode enables fast reacquisition after a short signal outage such as the case of scintillation. The coasting of 1 s is not difficult to implement. For example, a receiver would change its tracking loop to Frequency Lock Loop (FLL) when Phase Lock Loop (PLL) is broken after deep fading. Once the signal comes back, the receiver would quickly change the tracking loop back to PLL with the correct Doppler information from FLL. Since the required coasting time is very short, better implementations of 1 s coasting are certainly expected under the current receiver technology. Remember that the Hatch filter must be reset right after the loss of phase lock. In order to guarantee the integrity, ambiguous carrier information while coasting must not be used for carrier smoothing purposes (Section 2.5, p. 31).

In order to satisfy the 1 s reacquisition time, a receiver need not perform extensive safety checks before reintroducing the lost channel into the position calculation. The 1 s reacquisition time here means that a receiver reestablishes tracking a lost channel and reintroduces the channel into the position calculation in 1 s. Hence, “reintroduction time” may be a better term but it is called “reacquisition time” in the WAAS MOPS. Under the current MOPS requirement allowing a 20 s reacquisition time, a receiver may perform extensive safety check even after a very brief outage, but a minimal safety check may be enough for very brief outages.

Note that the observation of Figure 6.1 is from a solar minimum period. As mentioned, strong scintillation with S_4 index of about 1.0 was sometimes observed during the period, but the signal fades were not as frequent as the case of solar

maximum (Figure 2.10, p. 30). Although a 1 s reacquisition time is not far from the performance of Figure 6.1, there are no real performance data from an aviation receiver under the very frequent fades of solar maxima. Under this stressing case, the aviation receiver may take a longer time than Figure 6.1 to reacquire lost channels, which should be validated in the next solar maximum.

6.4 New Performance Requirement Under Very Short and Frequent Signal Fades

The signal outages under scintillation are much briefer than the 30 s outages under RFI which are considered in the current MOPS requirement. Under brief outages (less than 1 s, close to 0.2 s) due to scintillation, there is no compelling reason for a receiver to take 20 s to reacquire the lost channel although the 20 s reacquisition time is allowed by the current requirement. In order to prevent the unnecessary delay of reacquisition during scintillation, an additional requirement for future dual frequency aviation receiver performance standards was suggested at the standards committee working group (RTCA Special Committee-159, Working Group-2) meeting on 24 June 2009 [Seo *et al.*, 2009d]. The proposed requirement is described below.

2.1.1.9 Satellite Reacquisition Time

2.1.1.9.1 Satellite Reacquisition Time under Short Signal Outages

For satellite signal outages of 30 seconds or less when the remaining satellites provide a GDOP of 6 or less, the equipment shall reacquire the satellite within 20 seconds from the time the signal is reintroduced. This requirement applies to a satellite with the minimum signal power in the presence of interfering signals as described in Appendix C.

Note: For SBAS satellites, the momentary loss of signal does not obviate any of the time out intervals defined for SBAS data in Section 2.1.1.4.9. The equipment can continue to use data until it times out.

2.1.1.9.2 Satellite Reacquisition Time under Very Short Signal Outages

For satellite signal outages of 1 second or less when the remaining satellites provide a GDOP of 6 or less, the equipment shall reestablish tracking the satellite within 1 second from the time the signal is reintroduced. This requirement applies to a satellite with the minimum signal power in the presence of interfering signals as described in Appendix C.

Note: Equipment should be able to reestablish tracking satellites within 1 second from the time the signal is reintroduced under conditions of strong ionospheric scintillation that could cause short (1 second or less) and frequent (every 5 seconds) signal fades during solar maxima at equatorial latitudes.

The requirement in the proposed Section 2.1.1.9.1 (Satellite Reacquisition Time under Short Signal Outages) is the same as the requirement in the current Section 2.1.1.9 (Satellite Reacquisition Time) in the WAAS MOPS [RTCA, 2006]. The proposed Section 2.1.1.9.2 (Satellite Reacquisition Time under Very Short Signal Outages) specifies an additional requirement for a scintillation environment. Basically, the current “Satellite Reacquisition Time” requirement is split into two different requirements which consider both “Satellite Reacquisition Time under Short Signal Outages” for RFI (a 20 s reacquisition time limit for outages of 30 s or less) and “Satellite Reacquisition Time under Very Short Signal Outages” for scintillation (a 1 s reacquisition time limit for outages of 1 s or less). A receiver should properly manage an RFI condition with longer outages and a scintillation condition with shorter outages accordingly.

6.5 Summary

It has been demonstrated in this study that a 1 s reacquisition time can provide more than 99% availability of LPV-200 during the worst 45 min of a day even under severe scintillation scenarios. During the observed strong scintillation of the past solar maximum, a 1 s reacquisition time could provide more than 99.9% availability of LPV-200 during the worst 45 min of the nine day campaign. In order to achieve this high level of availability in the equatorial area during the strong scintillation of solar maxima, a fast reacquisition after a brief loss of lock should be mandated in the aviation receiver performance standards. Since the current MOPS does not have a specific performance requirement under scintillation, this study suggested an additional requirement for future dual frequency aviation receiver performance standards. The 1 s reacquisition time limit after a less than 1 s outage in the suggested requirement is not difficult to achieve with current receiver technology. During the Brazil campaign, for example, a certified WAAS receiver already demonstrated its fast reacquisition capability.

Chapter 7

Conclusion

7.1 Overview

This research was motivated by the fact that the current WAAS MOPS does not have performance requirements of aviation receivers under scintillation. Hence, the performance of a certified aviation receiver under scintillation is not guaranteed by the current MOPS. The analyses of this study were based on real scintillation data sets and simulated fading process models. These analyses were used to create a simple and effective receiver strategy to provide high aviation availability under scintillation conditions. An additional requirement for future standards mandating this strategy was proposed, and the proposed requirement is under discussion at the standards committee working group.

The contributions of this research are summarized as follows. This research:

1. Characterized signal environment under ionospheric scintillation from the perspective of GPS aviation [Seo *et al.*, 2009a].
2. Analyzed scintillation impact on GPS aviation availability [Seo *et al.*, 2009b].

3. Suggested and validated a new requirement for future dual frequency aviation receiver performance standards [Seo *et al.*, 2009c; 2009d].

7.2 Proposed Strategy to Provide High Aviation Availability Under Strong Scintillation

By observing real scintillation data from the past solar maximum, it was noticed that a receiver's reacquisition time is a very important parameter related to the level of expected aviation availability under strong scintillation. Although a receiver may frequently lose its tracking lock under the frequent deep fades observed during strong scintillation, the receiver can avoid simultaneous loss of multiple satellites if it has fast reacquisition capability. If a receiver does not lose many satellites simultaneously under strong scintillation, it can still provide high aviation availability given the current GPS constellation.

Another important observation was that the duration of deep signal fading under scintillation was very brief. As the current certified WAAS receiver already demonstrated during the Brazil campaign, fast reacquisition of a lost channel after a brief signal outage is not difficult to achieve for a conventional GPS receiver. A conventional receiver design with the strategy of fast reacquisition after a brief outage has much less burden for aviation certification than a novel receiver design with an IMU integration or vector tracking loops. Therefore, this research proposes fast reacquisition after brief outages as a strategy to provide high aviation availability under scintillation.

7.3 Effectiveness of the Proposed Strategy

The fast reacquisition strategy would be very effective, especially when the signal fades of different satellite channels are not highly correlated. If signal fades of different satellites occur simultaneously with a high probability (i.e., high satellite-to-satellite correlation), a receiver with fast reacquisition capability would still experience simultaneous loss of multiple satellites frequently. Hence, the effectiveness of the proposed strategy would be significantly reduced.

The 45 min of worst-case scintillation data from the Ascension Island campaign during the past solar maximum was selected as an example of strong scintillation. By the correlation study, it was confirmed that the satellite-to-satellite correlation was actually very low even during the worst 45 min. Therefore, the proposed strategy could be very effective during the strong scintillation period. The availability study of this work demonstrated that a 1 s reacquisition time could provide more than 99.9% availability of LPV-200 and 100% availability of RNP-0.1 during the worst 45 min even under the conservative assumption of 100% probability of loss of lock at deep fades.

Compared to other scintillation observations of previous studies, the worst 45 min scintillation of this study is believed to be a very severe case even in the equatorial area during solar maxima. Nevertheless, it is admitted that GPS scintillation data from the past solar maximum are too limited to fully characterize the equatorial scintillation and even stronger scintillation may occur in the next solar maximum. Hence, this study proposed a correlated fading process model which can simulate the instances of deep fades with any fading rates and correlation levels. Using this model, severe scintillation was simulated such that the observed very frequent deep fades and the observed maximum satellite-to-satellite correlation always occur for all

satellite channels. (During the worst 45 min scintillation, the very frequent fades and maximum satellite-to-satellite correlation occurred for only small fractions of time.) The availability result showed that a 1 s reacquisition time can provide more than 95% availability of LPV-200 during the simulated severe scintillation under many conservative assumptions including 100% frequency-to-frequency correlation of deep fades.

Since this research intends to provide a proper guideline for future dual frequency aviation receiver performance standards, the expected availability benefit from the future L5 signal was also studied. First, a new VPL equation was suggested to take benefit from this new signal under scintillation. Then, possible strategies to bound temporal ionospheric delay error during a single frequency loss were discussed. Using the proposed VPL and the strategy bounding ionospheric delay error, it was shown that a 1 s reacquisition time can provide more than 99% availability of LPV-200 during the simulated severe scintillation if a frequency-to-frequency correlation coefficient between L1 and L5 channels is less than 0.8. El-Arini *et al.* [2009] reported the correlation coefficient of 0.7 between L1 and L2 channels. Since the frequency separation between L1 and L5 is larger than the separation between L1 and L2, the correlation coefficient between L1 and L5 is expected to be less than 0.7. However, direct application of this previous correlation result is not very meaningful because the definition of correlation coefficient in [El-Arini *et al.*, 2009] is different from the definition used in this study. Since L5 scintillation data are not yet available, the true correlation level between L1 and L5 should be confirmed in the next solar maximum.

7.4 Real World Action Regarding the Proposed Strategy

This research proposed and validated a simple and effective strategy to provide high aviation availability during observed strong scintillations and simulated severe scintillations. Based on this study, an additional performance requirement mandating a 1 s reacquisition time after a less than 1 s signal outage was proposed at the standards committee working group [Seo *et al.*, 2009d]. This requirement is under discussion for inclusion in future dual frequency aviation receiver performance standards. Aviation receiver manufacturers are also involved in the discussion. If the manufacturers modify their receiver software to satisfy this requirement, they can expand the market to the equatorial area where LPV service is not currently available. However, this software modification may cause non-trivial cost to the manufacturers because it must be demonstrated that their receivers still satisfy all other requirements, especially RFI requirements, after this modification.

As the current reacquisition time test specified in the WAAS MOPS (Section 2.5.6 Satellite Reacquisition Time Test of [RTCA, 2006]), receiver performance under very short and frequent signal outages can be also tested using an RF simulator. The manufacturers may have difficulties to satisfy the deterministic limit of a 1 s reacquisition time and other RFI requirements simultaneously. If it is the case, a probabilistic requirement (e.g., a 1 s reacquisition time with more than 95% probability and a 2 s reacquisition time with more than 99% probability) can be also considered. Since this study has not performed availability analysis with probabilistic reacquisition times, further analyses are required if a probabilistic requirement is applied.

7.5 Direction of Future Work

Many conservative steps and assumptions were applied throughout the availability analyses of this work. This is mainly due to the lack of high rate GPS scintillation data from past solar maxima. Once extensive GPS scintillation data would be available after the next solar maximum (around 2013), the signal environment under scintillation can be better understood, and therefore those conservative assumptions can be reduced. For example, the fading rate of an L5 channel under strong scintillation is not yet known from real data. Ionospheric gradients accompanying scintillation in the equatorial area are not yet extensively studied. Although the parametric study showed that the availability results are not very sensitive to these parameters, a better characterization of such parameters will be useful to estimate aviation availability more precisely. A particular interest is on the correlation of signal fades between the current L1 and the future L5 signals. Depending on the correlation level between two frequencies, a possible availability benefit from future dual frequency aviation under scintillation will vary. In order to answer all these questions, extensive high rate (20 Hz or preferably 50 Hz) GPS scintillation data collection campaigns by many institutions should be performed during the next solar maximum.

Another effort should be focused on testing the performance of the current certified GPS aviation receivers under real scintillation. Since a certified GPS aviation receiver was not available during the past solar maximum, real performance data of an aviation receiver under scintillation of solar maxima are not yet available. Future dual frequency MOPS should provide standard procedures to test the fast reacquisition capability of a receiver under scintillation, if it mandates the fast reacquisition as suggested by this study. The standard test procedures using an RF simulator is necessary for the certification process, but a specific test procedure is not suggested

by this research. For the performance test under real scintillation and the development of standard test procedures, collaboration with aviation receiver manufactures is highly desired. Eventually, the standards committee will recommend specific requirements and test procedures to overcome ionospheric scintillation for worldwide GPS aviation expected in 2020 time-frame.

Appendix A

Acronyms

AFRL	Air Force Research Laboratory
ARAIM	Advanced/Absolute RAIM
ARNS	Aeronautical Radionavigation Service
CONUS	Conterminous United States
FAA	Federal Aviation Administration
FLL	Frequency Lock Loop
GDOP	Geometric Dilution Of Precision
GEAS	GNSS Evolutionary Architecture Study
GIC	GNSS Integrity Channel
GNSS	Global Navigation Satellite System
GPS	Global Positioning System
HAL	Horizontal Alert Limit
HPL	Horizontal Protection Level
IF	Intermediate Frequency
ILS	Instrument Landing System
IMU	Inertial Measurement Unit

IPP	Ionospheric Pierce Point
LAAS	Local Area Augmentation System
LPV	Localizer Performance with Vertical guidance
MAAST	Matlab Algorithm Availability Simulation Tool
MOPS	Minimum Operational Performance Standards
PDF	Probability Density Function
PLL	Phase Lock Loop
PRN	Pseudo-Random Noise
RAIM	Receiver Autonomous Integrity Monitoring
RF	Radio Frequency
RFI	RF Interference
RNP	Required Navigation Performance
RRAIM	Relative RAIM
RTCA	Radio Technical Commission for Aeronautics
SBAS	Space-Based Augmentation System
URA	User Range Accuracy
VAL	Vertical Alert Limit
VPL	Vertical Protection Level
VPLL	Vector Phase Lock Loop
WAAS	Wide Area Augmentation System
WBMOD	Wideband Scintillation Model

Appendix B

Covariance Between Correlated Poisson Random Variables

This appendix proves $\text{Cov}[V_1(t), V_2(t)] = \text{Var}[C(t)]$ for a given t , where $V_1(t)$, $V_2(t)$, and $C(t)$ are given as in Figure 4.7 (p. 73).

Since the Poisson random variables $P_1(t)$, $P_2(t)$, and $C(t)$ in Figure 4.7 for a given t are all independent,

$$\begin{aligned} \text{E}[V_1(t)V_2(t)] &= \text{E}[\{P_1(t) + C(t)\}\{P_2(t) + C(t)\}] \\ &= \text{E}[P_1(t)P_2(t) + P_1(t)C(t) + P_2(t)C(t) + C(t)^2] \\ &= \text{E}[P_1(t)] \text{E}[P_2(t)] + \text{E}[P_1(t)] \text{E}[C(t)] + \text{E}[P_2(t)] \text{E}[C(t)] + \text{E}[C(t)^2] \end{aligned}$$

$$\begin{aligned} \text{E}[V_1(t)] \text{E}[V_2(t)] &= \text{E}[P_1(t) + C(t)] \text{E}[P_2(t) + C(t)] \\ &= \{\text{E}[P_1(t)] + \text{E}[C(t)]\} \{\text{E}[P_2(t)] + \text{E}[C(t)]\} \\ &= \text{E}[P_1(t)] \text{E}[P_2(t)] + \text{E}[P_1(t)] \text{E}[C(t)] + \text{E}[P_2(t)] \text{E}[C(t)] + \text{E}[C(t)]^2. \end{aligned}$$

Hence,

$$\begin{aligned}\text{Cov}[V_1(t), V_2(t)] &= \text{E}[V_1(t)V_2(t)] - \text{E}[V_1(t)]\text{E}[V_2(t)] \\ &= \text{E}[C(t)^2] - \text{E}[C(t)]^2 \\ &= \text{Var}[C(t)].\end{aligned}$$

Appendix C

Doubly-Correlated Fading Process Model

This appendix proposes a method to generate doubly-correlated fading process model. Figure C.1 illustrates the procedure to obtain four doubly-correlated Poisson processes $\{L_{1,SV1}(t), t \geq 0\}$, $\{L_{5,SV1}(t), t \geq 0\}$, $\{L_{1,SV2}(t), t \geq 0\}$, and $\{L_{5,SV2}(t), t \geq 0\}$ with rates $\lambda_1 + \lambda_{SV} + \lambda_{15}$, $\lambda_5 + \lambda_{SV} + \lambda_{15}$, $\lambda_1 + \lambda_{SV} + \lambda_{15}$, and $\lambda_5 + \lambda_{SV} + \lambda_{15}$, respectively. In the illustration of Figure C.1, a simplified notation $L_{1,SV1}$ is used for a Poisson process $\{L_{1,SV1}(t), t \geq 0\}$, for example. The rate of the Poisson process is shown in parentheses as $(\lambda_1 + \lambda_{SV} + \lambda_{15})$. Similarly, X_1 indicates a Poisson process $\{X_1(t), t \geq 0\}$ and its rate is (λ_1) in parentheses. In addition, the “+” sign in Figure C.1 notates the combination of two Poisson processes in the way of Figure 4.7 (p. 73). Following this notation, the Poisson process $\{V_1(t), t \geq 0\}$ in Figure 4.7, which is the combination of two Poisson processes $\{P_1(t), t \geq 0\}$ and $\{C(t), t \geq 0\}$, can be expressed as $V_1 = P_1 + C$.

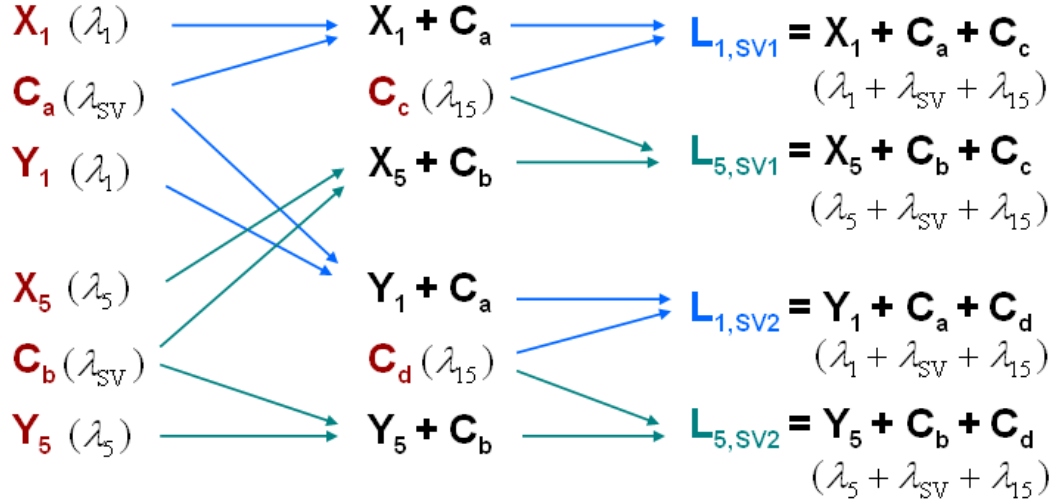


Figure C.1: Generation of four doubly-correlated Poisson processes $L_{1,SV1}$, $L_{5,SV1}$, $L_{1,SV2}$, and $L_{5,SV2}$ from eight independent Poisson processes X_1 , C_a , Y_1 , X_5 , C_b , Y_5 , C_c , and C_d . The combination of two Poisson processes notated with the “+” sign follows the way of Figure 4.7 (p. 73).

Once we generate three independent Poisson processes X_1 , C_a , and C_c with corresponding rates in parentheses, the Poisson process $L_{1,SV1}$ can be obtained by combining these three Poisson processes, i.e., $L_{1,SV1} = X_1 + C_a + C_c$. Similarly, $L_{5,SV1}$, $L_{1,SV2}$, and $L_{5,SV2}$ can also be obtained. Since $L_{1,SV1}$, $L_{5,SV1}$, $L_{1,SV2}$, and $L_{5,SV2}$ are Poisson processes, $L_{1,SV1}(t)$, $L_{5,SV1}(t)$, $L_{1,SV2}(t)$, and $L_{5,SV2}(t)$ for a given time t are Poisson random variables with means and variances of $(\lambda_1 + \lambda_{SV} + \lambda_{15})t$, $(\lambda_5 + \lambda_{SV} + \lambda_{15})t$, $(\lambda_1 + \lambda_{SV} + \lambda_{15})t$, and $(\lambda_5 + \lambda_{SV} + \lambda_{15})t$, respectively.

Now the covariance between two Poisson random variables $L_{1,SV1}(t)$ and $L_{5,SV1}(t)$ can be calculated. If the Poisson processes X_1 , X_5 , C_a , C_b , and C_c are all independently generated, the Poisson random variables $X_1(t)$, $X_5(t)$, $C_a(t)$, $C_b(t)$, and $C_c(t)$ for a given t are all independent. Hence,

$$\begin{aligned}
\mathbb{E}[L_{1,sv1}(t)L_{5,sv1}(t)] &= \mathbb{E}[\{X_1(t) + C_a(t) + C_c(t)\}\{X_5(t) + C_b(t) + C_c(t)\}] \\
&= \mathbb{E}[X_1(t)X_5(t) + X_1(t)C_b(t) + X_1(t)C_c(t) + C_a(t)X_5(t) \\
&\quad + C_a(t)C_b(t) + C_a(t)C_c(t) + C_c(t)X_5(t) + C_c(t)C_b(t) \\
&\quad + C_c(t)^2] \\
&= \mathbb{E}[X_1(t)] \mathbb{E}[X_5(t)] + \mathbb{E}[X_1(t)] \mathbb{E}[C_b(t)] + \mathbb{E}[X_1(t)] \mathbb{E}[C_c(t)] \\
&\quad + \mathbb{E}[C_a(t)] \mathbb{E}[X_5(t)] + \mathbb{E}[C_a(t)] \mathbb{E}[C_b(t)] + \mathbb{E}[C_a(t)] \mathbb{E}[C_c(t)] \\
&\quad + \mathbb{E}[C_c(t)] \mathbb{E}[X_5(t)] + \mathbb{E}[C_c(t)] \mathbb{E}[C_b(t)] + \mathbb{E}[C_c(t)^2] \\
\mathbb{E}[L_{1,sv1}(t)] \mathbb{E}[L_{5,sv1}(t)] &= \mathbb{E}[X_1(t) + C_a(t) + C_c(t)] \mathbb{E}[X_5(t) + C_b(t) + C_c(t)] \\
&= \{\mathbb{E}[X_1(t)] + \mathbb{E}[C_a(t)] + \mathbb{E}[C_c(t)]\} \\
&\quad \times \{\mathbb{E}[X_5(t)] + \mathbb{E}[C_b(t)] + \mathbb{E}[C_c(t)]\} \\
&= \mathbb{E}[X_1(t)] \mathbb{E}[X_5(t)] + \mathbb{E}[X_1(t)] \mathbb{E}[C_b(t)] + \mathbb{E}[X_1(t)] \mathbb{E}[C_c(t)] \\
&\quad + \mathbb{E}[C_a(t)] \mathbb{E}[X_5(t)] + \mathbb{E}[C_a(t)] \mathbb{E}[C_b(t)] + \mathbb{E}[C_a(t)] \mathbb{E}[C_c(t)] \\
&\quad + \mathbb{E}[C_c(t)] \mathbb{E}[X_5(t)] + \mathbb{E}[C_c(t)] \mathbb{E}[C_b(t)] + \mathbb{E}[C_c(t)]^2 \\
\text{Cov}[L_{1,sv1}(t), L_{5,sv1}(t)] &= \mathbb{E}[L_{1,sv1}(t)L_{5,sv1}(t)] - \mathbb{E}[L_{1,sv1}(t)] \mathbb{E}[L_{5,sv1}(t)] \\
&= \mathbb{E}[C_c(t)^2] - \mathbb{E}[C_c(t)]^2 \\
&= \text{Var}[C_c(t)] \\
&= \lambda_{15}t.
\end{aligned}$$

Therefore, the correlation coefficient between $L_{1,sv1}(t)$ and $L_{5,sv1}(t)$ is obtained

as follows.

$$\begin{aligned}
\rho_{L_{1,SV1}, L_{5,SV1}} &= \frac{\text{Cov}[L_{1,SV1}(t), L_{5,SV1}(t)]}{\sqrt{\text{Var}[L_{1,SV1}(t)]}\sqrt{\text{Var}[L_{5,SV1}(t)]}} \\
&= \frac{\lambda_{15}t}{\sqrt{(\lambda_1 + \lambda_{SV} + \lambda_{15})t}\sqrt{(\lambda_5 + \lambda_{SV} + \lambda_{15})t}} \\
&= \frac{\lambda_{15}}{\sqrt{\lambda_1 + \lambda_{SV} + \lambda_{15}}\sqrt{\lambda_5 + \lambda_{SV} + \lambda_{15}}}
\end{aligned}$$

Similarly, the correlation coefficients between other Poisson random variables are also obtained.

$$\begin{aligned}
\rho_{L_{1,SV2}, L_{5,SV2}} &= \frac{\lambda_{15}}{\sqrt{\lambda_1 + \lambda_{SV} + \lambda_{15}}\sqrt{\lambda_5 + \lambda_{SV} + \lambda_{15}}} \\
\rho_{L_{1,SV1}, L_{1,SV2}} &= \frac{\lambda_{SV}}{\sqrt{\lambda_1 + \lambda_{SV} + \lambda_{15}}\sqrt{\lambda_1 + \lambda_{SV} + \lambda_{15}}} \\
\rho_{L_{5,SV1}, L_{5,SV2}} &= \frac{\lambda_{SV}}{\sqrt{\lambda_5 + \lambda_{SV} + \lambda_{15}}\sqrt{\lambda_5 + \lambda_{SV} + \lambda_{15}}}
\end{aligned}$$

The four Poisson processes $L_{1,SV1}$, $L_{5,SV1}$, $L_{1,SV2}$, and $L_{5,SV2}$ are all doubly-correlated because $L_{1,SV1}(t)$ is correlated to $L_{5,SV1}(t)$ with a correlation coefficient $\rho_{L_{1,SV1}, L_{5,SV1}}$ and it is also correlated to $L_{1,SV2}(t)$ with a correlation coefficient $\rho_{L_{1,SV1}, L_{1,SV2}}$, and so forth.

The Poisson process $L_{1,SV1}$ models the fading process of the L1 channel of a satellite 1. The Poisson process $L_{5,SV1}$ models the fading process of the L5 channel of a satellite 1. For a satellite 2, $L_{1,SV2}$ models the fading process of its L1 channel and $L_{5,SV2}$ models the fading process of its L5 channel. Therefore, $\rho_{L_{1,SV1}, L_{1,SV2}}$ indicates a satellite-to-satellite correlation coefficient of the L1 channels and $\rho_{L_{5,SV1}, L_{5,SV2}}$ indicates a satellite-to-satellite correlation coefficient of the L5 channels. Similarly, $\rho_{L_{1,SV1}, L_{5,SV1}}$ represents a frequency-to-frequency correlation coefficient of a satellite

1 and ρ_{L_1,SV_2,L_5,SV_2} represents a frequency-to-frequency correlation coefficient of a satellite 2.

Now we have a method to generate four Poisson processes L_{1,SV_1} , L_{5,SV_1} , L_{1,SV_2} , and L_{5,SV_2} modeling both satellite-to-satellite correlation and frequency-to-frequency correlation between two satellites, from eight independent Poisson processes X_1 , C_a , Y_1 , X_5 , C_b , Y_5 , C_c , and C_d in Figure C.1 (p. 124), if their rates λ_1 , λ_{SV} , λ_1 , λ_5 , λ_{SV} , λ_5 , λ_{15} , and λ_{15} , respectively, can be determined.

For the simulation in Section 5.3.3 (p. 97), the fading rate of the L1 channel is obtained from the Ascension Island data (i.e., $\lambda_1 + \lambda_{SV} + \lambda_{15} = \frac{1}{9.71}$), and the fading rate of the L5 channel, $\lambda_5 + \lambda_{SV} + \lambda_{15}$, is assumed to be the same as the fading rate of the L1 channel, $\lambda_1 + \lambda_{SV} + \lambda_{15}$. Let satellite-to-satellite correlation coefficients be ρ_{SV} (i.e., $\rho_{L_1,SV_1,L_1,SV_2} = \rho_{L_5,SV_1,L_5,SV_2} = \rho_{SV}$). Then,

$$\begin{aligned} \rho_{L_1,SV_1,L_1,SV_2} = \rho_{L_5,SV_1,L_5,SV_2} &= \frac{\lambda_{SV}}{\sqrt{\lambda_1 + \lambda_{SV} + \lambda_{15}}\sqrt{\lambda_1 + \lambda_{SV} + \lambda_{15}}} \\ &= \frac{\lambda_{SV}}{\lambda_1 + \lambda_{SV} + \lambda_{15}} \\ &= \rho_{SV} \end{aligned}$$

$$\lambda_{SV} = \rho_{SV}(\lambda_1 + \lambda_{SV} + \lambda_{15}) = \frac{\rho_{SV}}{9.71}. \quad (\text{C.1})$$

Once a frequency-to-frequency correlation coefficient between the L1 and L5 channels is given as ρ_{15} (i.e., $\rho_{L_1,SV_1,L_5,SV_1} = \rho_{L_1,SV_2,L_5,SV_2} = \rho_{15}$), λ_{15} is determined as follows.

$$\rho_{L_1,SV_1,L_5,SV_1} = \rho_{L_1,SV_2,L_5,SV_2} = \frac{\lambda_{15}}{\lambda_1 + \lambda_{SV} + \lambda_{15}} = \rho_{15}$$

$$\lambda_{15} = \rho_{15}(\lambda_1 + \lambda_{SV} + \lambda_{15}) = \frac{\rho_{15}}{9.71} \quad (\text{C.2})$$

Finally, λ_1 and λ_5 are also determined for the given ρ_{SV} and ρ_{15} .

$$\lambda_1 + \lambda_{SV} + \lambda_{15} = \lambda_5 + \lambda_{SV} + \lambda_{15} = \frac{1}{9.71}$$

$$\begin{aligned} \lambda_1 = \lambda_5 &= \frac{1}{9.71} - \lambda_{SV} - \lambda_{15} \\ &= \frac{1}{9.71} - \frac{\rho_{SV}}{9.71} - \frac{\rho_{15}}{9.71} \\ &= \frac{1 - \rho_{SV} - \rho_{15}}{9.71} \end{aligned} \tag{C.3}$$

Since the rates of Poisson processes λ_{SV} , λ_{15} , λ_1 , and λ_5 are now determined from Equations (C.1)–(C.3) for a given satellite-to-satellite correlation coefficient ρ_{SV} and a frequency-to-frequency correlation coefficient ρ_{15} , eight independent Poisson processes X_1 , C_a , Y_1 , X_5 , C_b , Y_5 , C_c , and C_d in Figure C.1 (p. 124) can be generated with corresponding rates. Therefore, doubly-correlated Poisson processes $L_{1,SV1}$, $L_{5,SV1}$, $L_{1,SV2}$, and $L_{5,SV2}$ modeling the L1 and L5 fading channels of satellites 1 and 2 are obtained by combining these eight independent Poisson processes as shown in Figure C.1.

Note that the rates of Poisson processes λ_1 and λ_5 in Equation (C.3) must be positive. Hence, $\rho_{SV} + \rho_{15} < 1$. This means that the sum of a simulated satellite-to-satellite correlation coefficient and a frequency-to-frequency correlation coefficient must be less than 1. Therefore, if a satellite-to-satellite correlation coefficient is selected as 0.15 as in Section 5.3.3 (p. 97), a simulated frequency-to-frequency correlation coefficient must be less than 0.85.

Bibliography

- [Aarons, 1982] J. Aarons. Global morphology of ionospheric scintillations. *Proceedings of the IEEE*, 70(4):360–378, 1982.
- [Basu, 1981] S. Basu. Equatorial scintillations – a review. *Journal of Atmospheric and Terrestrial Physics*, 43(5-6):473–489, 1981.
- [Basu *et al.*, 1985] S. Basu, S. Basu, E. MacKenzie, and H. E. Whitney. Morphology of phase and intensity scintillations in the auroral oval and polar cap. *Radio Science*, 20(3):347–356, 1985.
- [Beach and Kintner, 2001] T. L. Beach and P. M. Kintner. Development and use of a GPS ionospheric scintillation monitor. *IEEE Transactions on Geoscience and Remote Sensing*, 39(5):918–928, 2001.
- [Beniguel and Adam, 2007] Y. Beniguel and J.-P. Adam. *Effects of scintillations in GNSS operation*. Springer Netherlands, 2007.
- [Cabler and DeCleene, 2002] H. Cabler and B. DeCleene. LPV: New, improved WAAS instrument approach. In *Proceedings of the 15th International Technical Meeting of the Satellite Division of the Institute of Navigation*, pages 1013–1021, 2002.

- [Chiou *et al.*, 2008] T.-Y. Chiou, J. Seo, T. Walter, and P. Enge. Performance of a Doppler-aided GPS navigation system for aviation applications under ionospheric scintillation. In *Proceedings of the 21st International Technical Meeting of the Satellite Division of the Institute of Navigation*, pages 1139–1147, 2008.
- [Conker *et al.*, 2003] R. S. Conker, M. B. El-Arini, C. J. Hegarty, and T. Hsiao. Modeling the effects of ionospheric scintillation on GPS/satellite-based augmentation system availability. *Radio Science*, 38(1):23, 2003.
- [Crane, 1977] R. K. Crane. Ionospheric scintillation. *Proceedings of the IEEE*, 65(2):180–199, 1977.
- [Datta-Barua *et al.*, 2008] S. Datta-Barua, T. Walter, J. Blanch, and P. Enge. Bounding higher-order ionosphere errors for the dual-frequency GPS user. *Radio Science*, 43(5), 2008.
- [de Paula *et al.*, 2007] E. R. de Paula, I. J. Kantor, A. A. N. Campos, P. F. Smorigo, L. F. C. de Rezende, P. Doherty, S. Delay, T. Walter, K. Groves, and P. M. Kintner. 4 different GPS receivers performance during scintillation under solar minimum conditions (2005/2006), presented at SBAS-iono meeting, Boston, MA, 15 June, 2007.
- [El-Arini *et al.*, 2003] M. B. El-Arini, R. S. Conker, S. D. Ericson, K. W. Bean, F. Niles, K. Matsunaga, and K. Hoshinoo. Analysis of the effects of ionospheric scintillation on GPS L2 in Japan. In *Proceedings of the 16th International Technical Meeting of the Satellite Division of the Institute of Navigation*, 2003.
- [El-Arini, 2009] M. B. El-Arini. Estimating time between fades at Naha, Japan (a case study), personal communication, 22 April, 2009.

- [El-Arini *et al.*, 2009] M. B. El-Arini, J. Secan, J. A. Klobuchar, P. H. Doherty, G. Bishop, and K. Groves. Ionospheric effects on GPS signals in the arctic region using early GPS data from Thule, Greenland. *Radio Science*, 44:14, 2009.
- [Enge *et al.*, 1996] P. Enge, T. Walter, S. Pullen, C. Kee, Y. C. Chao, and Y. J. Tsai. Wide area augmentation of the global positioning system. *Proceedings of the IEEE*, 84(8):1063–1088, 1996.
- [Enge, 1999] P. Enge. Local area augmentation of GPS for the precision approach of aircraft. *Proceedings of the IEEE*, 87(1):111–132, 1999.
- [Fremouw and Ishimaru, 1992] E. J. Fremouw and A. Ishimaru. Intensity scintillation index and mean apparent radar cross-section on monostatic and bistatic paths. *Radio Science*, 27(4):539–543, 1992.
- [Fremouw *et al.*, 1978] E. J. Fremouw, R. L. Leadabrand, R. C. Livingston, M. D. Cousins, C. L. Rino, B. C. Fair, and R. A. Long. Early results from DNA wideband satellite experiment – complex-signal scintillation. *Radio Science*, 13(1):167–187, 1978.
- [Fremouw *et al.*, 1980] E. J. Fremouw, R. C. Livingston, and D. A. Miller. On the statistics of scintillating signals. *Journal of Atmospheric and Terrestrial Physics*, 42(8):717–731, 1980.
- [Gallager, 1996] Robert G. Gallager. *Discrete stochastic processes*. The Kluwer international series in engineering and computer science. Kluwer Academic Publishers, Boston, 1996.

- [Ganguly *et al.*, 2004] S. Ganguly, A. Jovancevic, A. Brown, M. Kirchner, S. Zigic, T. Beach, and K. M. Groves. Ionospheric scintillation monitoring and mitigation using a software GPS receiver. *Radio Science*, 39(1):9, 2004.
- [Gao *et al.*, 2009a] G. X. Gao, A. Chen, S. Lo, D. De Lorenzo, T. Walter, and P. Enge. Compass-M1 broadcast codes in E2, E5b, and E6 frequency bands. *IEEE Journal of Selected Topics in Signal Processing*, 3(4):599–612, 2009.
- [Gao *et al.*, 2009b] G. X. Gao, L. Heng, D. De Lorenzo, S. Lo, D. Akos, A. Chen, T. Walter, P. Enge, and B. Parkinson. Modernization milestone: observing the first GPS satellite with an L5 payload. *Inside GNSS*, (May/June):30–36, 2009.
- [Gunawardena *et al.*, 2009] S. Gunawardena, Z. Zhu, and M. Braasch. First look: observing the GPS L5 test transmission from SVN49 using software radio processing. *Inside GNSS*, (May/June):22–29, 2009.
- [Gwal *et al.*, 2004] A. K. Gwal, S. Dubey, and R. Wahi. *A study of L-band scintillations at equatorial latitudes*, volume 34 of *Advances in Space Research*, pages 2092–2095. Pergamon-Elsevier Science Ltd, Kidlington, 2004.
- [Hatch, 1982] R. Hatch. The synergism of GPS code and carrier measurements. In *Proceedings of the 3rd International Geodetic Symposium on Satellite Doppler Positioning*, pages 1213–1231, 1982.
- [Hegarty and Chatre, 2008] C. J. Hegarty and E. Chatre. Evolution of the global navigation satellite system (GNSS). *Proceedings of the IEEE*, 96(12):1902–1917, 2008.

- [Henkel *et al.*, 2008] P. Henkel, K. Giger, and C. Gunther. Multi-carrier vector phase locked loop for robust carrier tracking. In *Proceedings of the 12th European Navigation Conference*, 2008.
- [Humphreys *et al.*, 2009] T. E. Humphreys, M. L. Psiaki, J. C. Hinks, B. O’Hanlon, and P. M. Kintner. Simulating ionosphere-induced scintillation for testing GPS receiver phase tracking loops. *IEEE Journal of Selected Topics in Signal Processing*, 3(4):707–715, 2009.
- [ION, 1998] ION. *Global positioning system: papers published in Navigation (GPS redbooks)*, volume V. The Institute of Navigation, 1998.
- [Jan *et al.*, 2009] S. S. Jan, W. Chan, and T. Walter. Matlab algorithm availability simulation tool. *GPS Solutions*, 13(4):327–332, 2009.
- [Kaplan and Hegarty, 2006] Elliott D. Kaplan and C. Hegarty. *Understanding GPS : principles and applications*. Artech House mobile communications series. Artech House, Boston, 2nd edition, 2006.
- [Kayton and Fried, 1997] M. Kayton and W. Fried. *Avionics navigation systems*. J. Wiley, New York, 2nd edition, 1997.
- [Kelly and Davis, 1994] R. J. Kelly and J. M. Davis. Required navigation performance (RNP) for precision approach and landing with GNSS application. *Navigation. Journal of the Institute of Navigation*, 41(1):1–30, 1994.
- [Kim *et al.*, 2008] E. Kim, T. Walter, and J. D. Powell. Wide area augmentation system-based flight inspection system. *Journal of Aircraft*, 45(2):614–621, 2008.

- [Kintner *et al.*, 2007] P. M. Kintner, B. M. Ledvina, and E. R. De Paula. GPS and ionospheric scintillations. *Space Weather—the International Journal of Research and Applications*, 5(9):23, 2007.
- [Kintner *et al.*, 2009] P. Kintner, T. Humphreys, and J. Hinks. GNSS and ionospheric scintillation: how to survive the next solar maximum. *Inside GNSS*, (July/August):22–30, 2009.
- [Knight, 2000] M. F. Knight. *Ionospheric scintillation effects on global positioning system receivers*. PhD thesis, 2000.
- [Lee, 1992] Y. C. Lee. Receiver autonomous integrity monitoring (RAIM) capability for sole-means GPS navigation in the oceanic phase of flight. *IEEE Aerospace and Electronics Systems Magazine*, 7(5):29–36, 1992.
- [May *et al.*, 1999] M. May, A. Brown, and B. Tanju. Applications of digital storage receivers for enhanced signal processing. In *Proceedings of the 12th International Technical Meeting of the Satellite Division of the Institute of Navigation*, pages 2199–2208, 1999.
- [Misra and Enge, 2006] P. Misra and P. Enge. *Global positioning system : signals, measurements, and performance*. Ganga-Jamuna Press, Lincoln, MA, 2nd edition, 2006.
- [Murphy *et al.*, 2005] T. Murphy, M. Harris, P. Geren, T. Pankaskie, B. Clark, and J. Burns. More results from the investigation of airborne multipath errors. In *Proceedings of the 18th International Technical Meeting of the Satellite Division of the Institute of Navigation*, pages 2670–2687, 2005.

- [Normark and Stahlberg, 2005] P.-L. Normark and C. Stahlberg. Hybrid GPS/Galileo real time software receiver. In *Proceedings of the 18th International Technical Meeting of the Satellite Division of the Institute of Navigation*, pages 1906–1913, 2005.
- [Parkinson and Gilbert, 1983] B. W. Parkinson and S. W. Gilbert. Navstar – global positioning system – 10 years later. *Proceedings of the IEEE*, 71(10):1177–1186, 1983.
- [Pullen *et al.*, 2009] S. Pullen, Y. S. Park, and P. Enge. Impact and mitigation of ionospheric anomalies on ground-based augmentation of GNSS. *Radio Science*, 44, 2009.
- [RTCA, 2006] RTCA. *Minimum operational performance standards for global positioning system/wide area augmentation system airborne equipment, Doc. DO-229D*. Washington, D. C., 2006.
- [Secan *et al.*, 1997] J. A. Secan, R. M. Bussey, E. J. Fremouw, and S. Basu. High-latitude upgrade to the wideband ionospheric scintillation model. *Radio Science*, 32(4):1567–1574, 1997.
- [Seo *et al.*, 2009a] J. Seo, T. Walter, T. Y. Chiou, and P. Enge. Characteristics of deep GPS signal fading due to ionospheric scintillation for aviation receiver design. *Radio Science*, 44, RS0A16, 2009.
- [Seo *et al.*, 2009b] J. Seo, T. Walter, and P. Enge. Availability impact on GPS aviation due to strong ionospheric scintillation. *IEEE Transactions on Aerospace and Electronic Systems*, submitted, 2009.

- [Seo *et al.*, 2009c] J. Seo, T. Walter, and P. Enge. Correlation of GPS signal fades due to ionospheric scintillation for aviation applications. *Advances in Space Research*, submitted, 2009.
- [Seo *et al.*, 2009d] J. Seo, T. Walter, and P. Enge. Possible modification to the WAAS MOPS regarding ionospheric scintillation, presented at RTCA Special Committee-159, Working Group-2 meeting, 24 June, 2009.
- [Singleton *et al.*, 1961] D. Singleton, G. J. E. Lynch, and J. A. Thomas. Field-aligned ionospheric irregularities and scintillation of satellite radio transmissions. *Nature*, 189(475):30, 1961.
- [Van Dierendonck and Hegarty, 2000] A. J. Van Dierendonck and C. Hegarty. The new L5 civil GPS signal. *GPS World*, (September):64–72, 2000.
- [Walter *et al.*, 2004] T. Walter, S. Datta-Barua, J. Blanch, and P. Enge. The effects of large ionospheric gradients on single frequency airborne smoothing filters for WAAS and LAAS. In *Proceedings of the 2004 National Technical Meeting of the Institute of Navigation*, pages 103–109, 2004.
- [Walter *et al.*, 2008] T. Walter, P. Enge, J. Blanch, and B. Pervan. Worldwide vertical guidance of aircraft based on modernized GPS and new integrity augmentations. *Proceedings of the IEEE*, 96(12):1918–1935, 2008.
- [Woo, 2000] K. T. Woo. Optimum semicodeless carrier-phase tracking of L2. *Navigation. Journal of the Institute of Navigation*, 47(2):82–99, 2000.